9th International Conference on Green Energy and Environmental Engineering (GEEE-2023)

Proceedings of Engineering & Technology
-PET-

Editor: Dr. Ahmed Rhif

ICID

Centre International d'Innovation et de Développement

Proceedings of Engineering & Technology
-PET-

9th International Conference on Green Energy and Environmental Engineering (GEEE-2023)

Editor:

Dr. Ahmed Rhif (Tunisia)

PET-Vol. 75
ISSN : 1737-9934

Committees

Honorary General Chairs:

Jalila Bouanani El Idrissi (MOR)
Mihoub Ouahiba (ALG)
Olfa Kammoun (TUN)

General Chairs:

Ahmed Rhif (TUN)
Fatima Zohra Boufadi (ALG)
Jeru Achyl Hounogbe (SEN)
Tayane Souad (MOR)

Steering Committee:

Abdoulaye Bouya Diop (SEN)
Akrouch Soukaina (MOR)
Allé Dioum (SEN)
Belatel Mimi (ALG)
Djeghlal M.Lamine (ALG)
Georges Descombes (FR)
Ines Ben Sassi (TUN)
Kasbadji Merzouk Nachida (ALG)
Meriem Hayani Mechkouri (MOR)
Nada Chtioui (TUN)
Nawel Seddiki (ALG)
Rekioua Djamila (ALG)
Sara Zatir (ALG)
Sahbeni Kawther (TUN)
Salma El Aimani (MOR)
Yosra Lahdheri (TUN)
Youcef Soufi (ALG)

Technical Committee:

Abdelkrim Khireddine (ALG)
Abdellah Mechaqrane (MOR)
Ahmed Maher (EGY)
Amer Ragab Ali Zerek (LBY)
Barara Mohamed (FR)
Berbaoui Brahim (ALG)
Bedoud khouloud (ALG)
Cherkaoui Abdeljzbbar (MOR)
Djalila Boudemagh (ALG)
El Fadar Abdellah (MOR)
Esther Muchiri (KEN))
Fatima Laassiri (MOR)
Fatima Zahra Messaoud (ALG)
Fateh Mebarek-Oudina (ALG)
Gherbi Mohamed (ALG)
Hadja Fatima Mehnane (ALG)
Haitham Saad Mohamed Ramadan (FR)
Kamal Reklaoui (MOR)
Kenz Amhmed Bozed (LBY)
Khaled Tarmissi (SAU)
Kheiri Abdelhamid (FR)
Kouzou Abdallah (ALG)
Lamia Iftekhar (BGD)
Madiha Yessari (MOR)
Manal Marzouq (MOR)
Mary Ahuna (KEN)
Mhamed Hammoudi (ALG)
Mounir Gaidi (UAE)
Mustapha Hatti (ALG)
Nadezhda Kunicina (LVA)
Olga Boiprav (BLR)
Rabhi Selma (ALG)
Rachid Benchrifa (MOR)
Rafika Boudries (ALG)
Rahmouni Soumia (ALG)
Sana Ahmed Abdaljlil (LBY)
Sapna Gambhi (IND)
Sellam Mebrouk (ALG)
Slimane Semghouli (MOR)
Sofiane Amara (ALG)
Stephen Okwiri (KEN)
Youssef Errami (MOR)
Yousef Jaradat (JOR)
Zohra Ameur (ALG)

Summary

9th International Conference on Green Energy & Environmental Engineering (GEEE-2023)
Proceedings of Engineering & Technology-PET-Vol 75

Improvement of the defluoridation conditions of industrial wastewater by precipitation

Imen Ben Belgacem[#1] and Abdessalem Ezzeddine[*2]

 # Sfax University/ Laboratory Materials sciences and Environment (MES-LAB) , Sfax University, Faculty of Sciences, Sfax, Tunisia.

[1]imen_ben_belgacem@yahoo.fr
[2]abdessalem.ezzeddine@enig.rnu.tn

* *Gabès University / Laboratory Engineering Process and Systems (LGPS)/ National School of Engineers, Gabès, Tunisia.*

***Abstract*— The treatment of real industrial wastewater by precipitation-neutralization using lime has been investigated. Effects of experimental conditions such as lime dose, and the final pH have been evaluated. Results of this study indicated that precipitation-neutralization processes can be successfully used to remove more than 90% of fluoride from wastewater. The treatment of this effluent containing different fluoride concentrations by precipitation with lime using $[Ca^{2+}]/[F^-]$ molar ratio of 0.8 led to fluoride removal higher than 95% with a final pH within the range 6.5 to 8.5. Synthetic calcium fluoride generated by precipitation-neutralization with lime (SCFL) contains 77.9% of CaF_2.**

***Keywords*—, Fluoride; Precipitation–neutralization; Lime; Synthetic calcium fluoride; Industrial wastewater; defluoridation.**

I. INTRODUCTION

Fluoride is a common element in the earth's crust and is highly soluble in water. Intake of fluoride is mainly through consuming drinking water containing fluoride. Fluoride intake at 0.5-1.5 mg/day will benefit teeth and bone development [1]. However, excessive fluoride intake can lead to dental and skeletal fluorosis, a chronic endemic disease. Fluorosis is a worldwide health problem and is endemic in certain areas in Tunisia, Algeria, Senegal, China, India, etc. In addition, exposure to excessive fluoride can also cause metabolic, structural and functional damages in such organs as nervous system [2], endocrine glands [3], reproductive system [4], hypertension [5] kidney and liver [6].

Fluoride pollution occurs through two different sources including natural and artificial sources. In groundwater sources, the natural concentration of fluoride depends on the geological, chemical and physical characteristics of the aquifer. Fluoride ions can also found in wastewater from the fluoride chemical industries, such as aluminum fluoride-manufacturing, semiconductor, fertilizer and glass-manufacturing industries. Some of these wastewaters were discharged into natural environment without any treatment. In Tunisia during manufacturing of aluminum fluoride large quantities of hydrofluoric acid (HF) are used. Hence, effluents from this process contain high levels of fluoride. Typical fluoride concentrations are from 100 to 6500 mg/L. The international legal requirement for effluent discharge needs an efficient treatment to remove fluoride ions contained in this effluent prior its discharge into the environment.

Several research efforts aiming to the development of efficient technologies for the reduction of the fluoride anions in industrial effluents have been reported in the literature and several methods such as coagulation [7], adsorption [8,9], reverse osmosis (RO) [10,11], nanofiltration [12], electrodialysis [13], Donnan dialysis [14], ion-exchange [15] and electrolytic methods [16,17] have been employed or tested for defluoridation. These studies have shown that several methods are successful to remove fluoride contained in industrial wastewaters but their feasibility is case specific. The disadvantages of most of these methods are high operational and maintenance costs and complicated procedure involved in the treatment. For example, the coagulation methods have generally been found effective in defluoridation but they are unsuccessful in bringing fluoride to desired concentration levels. Furthermore, membrane processes do not require additives but these are relatively expensive to install and operate and prone to fouling, scaling, or membrane degradation. Also, the electrochemical techniques, in general, suffer due to the high cost factor, during installation and maintenance [18] treatment [19]. This process produces calcium fluoride (CaF_2) particles through the addition of lime or any other calcium salt, such as, $CaCO_3$, $CaSO_4$ and $CaCl_2$ according to equation (1):

$$Ca(OH)_2\,(s) + 2\,F^-(aq) \rightarrow CaF_2(s) + 2\,OH^- \qquad (1)$$

The present work aims to (i) evaluate the feasibility of precipitation process using $Ca(OH)_2$ to treat high fluoride-content wastewater (ii) evaluate the ability of this processes to reduce fluoride load and to adjust medium pH, (iii) investigate the influence of different experimental parameters

ISSN: 1737-9334

such as initial pH, initial fluoride concentration, calcium/fluoride molar ratio on the effectiveness of fluoride treatment contained in industrial wastewater, (iv) determine the optimal conditions allowing the highest removal efficiency with these process in order to fulfill the normative requirements and (v) compare quantitatively the performance of these processes: neutralization-precipitation by lime, to decrease fluoride concentration to desirable values in accordance with international environmental regulations [20].

II. MATERIAL AND METHODS

A. Chemicals and reagents

Chemicals used in the present study were of analytical reagent grade. Calcium hydroxide $Ca(OH)_2$ (see characteristics in Table 1), procured by a local suppliers' (Interchaux). Double–distilled water was used in all the experimental runs.

B. Industrial fluoride effluent

An industrial wastewater was used in this study. For all fluoride-containing solutions, only polypropylene (PP) vessels were used for sample preparation and storage.

C. Precipitation process

The treatment experiments were performed in a batch thermostated polypropylene reactor of 0.5 Liter capacity. All measurements were made at room temperature (25 ± 1◦C) and atmospheric pressure under stirring conditions. A specific quantity of reagents lime or limestone) was added at the beginning of the treatment to desired volume of fluoride solution under vigorous magnetic stirring. The mixed solution was stirred for 120 minutes to allow the precipitation reaction. Sample was taken at certain time intervals (every 10 minutes), followed by immediate analysis to determine pH and fluoride concentration.

D. Analytical methods

The fluoride concentration was determined using the potentiometric standard method with Metrohm 781 pH/Ion Meter equipped by an ion-selective electrode (Metrohm 6.0502.150) and Ag/AgCl reference electrode (Metrohm 6.0726.100). The conductivity was measured using Metrohm 856 Conductivity Module at 25 ± 1◦C. The precipitated solids were filtered using a membrane filter (0.45 m) and dried at 110 ± 0.2 ◦C overnight.

X-Ray Fluorescence spectrometer (XRF) PANalytical model AXIOS were used to characterize the obtained precipitates. The pH of the wastewater was measured by Metrohm 780 pH meter equipped by a HF resistant glass electrode (Metrohm 6.0421.100). The instrument was calibrated each time the analysis was done. All quantitative analyses were run in triplicate for reproducibility of data and results in the figures and tables were the average ones.

III. RESULTS AND DISCUSSIONS

A. Characterisation of industrial effluent

Industrial wastewater was known by important fluctuations for the content of the element fluoride. So ten samples witch cover the range of variation of contents in this element were taken. Table 3 represents compositions of a representative industrial effluent. The major anions are fluoride and sulfate; their concentrations are 3300 and 345 mg/L, respectively. The major cation is aluminium (789 mg/L). The values of pH and conductivity make this effluent clearly different from those reported in similar published studies [22]. All these physicochemical characteristics confirm its toxicity and shows that it is mandatory to be treated before it is discharged into the environment.

B. Effect of lime dose

$Ca(OH)_2$ dose is an important factor to determine the performance of precipitation-neutralization process using lime [23]. Fig. 1 shows changes of fluoride concentration with time during the treatment of wastewater containing 167 mg F/L with different doses of lime. The results of Fig. 1 show that fluoride removal is largely affected by lime dose in the range from 0.25 g/L to 20 g/L. As it can be seen, the increase of $Ca(OH)_2$ dose from 0.25 g/L to 1 g/L decreases fluoride concentration from 167 mg/L to 105 mg/L and 9 mg/L, respectively after 30 minutes. However, increasing lime dose higher than 1.0 g/L does not enhance fluoride removal.

Furthermore, Fig. 2 presents the changes of pH with time during the treatment of AFMW using different doses of lime. This figure shows that the pH increased with the increase of the $Ca(OH)_2$ dose from initial pH 2.5 ± 0.1 to 3.5 ± 0.1, 5.5 ± 0.1, 8.0 ± 0.1, 10.5 ± 0.1 and 11.6 ± 0.1 for Ca(OH)2 doses of 0.25, 0.33, 0.5, 1.0, 2 and 5 g/L, respectively after 30 minutes contact time. For higher lime dose than 5.0 g/L, pH values higher than 11.6 ± 0.1 were obtained at the end of the treatment. For low doses of lime (0.25 g/L) corresponding to $[Ca^{2+}]/[F^-]$ molar ratio of 0.4, the final pH of treated wastewater was acidic (pH 3.5 ± 0.1). However, increasing lime dose from 0.25 g/L to 0.33 g/L and 0.5 g/L (corresponding to $[Ca^{2+}]/[F^-]$ molar ratios of 0.5 and 0.8, respectively), pH increased rapidly with time and reached a final pH of 5.7 ± 0.1 and 8.0 ± 0.1, respectively. A rapid increase of pH from initial pH 2.5 ± 0.1 to pH 10.5 ± 0.1, ± 0.1 and 11.6 ± 0.1 was observed for lime doses of 1, 2 and 5 g/L ($[Ca^{2+}]/[F^-]$) molar ratios of 1.5, 3 and 7.5), after 30 minutes, and then pH remains constant till the end of treatment.

Considering both fluoride removal efficiency and final pH of treated wastewater, dose of lime of 0.5 g/L corresponding to molar ratio equal to 0.8, is optimal to leading to more than 90 % fluoride removal with

ISSN: 1737-9334

dischargeable pH conditions (pH ranged from 6.5 to 8.5). This result of pH is consistent with those of M. F. Chang and J.C. Liu [24], who observed maximum fluoride removal at pH 6.5-8.5. While, for the parameter ratio of calcium to fluoride, [Ca2+]/[F-] obtained in this study (0.8) is higher than the ratio of 0.5 find by these authors. These results can be interpreted as follows:

- For low lime doses (< 0.5 g/L), calcium cation Ca^{2+} are not enough to totally precipitate fluoride ions and to attain desired environmental pH.
- Increasing progressively lime dose to 0.5 g/L, increases Ca^{2+} in the medium, and then precipitates further fluoride ions and neutralizes pH.
- For lime doses higher than 0.5 g/L, the solubility of calcium fluoride ($K=3.46\ 10^{-11}$) is exceeded and fluoride is converted from AFMW into solid crystal. Mechanism includes the following reactions:

$$HF \rightarrow H^+(aq) + F^-(aq) \quad (2)$$

$$Ca(OH)_2(s) \rightarrow Ca^{2+}(aq) + 2\ OH^-(aq) \quad (3)$$

$$Ca^{2+}(aq) + 2\ F^-(aq) \rightarrow CaF_2(s) \quad (4)$$

An excess of hydroxyl anions (OH-) is also generated which explain highly alkaline conditions obtained at the end of the treatment (pH~8.5 ± 0.1).

IV. FIGURES AND TABLES

Chemical characteristic (weight %)		**Physical characteristics**	
$Ca(OH)_2$	94.1	Grading	undersize 90 µm > 92%
CO_2 residual	2.1		undersize 200 µm > 98%
SiO2	1.9	Apparent density	1.5
MgO	0.4	-	-
Fe_2O_3	0.4	-	-
Al_2O_3	0.3	-	-

TABLE1 Chemical and physical specification of lime.

Parameters	**Unity**	**Value**
Conductivity at 25°C	mS/cm	33.5
pH	-	2.5
F^-	mg/L	3300
Cl^-	mg/L	295
Na^+	mg/L	141
K^+	mg/L	10.0
Ca^{2+}	mg/L	5,91
Al^{3+}	mg/L	789
Mg^{2+}	mg/L	0.24
Fe^{3+}	mg/L	1.20
Si	mg/L	4340
SO_4^{2-}	mg/L	345
PO_4	mg/L	7.0
Suspended solids	mg/L	470

TABLE 2 Composition of a representative sample of the industrial effluent.

	Calcium fluoride commercial grades		
Weight (%)	**Metallurgical grade**	**Ceramic grade**	**Acid grade**
CaF_2	60 to 85	85 to 97	> 97
SiO_2	-	> 3	< 1
$CaCO_3$	-	> 1.5	< 1.5
Fe_2O_3	-	< 0.14	< 0.5
P_2O_5	-	< 0.1	< 0.03
S (sulfur)	-	Traces	Traces
Zn	-	Traces	Traces

TABLE 3 *Commercial fluorspar grades.*

Composition	**CaF_2**	**CaO**	**SiO_2**	**Fe_2O_3**	**Al_2O_3**	**P_2O_5**
Weight (%)	77.9	18.1	1,9	0.62	0.35	0.048

TABLE 4 *Chemical analyses of SCFL.*

ISSN: 1737-9334

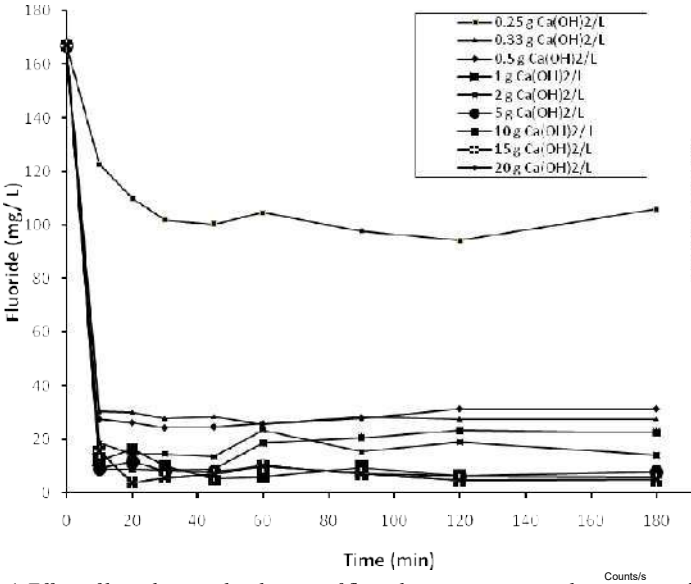

FIG.1 *Effect of lime dose on the changes of fluoride concentration with time. (initial pH 2.5 ± 0.1, initial fluoride concentration 167 mg/L and temperature 25 ± 1°C).*

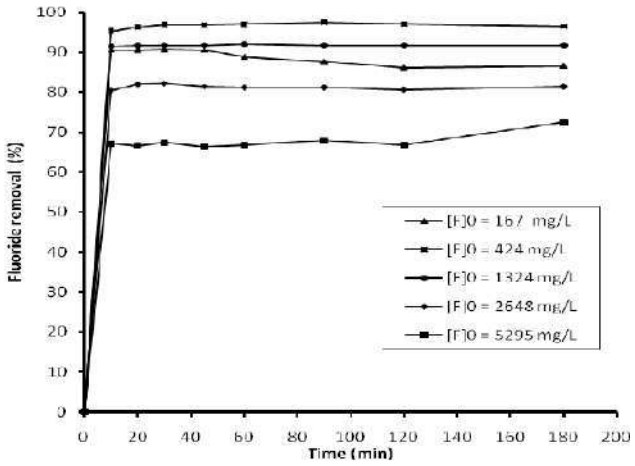

FIG.3 *Effect of fluoride content on the changes of fluoride removal with time (initial pH 2.5 ± 0.1, $[Ca^{2+}]/[F^-]$ 0.8 and temperature 25 ± 1°C).*

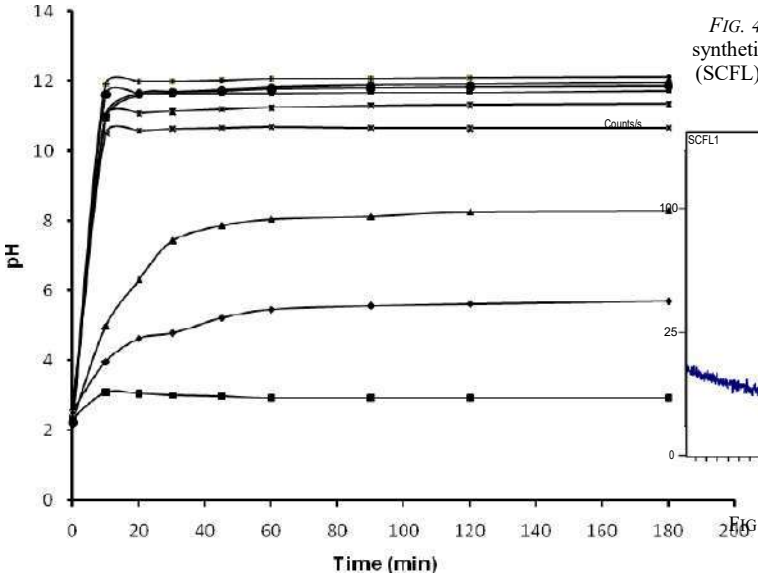

FIG. 2 *Effect of lime dose on the changes of pH with time (initial pH 2.5 ± 0.1, initial fluoride concentration 167 mg/L and temperature 25 ± 1°C).*

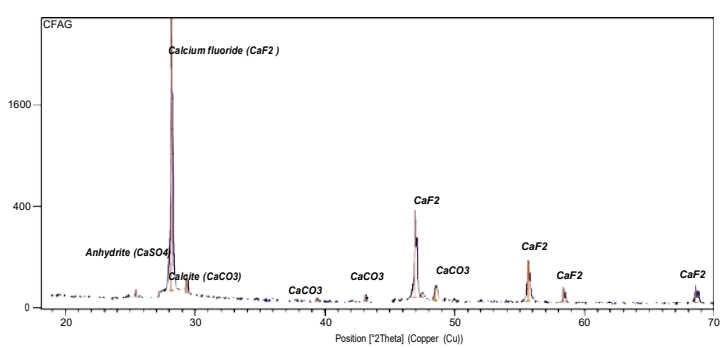

FIG. 4 XRD pattern : (a) Calcium fluoride acid grade (CaF2 > 97%); (b) synthetic calcium fluoride generated by precipitation-neutralization with lime (SCFL); (c) synthetic calcium fluoride generated by lime stone treatment of wastewater (SCFLS).

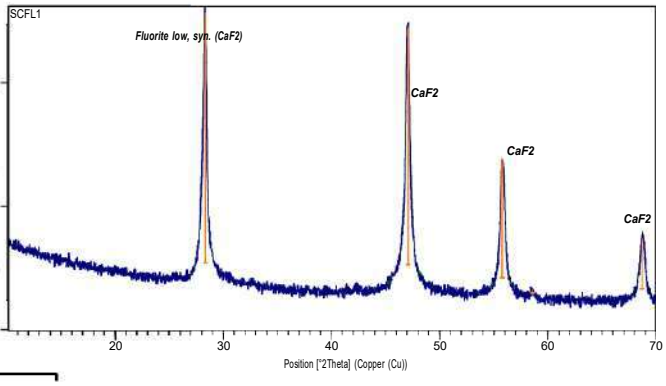

FIG. 5 Scheme of HF and AlF_3 production with integration of SCFL

ISSN: 1737-9334

V. CONCLUSIONS

The results found in this work demonstrate that the precipitation-neutralization and process are very efficient to reduce the concentration of fluoride anions contained in industrial wastewater in order to meet environmental regulation for wastewater discharge in terms of residual fluoride concentration and medium pH. Chemical precipitation-neutralization using $Ca(OH)_2$ has the advantage to obtain synthetic calcium fluoride to be reused in the hydrofluoric acid manufacture, making the process more technically and economically feasible.

REFERENCES

[1] E. Varol, S. Akcay, I.H. Ersoy, M. Ozaydin, B.K. Koroglu, S. Varol, (2010). Aortic elas-ticity is impaired in patients with endemic fluorosis. Biol. Trace Elem. Res. 133, 121–127.

[2] L. Valdez-Jimenez, C. Soria Fregozo, M.L. Miranda Beltran, O. Gutierrez Coronado, M.I. Perez Vega, (2011). Effects of the fluoride on the central nervous system. Neurologia 26, 297–300.

[3] E.A. Garcia-Montalvo, H. Reyes-Perez, L.M. Del Razo, (2009). Fluoride exposure impairs glucose tolerance via decreased insulin expression and oxidative stress. Toxicology 263, 75–83.

[4] P. Hao, X. Ma, X. Cheng, Y. Ba, J. Zhu, L. Cui, (2010). Effect of fluoride on human hypothalamus-hypophysis-testis axis hormones. Wei Sheng Yan Jiu 39 53–55. (in Chinese)

[5] L. Sun, Y. Gao, H. Liu, W. Zhang, Y. Ding, B. Li, M. Li, D. Sun, (2013). An assessment of the relationship between excess fluoride intake from drinking water and essential hypertension in adults residing in fluoride endemic areas, Sc. Total Environ. 443, 864–869.

[6] A. Chattopadhyay, S. Podder, S. Agarwal, S. Bhattacharya, (2011). Fluoride-induced histopathology and synthesis of stress protein in liver and kidney of mice, Arch.Toxicol. 85, 327–335.

[7] W.X. Gong, J.H. Qu, R.P. Liu, H.C. Lan, (2012). Effect of aluminum fluoride complexation on fluoride removal by coagulation, Colloids and Surfaces A: Physicochem. Eng. Aspect 395 88–93.

[8] P. Koilraj, S. Kannan, (2013). Aqueous fluoride removal using ZnCr layered double hydroxides and their polymeric composites: Batch and column studies, Chem. Eng. J. 234 406-415.

[9] V. Tomar, S. Srasad, D. Kumar, (2014). Adsorptive removal of fluoride from aqueous media using Citrus limoum (Lemon) leaf, Microchem. J. 112 97-103.

[10] S. Nicolas, L. Guihard, A. Marchand, B. Bariou, A. Amrane, A. Mazighi, N. Mameri, A. El Midaoui, (2010). Defluoridation of brackish northern Sahara groundwater-Activity.

ISSN: 1737-9334

Influence of drying plant material on yield, chemical composition, antioxidant and anti-inflammatory activities of essential oil extracted from the Tunisian *Cupressus sempervirens* leaves.

Hayfa Argui[#1,2], Fatiha Bradai[*3], Oumaima Ben Youchret-Zallera[#1], Coskun Yalçin[#4], Mossadok Ben-Attia[#2], Hechmi Said[#1], Marie-Laure Fauconnier[#5]

[#1]*Department of Chemistry, University of Carthage, 7021 Jarzouna, Tunisia.*

[#2]*Biomonitoring of the Environment Laboratory (LR01 / ES14), Faculty of Sciences of Bizerte, University of Carthage, 7021-Jarzouna, Tunisia*

[1,2]arguihayfa.tn@gmail.com, [1]oumayma_2005@yahoo.fr, [2]Mossadok.benattia@fsb.u-carthage.tn, [1]hechmi.said@gmail.com

[#4]*Department of Plant Production and Animal Husbandry, Canakkale Onsekiz Mart University, 17800 Çanakkale, Turkey*

[4]yalcin33coskun@gmail.com

[#5]*Agro-Bio Chem Department, University of Liege, Gembloux Agro-Bio Tech, 2, Passage of deportees, B-5030 Gembloux, Belgium.*

[5]Marie-Laure.Fauconnier@uliege.be

[*3]*Science of nature and life Department, University Center of Tipaza Morsli Abdellah, 42 00 Tipaza Algérie*

[3]fetihabradai@gmail.com

***Abstract*— The present study aims to assess the effectiveness of the drying time on the yield, chemical composition, antioxidant and anti-inflammatory properties of the essential oils (EOs) obtained from the Tunisian *Cupressus sempervirens* leaves. Adequate oils extraction conditions were determined. The drying time affected significantly the EOs yield of this plant. The major compounds found were; α-pinene, β-selinene, δ-3-carene, α-cubebene, β-caryophyllene and α-cedrol. Also, oils extracted from dried (60 and 90 days) leaves have high antioxidant properties due to the high content of (α-pinene and β-caryophyllene). Those constituents were known for their antioxidant activities. For the anti-inflammatory study, the inhibition was higher for the 60 days of drying at 100 µg mL^{-1}.**

***Keywords*— *Cupressus sempervirens;* leaf; essential oils; Microwave-assisted hydrodistillation; antioxidant activity; anti-inflammatory**

I. INTRODUCTION

In Tunisia, the *Cupressus sempervirens* L. was involved in traditional medicine, its fruit was known for the diabetes treatment and as an antiseptic. Essential oils (EO) occupy a large place in scientific research due to their antioxidant, antibacterial and antifungal activities [1]. The EOs chemical composition, as the volatiles compounds have also been extensively examined in medicinal plants [2]. The microwave assisted extraction (MAHD) is a new technology that has been applied to reduce the extraction time, organic solvent consumption, improve extraction yield, enhance extract quality, prevent pollution and reduce sample preparation costs. Up to now there is no report on the MAHD extraction of leaves EOs of *C. sempervirens*. Many studies have been conducted on the biological activities of the EO of this specie EO [3] but no studies or little were done on the effect of drying *C. sempervirens* leaves on the EO yields. This work aimed to study the effect of drying *Cupressus* leaves on the qualitative and quantitative characteristics of EO by applying a new method of distillation assisted by microwaves.

II. MATERIALS AND METHODES

A. Plant material

The fresh leaves of *C. sempervirens* were collected from the forest of Rimmel located in the North (Latitude: 37° 17’ 48’’ north; longitude: 10° 0′ 2″ east) of Tunisia, in January 2018. The specie was identified by Naziha Boughanmi, botanist Professor. The plant leaves were washed and dried in the shade for 30, 60 and 90 days. Fresh leaves were used as a control.

B. Determination moisture content

The moisture content was determined according to the method of Twidwell et al. [4]. Fresh plant material was dried in an oven at 105°C for 24 hours. It was calculated according to the following equation:

$$MC = ((m_f - m_d)/m_d) \times 100\%$$

where MC is the percentage of moisture after 24, m_f and m_d were, respectively, the mass of fresh and dried leaves (g).

C. Determination of dry matter

ISSN: 1737-9334

Leaf dry matter content were determined according to standard NF B 51-004 [5]. A mass of 5 g of vegetable matter is introduced into a porcelain crucible then dried in an oven at 105°C until a constant mass is obtained. After cooling in a desiccator, the crucible was weighed. Dry matter content was determined according to the following formula:

$$DM = (m_2/m_1) \times 100\%$$

Where DM is the percentage of dried matter after 24 hours of drying, m_1 is the mass of sample and m_2 is the mass of the crucible removed from the desiccator.

D. Extraction of EOs by Microwave-assisted hydrodistillation (MAHD)

After drying in the shade for (30, 60 and 90 days), crushed leaves (200g) were introduced in a reactor of 2L capacity and all microwave parameters were adjusted.

- *Influence of Heating Power on EO Yield.* In this assay, *MAHD* was performed at 400 rpm for 5 powers (250, 300, 400, 500 Watt).

- *Influence of the number of turns on the EO Yield*. This test was carried out for 3 revolutions (250, 300 and 400).

E. Evaluation of antioxidant activity of EOs

For the assessment of the antioxidant potential of the oils two methods were used:

- *The DPPH radical scavenging activity assay*

The antiradical activity was evaluated according to Bicas et al. [6], with slight modifications. One mL of a methanolic solutions of EOs (25, 50, 75 and 100 $\mu g.mL^{-1}$) was mixed with 1 mL of a methanolic DPPH solution (0.004% w/v). The mixture was incubated for 30 min at room temperature, and the absorbance was measured at 517 nm using an Ultraspec 7000 UV-vis dual beam spectrophotometer (GE Healthcare, Chicago, IL, USA). For comparison, the inhibition of the free radical DPPH with Trolox was also analysed under the same conditions as the samples. Trolox was used as a positive control. All tests were performed in triplicate. Percent inhibition PI (%) was calculated as described by Hazzit et al. [7]:

$$PI = (A_b - A_a)/A_b) \times 100\%$$

where PI is the percentage of inhibition, A_a is the absorbance of the sample and A_b is the absorbance of the reaction medium without oil.
PI (%) was plotted against sample concentrations to obtain the IC50 index, which was defined as the concentration of antioxidant required to decrease the initial DPPH concentration by 50% [8].

- *The FRAP (Ferric Reducing Antioxidant Power) assay*
The reducing power of essential oils and Trolox were determined according to the method of *Lamia et al.* [9]. First, one mL of sample (25, 50, 75 and 100 $\mu g.mL^{-1}$) was mixed with sodium phosphate buffer (1 mL, 0.2 M, pH=6.6) and 1 mL of potassium ferricyanide ($K_3Fe(CN)_6$) solution (1%). Then, the mixture was incubated for 20 min at 50°C and to stop the reaction, one mL of Trichloroacetic acid (TCA) at 10% (v/v) was added to the solution. Centrifugation at 3000 g was carried out for 10 min at room temperature. Finally, one mL of supernatant was recovered and mixed with 1.5 mL of distilled water and 150 µl of $FeCl_3$ (0.1%). The absorbance was measured at 700 nm. The increase absorbance of the reaction mixture (according to the blank) indicated an increase in the reducing power.

F. Evaluation of anti-inflammatory activity

The in vitro inhibitory effect of the oil of *C. sempervirens* was determined using the protein denaturation method described by Rahman et al. [10], with some modifications. One mL of human serum albumin solution (5%) was mixed with 1 mL of the extracts at different concentrations (25, 50, 75 and 100 $\mu g.mL^{-1}$). The pH of the reaction medium was adjusted to 6.6 and incubated at 37°C for 20 min and at 72°C for 5 min. The BSA buffer (2.5 ml) was added. The absorbance was measured at 660 nm. A blank for each extract was prepared under the same conditions, replacing albumin with Tris HCl. The control consists of albumin and distilled water, Diclofenac was used as a standard and tested under the same conditions.
The percentage of inhibition of albumin denaturation was calculated by the following formula [11]:

$$PI = ((A_c - A_t)/A_c) \times 100(\%)$$

where A_c is the absorbance of the reactional media without inhibitor essential oils, A_t is the absorbance of the sample.

III. RESULTS AND DISCUSSION

A. Moisture content and dry matter

The moisture content and the dry matter rate of *C. sempervirens* leaves were shown in the Table 1. Analysis of the *C. sempervirens* samples revealed a high humidity level (62%), which means that the majority of the weight of the plant is fresh.

TABLE 1. Moisture content and dry matter of *C. sempervirens leaves*.

Plant matter	Moisture content (%)	Dry matter (%)
C. sempervirens leaves	62	38

A. Optimal conditions for C. sempervirens EOs extraction

Results have shown that the optimal conditions obtained were 20 min as time of extraction, Heating power at P = 600 W, turns number of 400 rpm and a water/plant material ratio at approximately (200mL/200g).

ISSN: 1737-9334

B. Essential oils yields

Figure 2 shows the variation of the oil content according to the drying time. The yield of oil increased when the leaves were dried for 30 days achieving a maximum of 0,207%, beyond this period, a decrease in performance was observed. The yield of EO decreased with the increase of the time of leaves drying. The variation of the EO content obtained from *C. sempervirens* leaves before the extraction procedure according to the duration of drying was studied for the first time.

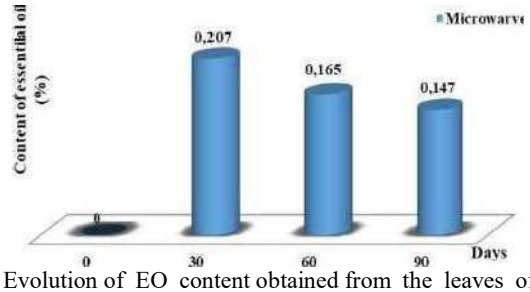

Fig. 1. Evolution of EO content obtained from the leaves of *C. sempervirens* after drying.

Increasing the concentration of EO, expressed in dry weight during the 30 days of drying may be explained by an important physiological activity (enzymatic reactions). So, the biosynthesis of EO continues accelerating as a response to drying process due to water stress. A severe dehydration decreased reactions after 30 days and could causes the death of cells. It was already shown that the moisture content in plant material affect the yield of EO [12]. Water evaporation caused the oil cell rupture, this allows the entering of the vapor in the cells which pull the oil out of cells [13][14]. According to Périno-Issartier et al. [15], damage affect the cells and so the oil and their volatile compounds content could be taken easier. The best distillation treatment delays process for 8 days, it affected the decrease in moisture content and damage to the texture of the distilled material. Where the longer the delay process, the more EO will be produced.

C. Chemical composition of Cupressus EOs

Chemical composition of the oil of *C. sempervirens* leaves was identified by GC-MS. According to the drying time, the total of identified components were: 39 (30 days), 57 (60 days) and 66 (90 days) and percentages were (99.741 ± 1.138), (99.438 ± 1.875%) and (99.403 ± 3.097%) after, respectively, 30, 60 and 90 days of drying leaves. Oil issue from the 30 days was predominantly composed of monoterpene hydrocarbons (42.102 ± 0.327%) where α-pinene (24.877 ± 0.138%), β-selinene (9.1 7ȝ± 0.061%) and α-cubebene (9.557 ± 0.075%) represented the maincompounds. Both oils of 60- and 90-days treatments were mainly composed of sesquiterpene hydrocarbons with respectively (39.666 ± 0.365%) and (38.362 ± 0.883%), where α-pinene is the major compound (16.237 ± 0.163% and 15.087 ± 0.171%). β-selinene covered the second highest percentage (9.027 ± 0.048%) in the oil after 60 days, while α-cubebene was the second most important compounds (7.700 ± 0.204%) after 90 days.

The chemical constituents confirmed that these oils are rich in principal phytochemical compound including monoterpene hydrocarbons, oxygenated monoterpenes, sesquiterpene hydrocarbons, sesquiterpene oxygenated, diterpenes, diterpenoids and unknown. Also, results showed that the amounts of monoterpenes and sesquiterpene hydrocarbons decreased with the increasing of the drying time. The most significant variations were observed in α-pinene (24.877 ± 0.138 - 15.087 ± 0.171%), α-fenchene (0.373 ± 0.017 - 0.277 ± 0.007%), β-caryophyllene (6.487 ± 0.05 - 4.923 ± 0.033%), γ-elemene (2.563 ± 0.094 - 2.313 ± 0.078%), alloaromadendrene (3.233 ± 0.038 - 2.867 ± 0.078%) and β-selinene (9.557 ± 0.075 - 7.62 ± 0.026%).

During the drying time, remarkable modification in the chemical composition of EO was registered at the level of two majorities compounds: α-Pinene and α-Cedrol. Where th α-Cedrol rate increased and went from (4.357 ± 0.052%) to (5.540 ± 0.076%) while the α-pinene dropped from (24.877 ± 0.138%) to (15.087 ± 0.171%), after 90 days of drying (Fig. 2).

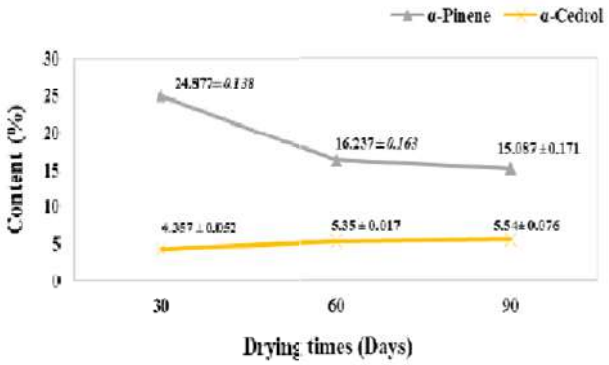

Fig. 2 Variation of α-pinene and α-Cedrol contents in the EOs of *C. sempervirens* according to the drying time of the plant material.

Fig. 3 showed variations of the fifteen major compounds depending on the drying time. However, eighteen compounds including α-Thujene, p-Cymene, Trans Sabinene hydrate, Isopulegol acetate, Linalyl acetate, β-Bourbonene, β-Elemene, β-Bisabolene, δ-Cadinol, Elemol, Caryophyllene oxide, 10-epi-γ-Eudesmol, ζ-cadinol, α-Cadinol, Khusinol, Abienol, Ferruginol and unknown, were present in the oil issue after 60 and 90 days of drying lants. In addition, (Z)-β-Ocimene, Trans-Pinocarveol, Camphor, α-

ISSN: 1737-9334

Phellandrene, (E)-β-Ocimene, α-Terpineol, Unknown_1, Carvacrol, δ-Elemene, Unknown_3 and Sempervirol, were present in the oil of 90 days dried samples.

The mean percentage of 9 compounds namely α-pinene (16.237 ± 0.163 - 15.087 ± 0.171%), β-selinene (9.557 ± 0.075 - 7.62 ± 0.026%), β-caryophyllene (6.487 ± 0.05 – 4.923 ± 0.033%), Alloaromadendrene (3.233 ± 0.038 – 2.867 ± 0.078%), γ-Elemene (2.563 ± 0.094 – 2.313 ± 0.078%), β-Terpinyl acetate (3.233 ± 0.037 – 0.00%), Dehydrobitan (1.227 ± 0.023 – 1.097 ± 0.055%), Pulegone (1.073 ± 0.087 – 0.00%) and α-Fenchene (0.373 ± 0.017 – 0.277 ± 0.007%) significantly ($P < 0.05$) decreased with drying time.

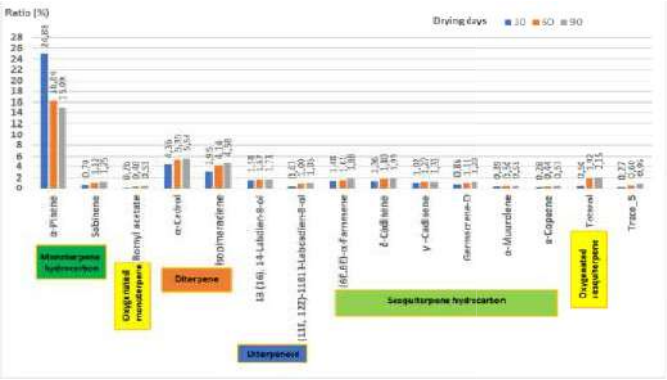

Fig. 3 Proportional evolution of the content of t e main compounds in the leaves of *C. sempervirens* during drying days.

The increase in the drying time (60 and 90 days) caused a significant ($P < 0.05$) increase in the percentage of the main compounds as; α-Cedrol (4.357 ± 0.052 - 5.540 ± 0.076%), Isopimaradiene (2.953 ± 0.033 - 4.583 ± 0.020%), 13 (16) 14 -Labdien-8-ol (1.583 ± 0.003 - 1.730 ± 0.75 %) and (6E, 6E)-α-Farnesene (1.483 ± 0.027- 1.877 ± 0.124%). However, the content of α-pinene (24.877 ± 0.138 - 15.0 7 ± 0.171%) was significantly ($P < 0.05$) decreased when t e time of drying increased.

The dominance of α-pinene (37.14%) and δ-3-carene (19.64%) were also observed in the oil of T nisian *Cupressus* by [16] and in Egypt with respectively (29.21%) and (18.92%) [17]. The differences in such composition have been proved to be mainly due to geographic, climatic, harvesting time and soil conditions (17).

D. Antioxidant activity

The DPPH free radical scavenging activity of *C. sempervirens* EO was evaluated by its inhibitory effect on a methanolic solution of DPPH. Table 2 gathers the different values of the percentage inhibition of the DPPH radical corresponding to the concentrations *C. sempervirens* EO obtained after 30, 60 and 90 days of plant drying.

Table 2. Percentages of DPPH radical inhibition for the different concentrations of *C. sempervirens* oils dried for 30, 60, 90 days. The Trolox used as a positive control.

Concentration (µg mL^{-1})	Time (days)			Trolox
	30	60	90	
25	6.25±1.20a	20.83±2.41a	18.42±1.52a	96.86±1.60a
50	16.67±1.76b	34.78±2.51a	34.21±1.52b	96.34±0.52a
75	21.74±1.26c	48.55±1.92b	43.24±1.56c	96.20±0.55a
100	33.33±1.20d*	50.00±2.41c*	54.05±1.56d*	96.86±1.60a^{ns}
LSD	*4.4886*	*7.5697*	*5.0222*	*3.8987*

*: Levels in the same column not connected by the same letter are significantly different (P<0,05).
^{ns}: Levels in the same column connected by the same letter are not significantly different (P≥0,05).

The present data were compared with that of the Trolox, which registered (96,86%) of inhibition of DPPH radical. Among oils obtained at the 30-, 60- and 90-days plant drying, maximal inhibition was registered by 90 days (54,05%), followed by 60 days (50,00%) and the 30 days (33,33%) at 100 µg mL^{-1} of oil concentration.

The main differences between these oil samples were found in the proportions of β-caryophyllene and α-pinène. The IC50 was determined from the antioxidant capacity of EOs of *C. sempervirens* leaves dried for 30, 60 and 60 days. These values were calculated over time from the regression line of PI (%) (Calculated from the GraphPad Prism 5) depending on the concentration of each tested sample. The IC50 values of EOs at different drying times as well as that of Trolox are shown in Table 3.

Table 3. IC50 values for *C. sempervirens* EOs at different drying times and the Trolox positive control.

Drying (Days)	*C. sempervirens* EO			Trolox*
	30	60	90	
IC_{50} (mg.mL^{-1})	47,67±3,97	36,12±4,60	36,60±3,32	8.543±0.154

Oils obtained from 60 dried leaves have the highest antioxidant property (IC50: 36,12 ± 4,60 µg.mL^{-1}), which is almost similar to that obtained from 90 days of drying leaves (IC50: 36,60 ± 3,32 µg.mL^{-1}), followed by 30 days of drying (IC50: 47,67 ± 3,97 µg.mL^{-1}) (Table 3). The antioxidant activity decreased with the decreasing of the majority of compounds. Results also demonstrated that dried 30, 60 and 90 days oils have high antioxidant proprieties, which could be due to the high content in α-pinene [18] and β-caryophyllene [19]. Those constituents were known for their antioxidant activities.

E. Reducing power

ISSN: 1737-9334

The reducing power of *C. sempervirens* EO originated from 30, 60 and 90 days after drying were studied by the transformation of Fe^{+3} to Fe^{+2}. High results were shown for the 60 days treatment at high level of concentrations. The β-caryophyllene is one of those compounds that may interact synergistically or antagonistically to create an effective system against free radicals [19].

F. *Anti-inflammatory activity*

The anti-inflammatory activity of *C. sempervirens* EO were determined in vitro using the anti-denaturation method of bovine albumin serum (BSA). Results showed that the PI (%) increased with the increasing of EO concentrations (Fig. 4). The EOs denatured the protein at 88 ± 3.079% (60 days of drying leaves) and 49.765 ± 1.248 % (90 days of drying leaves) at 100 µg.mL^{-1}. Moreover, the percentage of BSA protection was dependent on EO concentrations (p-value <0.05).

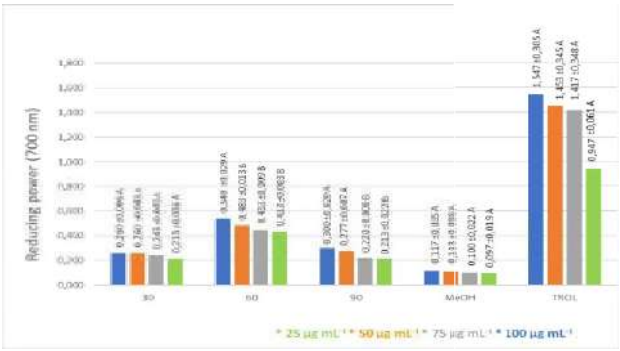

Fig. 4 The ferric-reducing power of EOs extracted from leaves of *C. sempervirens* and Trolox at various concentrations. Mean values and standard deviation values were presented (n = 3).

The effect of Diclofenac against denaturation is very significant (82.425 ± 0.417 %) at 100 µg.mL^{-1}. Oils obtained from *C. sempervirens* leaves dried over time have dose-dependent activities. Diclofenac had an IC50: 2.446 ± 0.073 µg.mL^{-1}, while oil issue from 60 and 90 days were 39.051 ± 0.028 and 48.706 ± 0.108 µg.mL^{-1}, respectively. IC50 values of the tested EOs and Diclofenac were also determined (39.051 ± 0.028 and 48,706 ± 0.108 µg.mL^{-1}) for respectively 60 and 90 days. The higher anti-inflammatory activity of the dried sample for 60 and 90 was probably due to their high content of α-humulene and β-caryophyllene.

IV. CONCLUSION

In this study, it would be appropriate to extract the EO after one month of *C. sempervirens* dried leaves, for a better industrial use of this oil, since their content would be at its maximum. Beyond this period, this oil loose its qualitative characteristic.

ACKNOWLEDGMENTS

This research work was carried out in the Laboratory of Volatolomics, Unit of General and Organic Chemistry, Gembloux Agro-Bio Tech, University of Liège, Gembloux, Belgium. A part of this work was funded by the Tunisian Ministry of Higher Education and Scientific Research and the University of Carthage (Bizerte).

REFERENCES

[1] D.R. Batish, H.P. Singh, R.K. Kohli, S. Kaur. Eucalyptus essential oil as a natural pesticide, *Forest Ecology and Management* 2008, 256(12):2166-2174.

[2] S. Rguez, N. Djébali, I.B. Slimene, G. Abid, M. Hammemi, S. Chenenaoui, S. Bachkouel, M. Daami-Remadi, R. Ksouri, I. Hamrouni-Sellami : *Cupressus sempervirens* essential oils and their major compounds successfully control postharvest grey mould disease of tomato. *Industrial crops and products* 2018, 123:135-141.

[3] G. Sacchetti, S. Maietti, M. Muzzoli, M. Scaglianti, S. Manfredini, M. Radice, R. Bruni. Comparative evaluation of 11 essential oils of different origin as functional antioxidants, antiradicals and antimicrobials in foods. *Food chemistry* 2005, 91(4):621-632.

[4] E.K. Twidwell et al. 2002, Extension extra, Paper 280.

[5] Norme N: B51-004, Wood-Determination of Moisture Content. In.: Association Française de Normalisation (AFNOR), France; 2010.

[6] J. Bicas, I. Neri-Numa, A. Ruiz, J. De Carvalho, G. Pastore : Evaluation of the antioxidant and antiproliferative potential of bioflavors. *Food and Chemical Toxicology* 2011, 49(7):1610-1615.

[7] M. Hazzit, A. Baaliouamer, A. Veríssimo, M. Faleiro, M.G. Miguel: Chemical composition and biological activities of Algerian Thymus oils. *Food chemistry* 2009, 116(3):714-721.

[8] F. Sharififar, M. Moshafi, S. Mansouri, M. Khodashenas, M. Khoshnoodi: In vitro evaluation of antibacterial and antioxidant activities of the essential oil and methanol extract of endemic Zataria multiflora Boiss. *Food control* 2007, 18(7):800-805.

[9] S.A. Lamia, B. Moussa, F. Marie-Laure, L. Georges: Chemical composition and antioxidant activity of Thymus fontanesii essential oil from Algeria. *The Natural Products Journal* 2020, 10(3):193-199.

[10] Rahman H, Eswaraiah MC, Dutta A: In-vitro anti-inflammatory and anti-arthritic activity of Oryza Sativa Var. joha rice (an aromatic indigenous rice of Assam). *Am Eurasian J Agric Environ Sci* 2015, 15(1):115-121.

[11] T.B. Thanh, L.V. Duc, H.N. Thanh, Tien VN: In vitro antioxidant and anti-inflammatory activities of isolated compounds of ethanol extract from Sanchezia speciosa Leonard's leaves. *Journal of basic and clinical physiology and pharmacology* 2017, 28(1):79-84.

[12] M. Khadidja, B. Nassima, B. Chahrazed, F. Xavier: Chemical composition and antimicrobial activity of essential oils isolated from Algerian Juniperus phoenicea L. and Cupressus sempervirens L. *Journal of Medicinal Plants Research* 2010, 4(10):959-964.

[13] M.T. Golmakani, K. Rezaei: Comparison of microwave-assisted hydrodistillation withthe traditional hydrodistillation method in the extractionof essential oils from Thymus vulgaris L. *Food chemistry* 2008, 109(4):925-930.

[14] M. Kosar, Z. Tunalier, T. Özek, M. Kürkcüoglu, Baser KHC: A simple method to obtain essential oils from Salvia triloba L. and Laurus nobilis L. by using microwave-assisted hydrodistillation. *Zeitschrift für Naturforschung C* 2005, 60(5-6):501-504.

[15] S. Périno-Issartier, C. Ginies, G. Cravotto, F. Chemat: A comparison of essential oils obtained from lavandin via different extraction processes: Ultrasound, microwave, turbohydrodistillation, steam and hydrodistillation. *Journal of Chromatography A* 2013, 1305:41-47.

[16] M. Boukhris, G. Regane, T. Yangui, S. Sayadi, M. Bouaziz: Chemical composition and biological potential of essential oil from Tunisian Cupressus sempervirens L. *Journal of arid land studies* 2012, 22(1):329-332.

[17] S.A. Fayed: Chemical composition, antioxidant, anticancer properties and toxicity evaluation of leaf essential oil of Cupressus sempervirens. *Notulae Botanicae Horti Agrobotanici Cluj-Napoca* 2015, 43(2):320-326.

[18] H. Argui, O.B. Youchret-Zalleza, S.C. Suner, C.D. Periz, G. Türker, S. Ulusoy, M. Ben-Attia, F. Büyükkaya, A. Oral, Y. Coskun: Isolation, Chemical Composition, Physicochemical Properties,

ISSN: 1737-9334

and Antibacterial Activity of Cupressus sempervirens L. Essential Oil. *Journal of Essential Oil Bearing Plants* 2021, 24(3):439-452.

[19] R. Torres-Martínez, Y.M. García-Rodríguez, P. Ríos-Chávez, A. Saavedra-Molina, J.E. López-Meza, A. Ochoa-Zarzosa, R.S. Garciglia: Antioxidant activity of the essential oil and its major terpenes of Satureja macrostema (Moc. and Sessé ex Benth.) Briq. *Pharmacognosy magazine* 2017, 13(Suppl 4):S875.

ISSN: 1737-9334

Parametric Investigation on the Performance of Flat Plate Solar Air Collector

Marwa Ammar[1], Ameni Mokni[2], Nahed Soussi[3], Hatem Mhiri[4]
[1] *ammarmriwa@gmail.com*
[1243]*Laboratory of Thermal and Thermodynamic of Industrial Processes, National School of Engineers of Monastir, road of Ouardanine, 5000 Monastir, Tunisia*

***Abstract*— The purpose of this new study is to examine potential improvements in the performance of flat plate solar air collector. An extensive parametric study is performed to optimize the collector design. A three dimensional CFD model of a flat plate solar air collector is developed and solved in steady-state conditions. We propose a suitable approach for assessing and optimizing a 1.28 m^2 surface collector's performance. We have then compared the performance of the different investigated structures. The new design presented in this study, deserves further exploitation as it seems to be a promising alternative for increasing thermal efficiency with a low cost and weight. It could be used in industrial and domestic applications.**

***Keywords*— FPC; Thermal Efficiency; Pump Power; Fins; TIM-PS**

I. INTRODUCTION

The concern for the sustainability of solar energy over time has led to persistent attempts to upgrade the capabilities of flat-plate solar air collectors. There is commonly one limitation associated with all solar air collectors; they exhibit a lower thermal efficiency than solar water collectors, which is related to the poor thermodynamic properties of air and the presence of a viscous sublayer near the hot wall Bopche and Tandale. [1]. The concept of boosting the heat transfer through artificial roughness was initiated nearly a century back Bhushan and Singh [2]. Chabane et al. [3] have elaborated experimentally a finned collector fitted with five longitudinal semi-cylindrical fins against the absorber. The greatest observed thermal efficiency was 51.5% for a finned collector with a solar heat flux of 480 W/m^2. Kumar et al. [4] and Kumara et al. [5] have investigated the several arrangements of blocking such as transverse perforated blocking, angular perforated blocking, solid V-blockage, V-blockage with gap and perforated V-blockage with gap and perforated V-blocks. The survey revealed that the perforated V-blockage has the best thermal-hydraulic performance than with the other blocking types. Fana et al. [6] have suggested a novel multi-channel V-block absorber implemented as part of a flat ventilation system. The daily average optical and thermal efficiency of the new and conventional absorber is about 84.9 - 69.4% and 69.1 - 58.6%. The authors showed that the V-absorber design could reduce the pressure drop and pumping power up to four times compared to the conventional absorber.

A second main obstacle concerns the convection losses from the front of the collector. Due to its confinement between plates of different temperatures, the air gap between the high temperature absorber and the transparent cover is subject to very large free convection movements. N. Benz et al [7] reported in their study that the natural convection phenomenon does not occur in the collector at a pressure below 5 kPa and that the amount of loss is lowered by 30% relative to atmospheric pressure. Thus, we can emphasize that maintaining the vacuum condition in the air space, confined between the transparent cover and the absorber plate, ensures the suppression of natural convection in this space. Nevertheless, the vacuum state in this space is not easy to maintain for a long period of time. There are several ways to minimize the convection losses of flat plate solar collectors. The internal convection can be reduced by the incorporation of convective barriers inside the air gap. Some tests for this method can be seen in F. Bava et al. [8], M. Jami et al. [9], and R. Garcia et al. [10]. From a practical and economic perspective, it is crucial that the device designed can deliver the desired hot air on demand and throughout the year, while ensuring savings on design and maintenance costs by using a 100% renewable source and excluding any auxiliary energy source.

Thus, the present work has been undertaken to numerically analyze several approaches aimed at optimizing the thermal performance of the collector. The impact of the inclusion of fins and the adoption of a selective absorber, as well as the incorporation of a structure of parallel vertical and inclined transparent insulation material (TIM-PS) slats inside the air gap have been analyzed simultaneously. To the best of the author's knowledge and based on the above literature survey, relatively few studies exist regarding the application of TIM slats to solar collectors. The innovation of this research lies in the comparison of a number of approaches regarding both the performance weight and cost in order to identify the most cost-effective and simple technique.

II. METHODOLOGY

A. SOLUTION DOMAIN

Our numerical investigation is based on a 3D model of a flat plate solar collector. In order to validate our numerical model, a first model

ISSN: 1737-9334

interprets the geometry of the solar collector experimentally studied by N.Moummi [11].
The collector surface is 1.6*0.8 m², with a transparent cover in polycarbonate of 0.01 m thickness, an absorber sheet made of cooper; once it is black-painted α=0.95 and ε =0.9, second it has a selective coating α=0.95 and ε =0.1

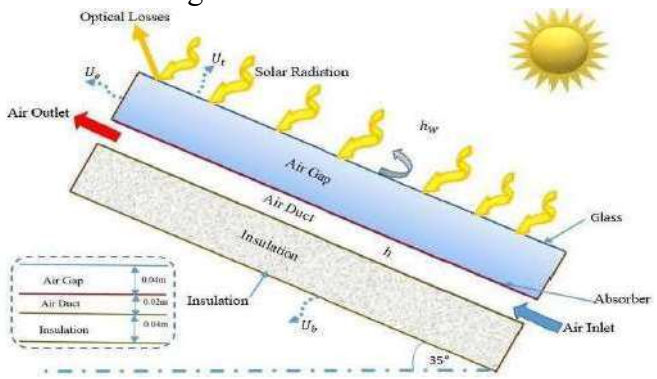

Fig.1 Structure of the FPC

B. Solution techniques

The numerical procedure chosen by the commercial code ANSYS FLUENT, for solving the Navier-Stokes equations, is based on the 'finite volume' method. In the software employed, the solver adopted is: three-dimensional 'Double-Precision', a 'serial' processing option is adopted to solve the problem. The data results are obtained from pressure-based segregation solver. The standard k-ε model was chosen as the computational procedure to close the system of the mean flow equation.

III. RESULTS AND DISCUSSIONS

A. Fins' Effect

Rectangular fins are as thin as the absorber and are about 0.4 mm thick, and were attached to the lower insulation plate. Fins' width is 50 mm; relative heights is e'/e=0.8. Eight fins are across the width of the collector. The interrupted fins mounted in staggered rows.

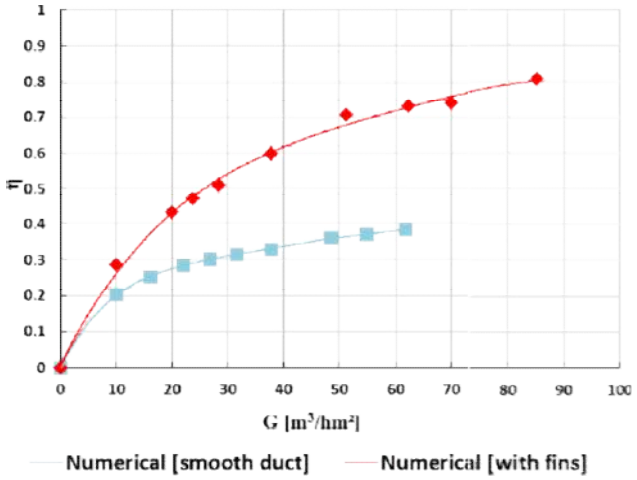

Fig. 2 Collector Efficiency of Smooth and Finned Duct Vs. The Air Volume Flow Rate at Φ=900 W/m².

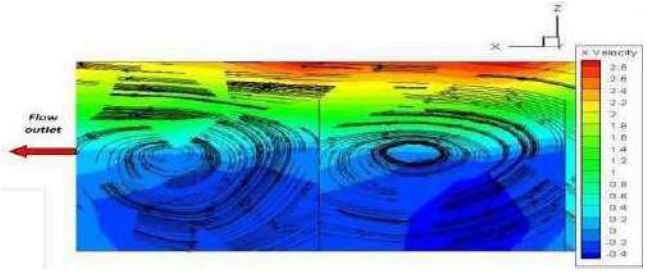

Fig.3 The velocity contours and streamlines for G = 51.28 m³/hm²

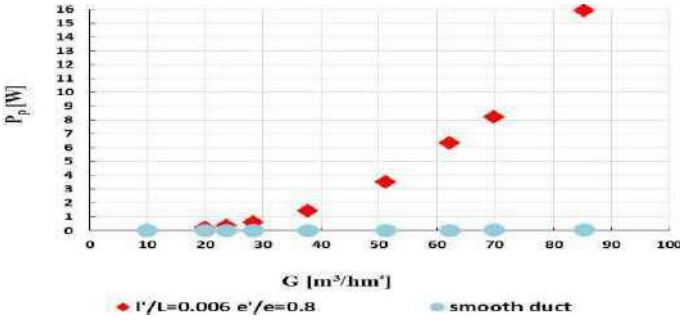

Fig.4 Pump Power Consumption

The improvement in heat transfer, due to the addition of rectangular fins, is obvious. The efficiency of the collector is shown in Fig.2; the results show that the efficiency is improved as the flow rate increases. The flow lines are drawn near the fins in Fig3; we can closely observe the complex flow pattern caused by the fins. We notice the formation of vortexes between the surfaces of the fins, which ensures the rolling action of the flow. The air flow deflects by 180° and creates a large separation vortex. The longer the fins, the more turbulent the flow and the thinner the laminar sub-layer; therefore, the heat transfer between the absorber and the air is greater. On the other hand, when the flow crosses a rough surface, it will be subjected to a frictional force due to the viscosity of the air and the presence of obstacles. This phenomenon is represented by the pressure drop (ΔP). The pressure drop in the air duct goes with the air volume flow rate; increasing the air flow rate induces a significant increase in friction loss. The frictional pressure drop is proportional to the square of the velocity. As a result, increasing pumping power occurs. The pumping work is shown in Fig.4; which compares the energy consumption of the pump for both cases. The energy consumption of the pump increases sharply with increasing volume flow. For the smooth duct manifold, the pump power consumption is up to 0.08 W, which is extremely low, while the pump power is up to 16 W for the collector with fins e'/e=0.8, the highest value.

This configuration containing 140 rows of fins have ameliorated the thermal performance to reach a value more than 80% but on the other hand, it leads to the

ISSN: 1737-9334

highest pump power. It is interesting to evaluate the minimizing of fins number.

B. Effect of Selective Absorber with Fins

As the impact of the radiant losses is more strictly linked to the absorber's optical properties, this part aim is to show how to boost the performance of the solar collector by optimizing the material's optical properties constituting the surface of its absorber.
For this part, we consider a highly selective absorber coating that exhibits optical properties as follows;
K= 380 W/mK, α=0.95 and =0.1.
The collector equipped with a selective absorber is more efficient than the one equipped with fins as long as the number of rows of fins remains lower than 140 rows (l'/L=0.006). To increase the efficiency of the collector with a minimum number of fins, without increasing the pumping power and the weight of the collector, we propose to use both a selective absorber and a low number of fins. The pumping power of the collector with a selective absorber and three rows of fins (l'/L=0.45) is insignificant compared to the pumping power for the collector with a non-selective absorber and 140 rows of fins (l'/L=0.006), the value does not exceed 0.05 W for the first type, but it reaches 16 w for the second type as shown in Fig.6.
Lower pumping power can extend the life of the pump as well as decrease the maintenance cost. The design of the selective absorber with three rows of fins has improved the thermal efficiency of the collector, and significantly reduces the pressure drop, pump power consumption, collector cost and collector weight compared to a collector with 140 rows of fins.

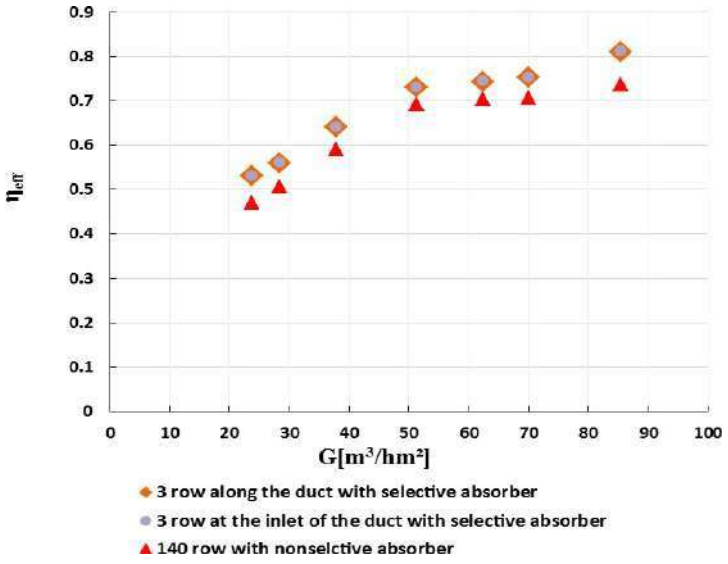

Fig.5 Comparison between Effective Efficiency

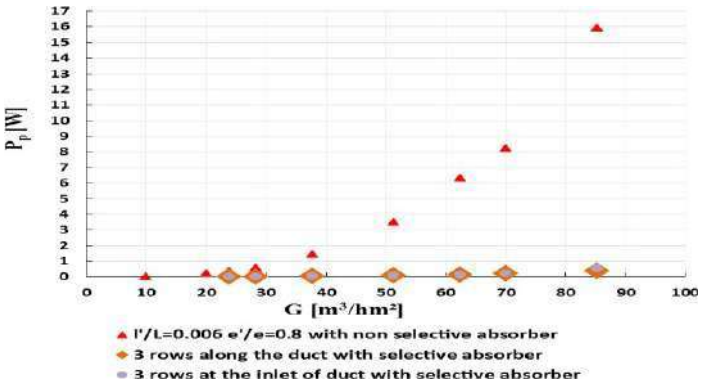

Fig. 6 Pump Power Consumption

C. Effect of Selective Absorber with TIM-PS

In order to take advantage of both the limitation of radiative losses by using a selective coating on the absorber plate (α=0.95, ε=0.1) and the limitation of convective losses by the use of parallel slats made of transparent insulating material (TIM-PS), we show a design with a selective absorber and TIM slats in the air gap attached to the transparent cover (Fig.7). These parallel slats are transparent to the solar radiation and have a thickness of 1 mm (Table 1), attached to the transparent cover and positioned so that they do not touch the absorber plate. We tested the model of collector with 1, 2, 3, 4 and 5 TIM-PS; the collector "without TIM-PS" is used as a reference model.

ISSN: 1737-9334

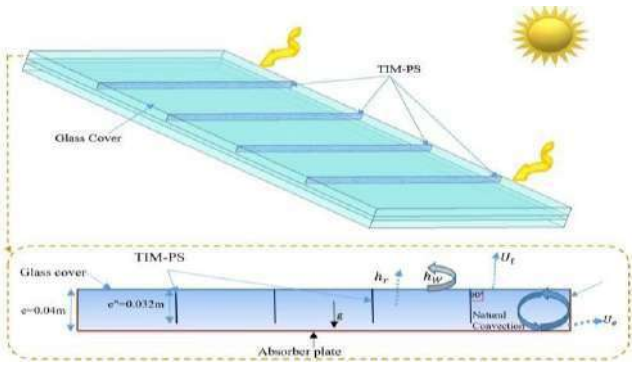

Fig. 7 Structure of the FPC with Vertical TIM-PS

TABLE 1 GEOMETRICAL CHARACTERISTICS OF THE TIM-PS

Parameters	Value
Width	0.8m
Thickness	1 mm
Relative Height e"/e	0.8
Material	PMMA

Fig.8 shows that with the increase of the air flow rate, the efficiencies of the collector increase. For the same air flow rate of 85.33 m^3/hm^2, the collector efficiency is 78, 76.7, 76.4, 75.2, 74.4 and 71% for the 4, 5, 3, 2, 1 slat and reference collector respectively. The efficiency of the collector increases with the TIM-PS number up to an optimal TIM-PS number of 4; beyond this number, the efficiency decreases with the number of TIM-PS. Increasing the number of TIM-PS allows a significant reduction of the convective transfer. By including the vertical TIM-PS within the air cavity, the flow structure was drastically modified, especially in the region near the top cold wall. The first reflex of the TIM-PS was to block the air flow, forcing the horizontal boundary layer flow along the top wall to separate from the transparent cover. The fluid circulation's take place in a thin layer in proximity to the absorber plate and the slats corners. The air circulating in the neighbourhood of the hot wall is then less cooled. Besides that, maintaining a gap between the TIM-PS and the selective absorber can minimize the coupling between conduction and radiation. Parallel transparent slats offer the possibility to improve the performance of the collector. They can reduce heat loss by providing high thermal resistance while transmitting solar energy efficiently, and on the other hand the addition of slats in the air gap does not affect the pressure drop, it does not increase the friction factor. The use of TIM-PS does not require additional pumping power.

The application of transparent parallel slats not only provides good insulation, but also affects the convective flow within the confined air space between the absorber plate and the transparent cover.

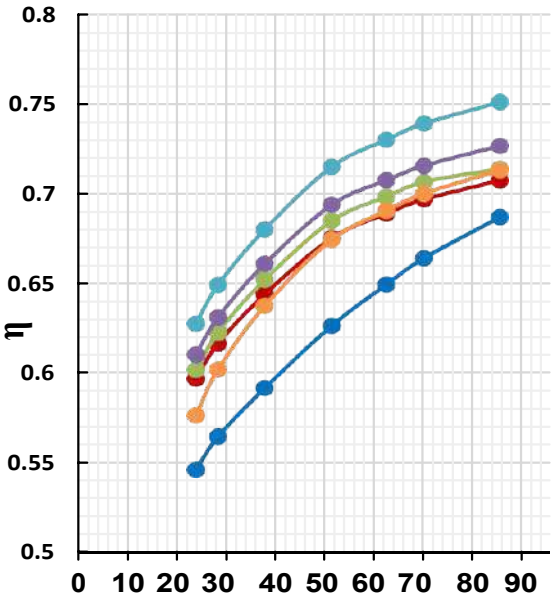

Fig. 8 Thermal Efficiency for Different TIM-PS Number

D. Effect of Slat Tilt Angle

In this part, we propose to study the effect of the tilting of the TIM-PS in the air gap (Fig.9). The novelty presented in this work lies in the fact that inclined slats are attached in the air gap, and that such a design of the solar air collector has not been studied before.

Fig.10 reveals that both of these +/-45 tilted slats provide an increase in collector performance, although it is clearly distinguishable that the improvement provided by the -45° tilted slats is significantly more significant than that achieved by the +45° tilted slats. The highest performance of the collector is achieved by the collector with twelve TIM-PS inclined at a negative angle (-45°). Thus TIM-PS inclined by +/-45° significantly affects the flow inside the air gap, therefore the

ISSN: 1737-9334

temperature fields, and thus the collector's performance. It is also worth noting that, TIM-PS inclined by -45° alters the air flow more than other positions of slats. In fact, when the TIM-PS is tilted by -45°, the unicellular structure of the airflow is dissociated thanks to the orientation of the -45° TIM-PS of many small cells with tilted shapes. The increase in the number of TIM-PS inclined by -45°, consequently increases the number of small cells, and thus decreases the rate of heat transfer between the hot and cold walls. For the optimization of the performance of the solar air collector, it is primordial to select the adequate inclination of the collector.

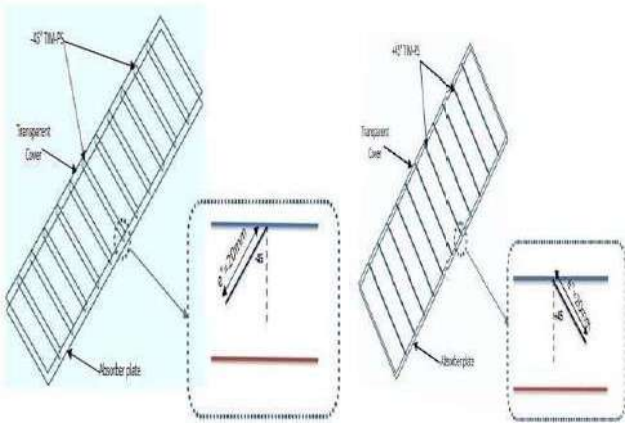

Fig.9 Configuration of Inclined Slats Sandwiched Between Absorber Plate and Transparent Cover

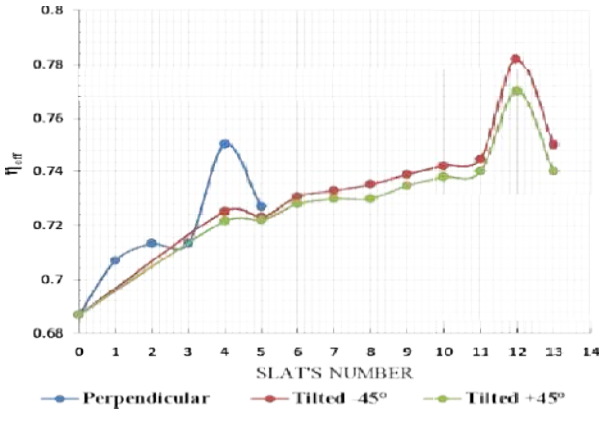

Fig.10 Effective Efficiency for Different TIM-PS Number and Tilted Angle, G=85.33 m³/hm²

E. Optimum Collector's Design

The most promising collector must achieve the best thermal efficiency and fill out high requirements of low weight, low pumping consumption, ease of manufacturing, and low cost. Optimized flat plate solar air collector modelled with a selective absorber and three rows of rectangular fins installed beneath the structure provides 81% of thermal efficiency. This collector's configuration provides a high efficiency but it can produce of friction factor then a pump power. The innovative facade collector including tilted TIM-PS can achieve a thermal efficiency around 80% with keeping the lightweight of the collector and the low cost, and without any increase in the friction factor and the pump power. Hence considering the factors of; the low pump power consumption, the low collector weight, the simplest geometry and low cost, the optimal design for solar air collector with tilted TIM-PS of e ′ /e= 0.8 corresponds to the optimal design. This CFD survey yielded the highest optimized and most cost-effective and simple to manufacture configuration for an air collector, its importance has been increased by the recent intensification of attempts to maximize the profitability of solar energy. This optimized configuration could be used in industrial and domestic applications. The new design of the TIM-PS inclined at an angle of -45◦ integrated collector, is the most suitable design, characterized by its high performance, for the usein agriculture sector for drying.

IV. Conclusions

One of the great challenges in designing a solar air collector is selecting of the suitable parameters of the collector components to achieve the best performance while keeping the lowest cost possible. In this paper, a parametric study of enhancement of collector's performance is illustrated. The new design of FPC including tilted TIM-PS is recommended to be used in industrial agriculture drying, as it seems to be a promising alternative for increasing thermal efficiency with a low cost. The results obtained in this work demonstrate the success of air heating system mode with TIM-PS.

Acknowledgment

The authors declare that they have no known competing financial interests or personal relationships that could have appeared to influence

ISSN: 1737-9334

REFERENCES

[1] Bopche, Santosh B., Tandale, Madhukar S., 2009. Experimental investigations on heat transfer and frictional characteristics of a turbulator roughened solar air heater duct. Int. J. Heat Mass Transfer 52,2834–2848. http://dx.doi.org/10.1016/j.ijheatmasstransfer.2008.09.039.

[2] Bhushan, Brij, Singh, Ranjit, 2010. A review on methodology of artificial roughness used in duct of solar air heaters. Energy 35, 202–212. http://dx.doi.org/ 10.1016/j.energy.2009.09.010.

[3] Chabane, Foued, Moummi, Noureddine, Benramache, Said, 2014. Experimental study of heat transfer and thermal performance with longitudinal fins of solar air heater. J. Adv. Res. 5, 183–192. http://dx.doi.org/10.1016/j.jare.2013.03.001.

[4] Kumar, Raj, Sethi, Muneesh, Chauhan, Ranchan, Kumar, Anil, 2017. Experimental study of enhancement of heat transfer and pressure drop in a solar air channel with discretized broken V-pattern baffle. Renew. Energy 101, 856e872. http://dx.doi.org/10.1016/j.renene.2016.09.033.

[5] Kumara, Raj, Kumara, Anil, Chauhana, Ranchan, Maithanib, Rajesh, 2018. Comparativestudy of effect of various blockage arrangements on thermal hydraulic performance in a roughened air passage. Renew. Sustain. Energy Rev. 81, http://dx.doi.org/10.1016/j.rser.2017.08.023, 447–46.

[6] Fana, Man, Youa, Shijun, Gaoa, Xinlei, Zhanga, Huan, Lic, Bojia, Zhenga, Wandong, Suna, Leizhai, Zhoua, Tingting, 2019. A comparative study on the performance of liquid flat-plate solar collector with a new V-corrugated absorber. Energy Convers. Manage. 184, 235–248. http://dx.doi.org/10.1016/j.enconman.2019.01.044.

[7] N. Benz, T. Beikircher, High efficiency evacuated flat-plate solar collector for process steam production, Solar Energy Vol. 65, No. 2, pp. 111–118, 1999, PI I:S0038 – 092X (98)00122 – 4.

[8] Bava F, Furbo S, Perers B. Simulation of a solar collector array consisting of two types of solar collectors, with and without convection barrier. International Conference on Solar Heating and Cooling for Buildings and Industry, SHC. 2014.

[9] Jamia M, Mezrhaba A, Ahmed, Bouzidib M'hamed, Lallemand Pierre. Lattice-Boltzmann computation of natural convection in a partitioned enclosure with inclined partitions attached to its hot wall. Phys A 2006;368:481–94. https://doiorg/10.1016/j.physa.2005.12.029.

[10] Paiva Garciaa Rafael, del Rio Oliveirab Santiago, Luiz Scalonb Vicente. Thermal efficiency experimental evaluation of solar flat plate collectors when introducing convective barriers. Sol Energy 2019;182:278–85. https://doi.org/10.1016/j.solener.2019.02.048.

[11] N. Moummi, S. Youcef-Ali, A. Moummi, J.Y. Desmons, Energy analysis of a solar air collectorwithrows of fins, Renewable Energy 29 (2004) 2053–2064, doi:10.1016/j.renene.2003.11.006.) 5, 183 19.

ISSN: 1737-9334

Modelling and Control of Wastewater Treatment Systems: Case of Activated Sludge Processes

Saïda Dhouibi[1], Raja Jarray[1,2], Soufiene Bouallègue[1,2]

[1]: *Research Laboratory in Automatic Control (LARA), National Engineering School of Tunis, University of Tunis El Manar, Tunis, Tunisia*
[2]: *High Institute of Industrial Systems of Gabès, University of Gabès, Zrig, 6072 Gabès, Tunisia*

Email: dhouibi.saida@yahoo.com
Email: raja.jarray@enit.utm.tn
Email: soufiene.bouallegue@issig.rnu.tn

***Abstract*— Wastewater Treatment Systems become a necessity around the world because of their crucial role to protect the environment and the human health. In this work, a Model Predictive Control (MPC) strategy of an Activated Sludge Process (ASP) based on the Takagi-Sugeno (TS) fuzzy modelling approach is proposed and successfully applied. A quasi-Linear Parameter-Varying (LPV) representation of such a wastewater treatment plant is established to build the corresponding TS fuzzy model by the use of a convex polytopic transformation. Such a global TS fuzzy model structure of the studied ASP is then used for the design of nonlinear MPC laws for the ASP's dynamics, i.e. effluent volume, concentrations of heterotrophic biomass, biodegradable substrate and dissolved oxygen. Demonstrative results and comparisons show the effectiveness and superiority of the proposed fuzzy MPC approach**

***Keywords*—Wastewater treatment systems, activated sludge bioreactor, Takagi-Sugeno fuzzy modelling, model predictive control, carbon removal.**

I. INTRODUCTION

In a natural environment, polluted and waste waters have a serious impact on both human health and ecosystems [1–5]. As these waters are rich in hazardous components like carbon, nitrogen and phosphorus, new treatment technologies are proposed to best reduce the content of these hazardous substances and therefore protect the environment from their adverse effects. Biological treatment through activated sludge purification processes currently represents the effective technology in the field of wastewater recycling [1,3,4]. In activated sludge processes, a suspension of bacterial biomass is responsible for the removal of pollutants.

Recently, many control approaches have been proposed in the literature for the activated sludge purification processes. As complex and high coupled systems, modeling and control of biochemical processes remain a difficult and tedious task because of the frequent changes of quality and flow rate of the load as well as the presence of complex biological phenomena intervening. The regulation of these plants requires advanced theories to achieve the desired purification performances [6–20]. In [6], a Parallel Distributed Compensation (PDC) technique has been designed for an activated sludge process in the case of carbon removal. The concept of Linear Matrices Inequalities (LMI) and pole-placement are used. In [7], a PI-based control of the dissolved oxygen in wastewater treatment plants has been investigated for the nitrogen removal. In [8], the same problem, i.e. dissolved oxygen control, is handled using a neural network-based adaptive PID algorithm. Authors in [9] proposed optimal control strategies using an economic-oriented model predictive dynamic. In [10], an intelligent control approach based on the multi-objective optimization has been proposed to minimize the operating cost of nitrogen. In [11], a robust H∞ state-space fuzzy parallel distributed compensation approach for a biological wastewater system described by a fuzzy Takagi-Sugeno model has been presented and applied. In [12], a fuzzy controller is designed to monitor the effluent quality and operational cost in a wastewater plant. In [13–15], various model predictive control strategies have been applied for the activated sludge processes. Other various control techniques and approaches have been studied and proposed in the literature for such family of wastewater treatment systems [16–20]. Through all this literature works' citation, one can observe that the use of the classical and most common nonlinear control techniques still difficult in terms of design and implementation. In many scenarios, these nonlinear approaches are non systematic and require prohibitive design time and resources. In recent years, intelligent and non conventional control techniques, particularly those based on the concepts of fuzzy logic control, have been emerged as a promising solution both for modeling and control design of these biochemical systems.

Based on these aforementioned observations and ideas, the use of Takagi-Sugeno fuzzy formalism presents a promising alternative for modeling and control design of such complex purification processes [21,22]. Such a logic fuzzy technique of modeling, using a given nonlinear model of standard activated sludge plants, allows the design of various efficient linear control strategies, e.g. proportional-integral-Derivative (PID), parallel distributed compensation (PDC), robust H∞ design, and particularly model predictive control (MPC). The main steps of such an advanced control design methodology are essentially based on the rewriting of the nonlinear model in a quasi-LPV form and the transformation of such a state-space representation within a global linear and time-invariant form thanks to the well-known convex polytopic transformation [21]. The operation of the nonlinear system is then described in different parts of the state-space using local stationary linear sub-models. The premise variables are partitioned in order to build all weighting functions and constant matrix of the state-space representation that is equivalent to the initial nonlinear system [21,22].

ISSN: 1737-9334

In this paper, a TS fuzzy model of activated sludge plants is established from a given standard nonlinear benchmark, i.e. Activated Sludge Model N°1 (ASM1) [23]. The modeling procedure is described and the obtained TS fuzzy model is then used to design advanced nonlinear MPC laws for biological variables involved in the case of carbon removal, i.e. the effluent volume and the concentrations of heterotrophic biomass, biodegradable substrate and dissolved oxygen. Demonstrative results are carried out and discussed. The remainder of this paper is organized as follows. In Section II, a TS fuzzy model of the studied activated sludge process is computed. In Section III, a fuzzy model predictive control strategy is designed. The effective parameters of such a control approach are selected and tuned thanks to a trials-and-errors-based iterative technique. In Section IV, numerical simulations are carried out to show the effectiveness and validity of the proposed TS fuzzy approach. Section V gives the conclusions of the paper.

II. Takagi-Sugeno Fuzzy Modelling of the Process

A. Activated Sludge Process Description

An activated sludge process for wastewaters purification is a biochemical system made up of a bioreactor, a clarifier, and a pipe for the sludge recycling process, see Fig. 1. Following a pre-treatment phase, the input wastewater circulates in the aeration tank in which the bacterial biomass degrades the organic polluting matter, i.e. carbon, nitrogen and others. In such a chemical reaction, the microorganisms agglomerate in flocks and produce sludge. The mixed liquor from the effluent is then sent to the decanter where the separation of the purified water and the bacterial flocks is done by gravity. A fraction of the settled sludge is recycled to the aerator to maintain its purification capacity.

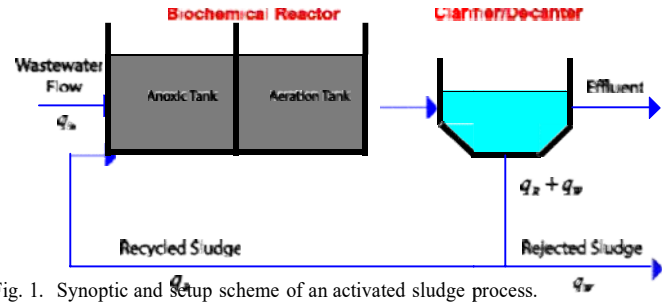

Fig. 1. Synoptic and setup scheme of an activated sludge process.

In the case of carbon removal, a reduced ASM1 form can be considered to describe the entire nonlinear dynamics of the activated sludge plant, i.e. effluent's volume, concentrations of heterotrophic biomass, biodegradable substrate and dissolved oxygen [6,22,23]. In this work, it is assumed that the purified water does not contain particulate substances and the concentrations of the soluble components are the same at the decanted inlet and outlet. Therefore, the following expressions are retained [6,22,23]:

$$\left(q_{in}(t)+q_R(t)\right)X_{BH}(t)=\left(q_R(t)+q_w(t)\right)X_{BH,R} \quad (1)$$

$$S_{S,R}(t)=S_S(t) \quad (2)$$

where X_{BH} and S_S are the heterotrophic biomass and biodegradable substrate concentrations, respectively, q_{in} , q_R and q_w are the effluent inlet, recycling and extraction flow rates, respectively.

As additional modeling hypothesis, the effluent's recycling and extraction flow rates represent fractions of the total inlet flow rate and can be defined as follows:

$$q_R(t)=f_R q_{in}(t), \quad 1\le f_R\le 2 \quad (3)$$

$$q_W(t)=f_W q_{in}(t), \quad 0<f_W<1 \quad (4)$$

Based on the homogeneity property of such a biochemical process, the output concentrations of heterotrophic biomass, biodegradable substrate and dissolved oxygen can be written as follows [6,22,23]:

$$X_{BH,out}=X_{BH}, S_{S,out}=S_S, S_{O,out}=S_O \quad (5)$$

On the other hand, the concentration of dissolved oxygen is assumed to be zero at the inlet of the bioreactor, i.e. $S_{O,in}=0$ .It is also assumed that the activated sludge process operates at a variable volume of the effluent described by the following law:

$$q_{out}=(1+f_R)q_{in}-\alpha_1(V_{ref}-V) \quad (6)$$

where $\alpha_1\in\mathbb{R}_+$ denotes the gain of a proportional regulation and V_{ref} presents the reference volume.

Based on all the aforementioned hypotheses, a reduced nonlinear model of the activated sludge process is derived in the case of carbon removal as follows:

$$\begin{cases}\dot{V}=\alpha_1(V_{ref}-V)\\ \dot{X}_{BH}=\frac{q_{in}}{V}X_{BH,in}-\frac{q_{in}(1+f_R)-f_W}{V}X_{BH}+\mu_H\frac{S_S}{K_S+S_S}\frac{S_O}{K_{OH}+S_O}X_{BH}-b_H X_{BH}\\ \dot{S}_S=\frac{q_{in}}{V}S_{S,in}-\frac{q_{in}}{V}S_S-\frac{1}{Y_H}\mu_H\frac{S_S}{K_S+S_S}\frac{S_O}{K_{OH}+S_O}X_{BH}\\ \qquad\quad +(1-f)b_H X_{BH}\\ \dot{S}_O=\frac{q_{in}}{V}S_{O,in}-\frac{1-Y_H}{Y_H}\mu_H\frac{S_S}{K_S+S_S}\frac{S_O}{K_{OH}+S_O}X_{BH}\\ \qquad\quad +\alpha_2 q_a(S_{O,sat}-S_O)\end{cases} \quad (7)$$

B. Takagi-Sugeno Fuzzy Modelling

Based on the above nonlinear model of the studied ASP, an equivalent quasi-LPV state-space representation is defined as follows [6,21,22]:

$$\begin{cases}\dot{X}(t)=\boldsymbol{A}(\theta(X,u))X(t)+\boldsymbol{B}(\theta(X,u))u(t)\\ y(t)=\boldsymbol{C}(\theta(X,u))X(t)\end{cases} \quad (8)$$

where $\rho(X,u) \in C^1(\mathbb{R}^n \times \mathbb{R}^m)$ is the vector of variable parameters, $X \in \mathbb{R}^n$ and $u \in \mathbb{R}^m$ are the state and input vectors, $A(\rho(X,u))$ and $B(\rho(X,u))$ denote the parameters-varying state and input matrices expressed as:

$$A(\rho(X,u)) = \begin{bmatrix} a_{1,1} & 0 & 0 & 0 \\ 0 & a_{2,2} & a_{3,2} & 0 \\ 0 & a_{4,2} & 0 & a_{4,4} \\ 0 & 0 & 0 & b_{4,4} \end{bmatrix} \quad (9)$$

$$B(\rho(X,u)) = \begin{bmatrix} b_{1,1} & 0 & 0 & 0 \\ 0 & b_{2,2} & b_{3,2} & 0 \\ 0 & 0 & b_{4,3} & 0 \end{bmatrix} \quad (10)$$

where:

$$\begin{aligned} a_{1,1} &= \rho_1, a_{2,2} = \rho_2 z_2 f_W (1+f_R) z_2 - b_H \\ a_{3,2} &= \rho_3 Y_H z_1 + (1-f_H) b_{H,a} z_2 = \rho_3 z_1 \\ a_{4,2} &= -Y_H \rho_4 z_1, a_{4,4} = \rho_4 z_3 \\ b_{1,4} &= \rho_5 b_{1,1} = b_{2,1} = b_{3,2} = z_2, b_{4,3} = z_{O,sat} \end{aligned} \quad (11)$$

From equations (9) and (10) that given the non-constant state-space matrices, three premise variables can be defined as follows:

$$z_1(\rho(X,u)) = \frac{S_S(t)}{K_S + S_S(t)} \frac{S_O(t)}{K_{OH} + S_O(t)} \quad (12)$$

$$z_2(\rho(X,u)) = \frac{q_{in}(t)}{V(t)} \quad (13)$$

$$z_3(\rho(X,u)) = q_a(t) \quad (14)$$

By using the convex polytopic transformation [21], these premise variables are partitioned as follows:

$$\begin{aligned} \rho_1(\rho(X,u)) &= z_1 F_1^1(z_1(t)) + z_1 F_2^1(z_1(t)) \\ \rho_2(\rho(X,u)) &= z_2 F_1^2(z_2(t)) + z_2 F_2^2(z_2(t)) \\ \rho_3(\rho(X,u)) &= z_3 F_1^3(z_3(t)) + z_3 F_2^3(z_3(t)) \end{aligned} \quad (15)$$

where: $z_{i\_} = \max\{z_i(X,u)\}; z_{i\_} = \min\{z_i(X,u)\}$ (16)

$$\begin{aligned} F_1^1(z_1(t)) &= \frac{z_1 - z_{1\_}}{z_{1\_} - z_{1\_}}; F_2^1(z_1(t)) = \frac{z_1 - z_{1\_}}{z_{1\_} - z_{1\_}} \\ F_1^2(z_2(t)) &= \frac{z_2 - z_{2\_}}{z_{2\_} - z_{2\_}}; F_2^2(z_2(t)) = \frac{z_2 - z_{2\_}}{z_{2\_} - z_{2\_}} \\ F_1^3(z_3(t)) &= \frac{z_3 - z_{3\_}}{z_{3\_} - z_{3\_}}; F_2^3(z_3(t)) = \frac{z_3 - z_{3\_}}{z_{3\_} - z_{3\_}} \end{aligned} \quad (17)$$

By making all the possible combinations of these premise variables, the defuzzification leads to the following global TS fuzzy model for the activated sludge process (7):

$$\dot{X}(t) = \sum_{i=1}^{8} \rho_i(z(t)) \{A_i X(t) + B_i u(t)\} \quad (18)$$

where the state-space matrices $A_i \in \mathbb{R}^{4\times4}$ and $B_i \in \mathbb{R}^{4\times4}$ are computed from (9)-(10) and (16), and the activation functions are given as follows:

$$\begin{aligned} \rho_1(X,u) &= F_1^1(S_S, S_O) F_1^2(V, q_{in}) F_1^3(q_a) \\ \rho_2(X,u) &= F_1^1(S_S, S_O) F_1^2(V, q_{in}) F_2^3(q_a) \\ \rho_3(X,u) &= F_1^1(S_S, S_O) F_2^2(V, q_{in}) F_1^3(q_a) \\ \rho_4(X,u) &= F_1^1(S_S, S_O) F_2^2(V, q_{in}) F_2^3(q_a) \\ \rho_5(X,u) &= F_2^1(S_S, S_O) F_1^2(V, q_{in}) F_1^3(q_a) \\ \rho_6(X,u) &= F_2^1(S_S, S_O) F_1^2(V, q_{in}) F_2^3(q_a) \\ \rho_7(X,u) &= F_2^1(S_S, S_O) F_2^2(V, q_{in}) F_1^3(q_a) \\ \rho_8(X,u) &= F_2^1(S_S, S_O) F_2^2(V, q_{in}) F_2^3(q_a) \end{aligned} \quad (19)$$

III. MODEL PREDICTIVE CONTROL DESIGN

A. Basic Concepts

As an advanced control approach, the MPC technique aims to compute a sequence of control laws where only the first element is applied to the process [13–15,24–27]. Such a control sequence is updated at each sampling time, i.e. $t = kT_s$, to minimize the following quadratic cost function:

$$\begin{aligned} J(t) = &\sum_{i=1}^{N_p} e^T(t+i \mid k) Q e(t+i \mid t) \\ &+ \sum_{i=0}^{N_c-1} \Delta u^T(t+i \mid t) R \Delta u(t+i \mid t) \end{aligned} \quad (20)$$

where $N_p \in \mathbb{N}$ and $N_c \in \mathbb{N}$ are the prediction and control horizons, respectively, $Q = Q^T > 0$ and $R = R^T > 0$ denote the weighting matrices of the MPC laws, $e(t+i \mid t)$ denotes the error between the set-point reference and system predicted outputs at the time $t+i$ given all measurements up to and including those at the sampling-time t.

In MPC framework, the main effective control parameters are the prediction/control horizons, and weighting coefficients often selected by repetitive and trials-errors-based procedures.

B. TS Fuzzy-based Model Predictive Control

To stabilize the biochemical dynamics of the studied ASP around their set-point values, a MPC control strategy is carried out based on the established TS fuzzy model. The equivalence between the two nonlinear and TS fuzzy model is exploited to apply with high efficiency the designed MPC laws for the real wastewater process as shown in Fig. 2. The designed fuzzy controllers share the same fuzzy sets with the fuzzy model in the premise parts. The defuzzification of the overall MPC laws is carried out as follows:

ISSN: 1737-9334

$$u_{MPC}(t) = \sum_{i=1}^{8} \mu_i(z(t))\, u_{MPC,i}(t) \quad (21)$$

where $u_{MPC,i}$, $i \in \{V, X_{BH}, S_S, S_O\}$, is the local fuzzy MPC law designed for the corresponding local sub-models.

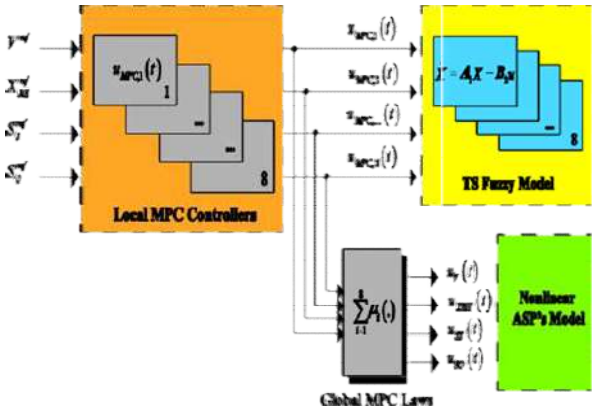

Fig. 2. Block diagram of the proposed TS fuzzy-based MPC strategy.

IV. Simulations Results and Discussion

To show the effectiveness of TS fuzzy modeling and MPC approaches, numerical simulations are carried out under MATLB/Simulink environment. The parameters of the studied wastewater plant are summarized in Table I. Input evolution profiles are chosen for effluent volume and concentrations of heterotrophic biomass, biodegradable substrate and dissolved oxygen dynamics. Modeling results allowing comparing the behaviors of the wastewater dynamics either while considering the nonlinear model and the equivalent TS fuzzy one.

TABLE I
Numerical values for the ASP's parameters

Param.	Designation	Values
K_S	Half-saturation coefficient of substrate	20g/m^3
K_{OH}	Oxygen half-saturation coefficient	g/m^3
$S_{O,Sat}$	Oxygen saturation concentration	10 g/m^3
α_1	Volume regulation gain	0.01
α_2	Oxygen regulation gain	2.3m^{-3}
b_H	Heterotrophic biomass mortality rate	0.4
μ_H	Heterotrophic biomass growth rate	3.733
Y_H	Substrate/heterotrophic conversion rate	0.6
f	Biomass fraction of products	0.1
f_R	Fraction rate of the recycling flow rate	1.1
f_W	Fraction rate of the extraction flow rate	0.03

A. TS Fuzzy Model Comparison and Validation

Numerical simulations lead to the time-domain responses of Fig. 3 to 6. Such responses of the nonlinear dynamics are compared with each other by considering the TS fuzzy and nonlinear models.

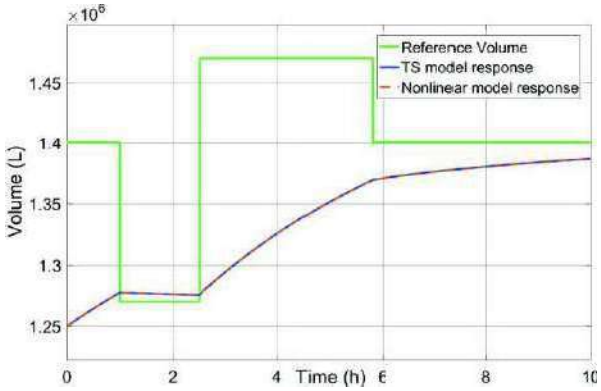

Fig. 3. Transient responses of the effluent volume dynamics.

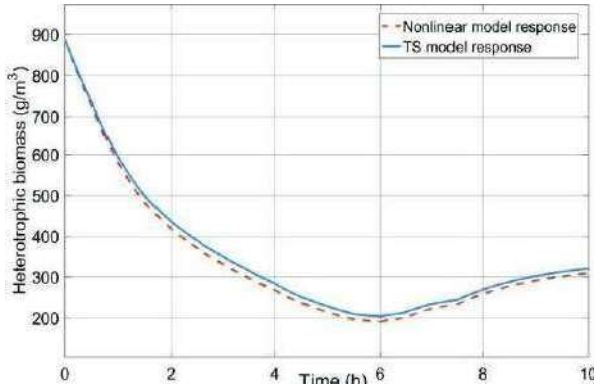

Fig. 4. Transient responses of the heterotrophic biomass concentration .

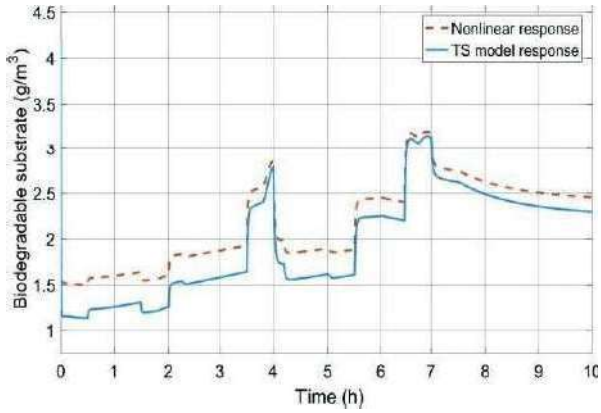

Fig. 5. Transient responses of the biodegradable substrate concentration.

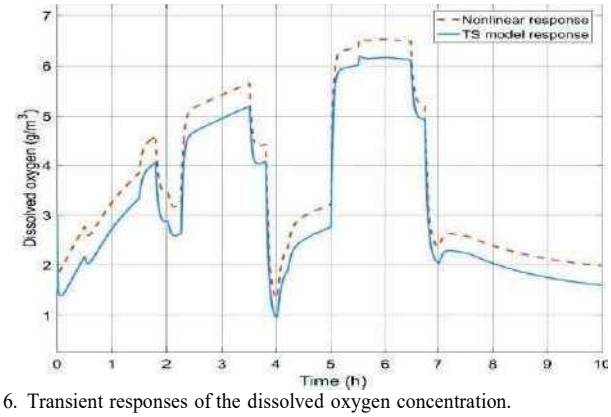

Fig. 6. Transient responses of the dissolved oxygen concentration.

ISSN: 1737-9334

The time-domain behaviors of the wastewater system's dynamics, by separately considering the initial nonlinear model and the computed TS fuzzy one, are displayed and compared. Looking at these demonstrative modeling results, one can observe that the effluent input flow rate clearly influences the three concentrations of the bioreactor in the case of carbon removal, namely the heterotrophic biomass, the biodegradable substrate and the dissolved oxygen. Simulation results show the resemblance between these two kinds of dynamic responses, i.e. evolutions of the concentrations and effluent volume are close to each other however with minor differences noted. So, one can conclude that the computed TS fuzzy model succeeds in reproducing with satisfied precision the dynamical nonlinear behavior of the studied biological wastewater process, i.e. the activated sludge plant. To more compare and quantify the resemblance of obtained modeling results, the behavior of the wastewater dynamics is evaluated and analyzed using the well-known Variance Accounted For (VAF) metric defined as follows:

$$VAF_i = \left(1 - \frac{\mathrm{var}(y_{NL} - y_{TS})}{\mathrm{var}(y_{NL})}\right) 100\ \% \quad (22)$$

where y_{NL} and y_{TS} denote the outputs of the nonlinear and TS fuzzy models, respectively, var $(.)$ is the mathematical variance function and $i \in \{V, X_{BH}, S_S, S_O\}$.

VAF (%) metrics' variations are shown in Fig. 7 for all modeled ASP's dynamics. The steady-state values for such a modeling metric further justify the modeling performance. As shown, VAF indices around 99% for the effluent's volume, 99.95% for the heterotrophic biomass concentration, 78% and 97% for the concentrations of biodegradable substrate and dissolved, respectively, are obtained and guaranteed with the proposed TS fuzzy modeling strategy.

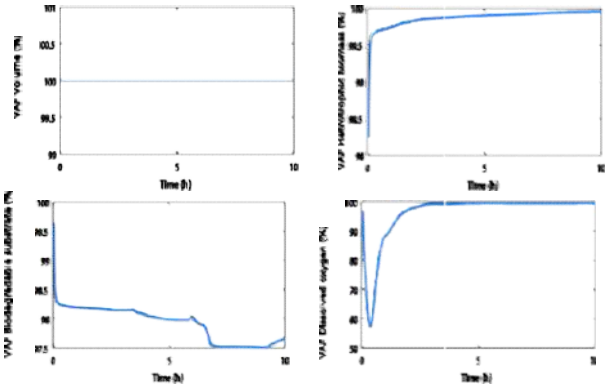

Fig. 7. VAF (%) metrics' variations of the modeled wastewater dynamics.

B. TS Fuzzy MPC Implementation

A trials-errors-based design procedure is investigated to tune the effective parameters of MPC algorithms, i.e. horizons of control and prediction, and weighting coefficients. The closed-loop responses are presented and compared in Fig. 8 to Fig. 11. Several prototyping trials have been carried out with different values of the design MPC parameters.

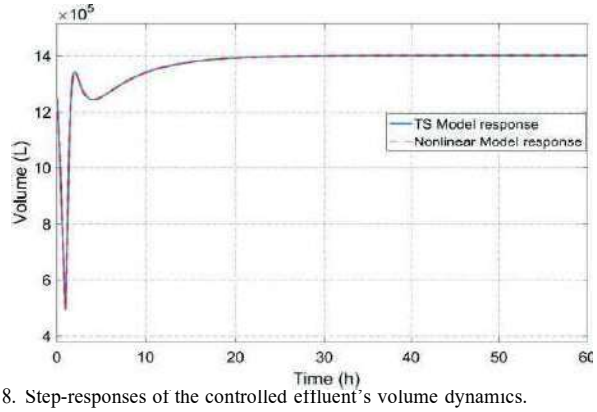

Fig. 8. Step-responses of the controlled effluent's volume dynamics.

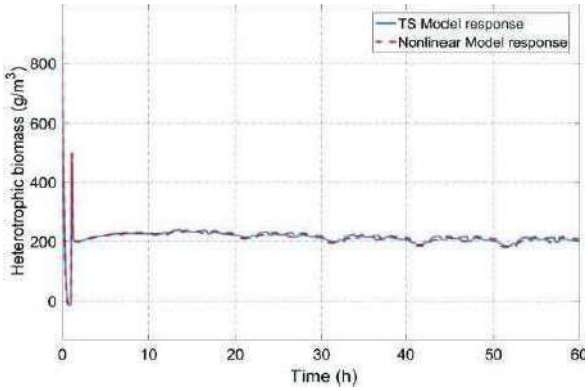

Fig. 9. Step-responses of the controlled heterotrophic biomass dynamics.

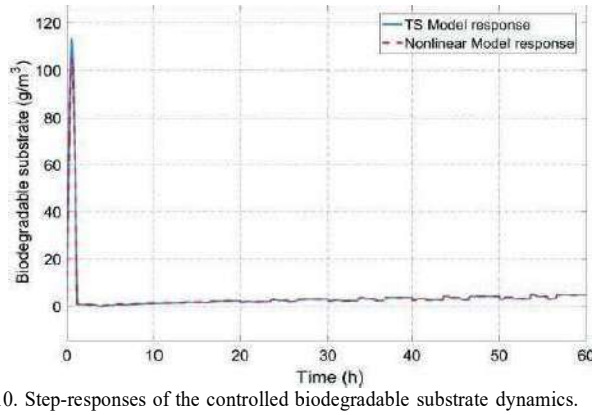

Fig. 10. Step-responses of the controlled biodegradable substrate dynamics.

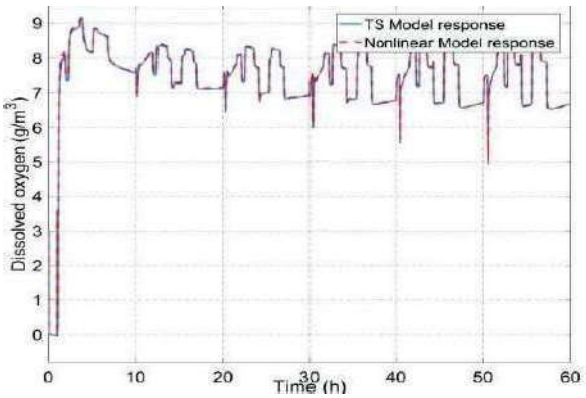

Fig. 11. Step-responses of the controlled dissolved oxygen dynamics.

ISSN: 1737-9334

Looking at these demonstrative results, one can conclude that the control performances in terms of stabilization around the set-point values are satisfied and significantly influenced by the choice of the effective MPC's parameters. Transient responses with small steady-state errors and damped behaviors are obtained for the dynamics of effluent's volume and biochemical concentrations. Steady-state performances are acceptable but still perfectible in terms of precision and robustness. The use of more sophisticated tuning techniques of MPC design presents a serious challenge. The resemblance between the nonlinear and TS fuzzy-based responses can validate the proposed fuzzy modeling and control approach of wastewater processes.

V. CONCLUSIONS

In this work, a Takagi-Sugeno fuzzy-based approach is proposed and successfully applied for modeling and control of an activated sludge process type of wastewater systems. In a carbon removal case, nonlinear dynamics of the process, i.e. effluent volume and concentrations of heterotrophic biomass, biodegradable substrate and dissolved oxygen, are stabilized in closed-loop around the imposed set-point values thanks to a proposed TS fuzzy-based MPC strategy. From a reduced nonlinear model of the standard ASM1 benchmark, an equivalent TS fuzzy state-space representation is computed and explored in the MPC design phase. While adopting a classical trials-errors-based design procedure, all effective MPC parameters for all TS fuzzy local sub-models are selected. Numerical simulations are carried out and demonstrative results are presented and discussed. These results are satisfactory and can be further improved in our future works. The closed-loop responses of the controlled process show the equivalence of the modeling representations. All results and comparisons prove the effectiveness of the proposed TS fuzzy approach for the wastewater processes.

REFERENCES

[1] Lefebvre, B. (Ed.). The activated Sludge Process: Methods and recent developments, Nova Science Publishers, New York, 2019.

[2] Crites, R.W., Middlebrooks, J., Bastian, R.K., Reed, S.C. Natural Wastewater Treatment Systems, 2nd edition, CRC Press, Taylor & Francis Group, New York, 2014.

[3] Van Haandel, A.C., Van der Lubbe, J.G.M. Handbook of Biological Wastewater Treatment Design and Optimisation of Activated Sludge Systems, 2nd edition, IWA Publishing, New York, USA, 2012.

[4] Wesley Eckenfelder, W., Grau, P. Activated Sludge Process Design and Control: Theory and Practice, 2nd edition, CRC Press, Taylor & Francis Group, New York, USA, 1998.

[5] Olsson, G., Newell, B. Wastewater Treatment Systems: Modelling, Diagnosis and Control. IWA Publishing, London UK, 1999.

[6] Dhouibi, S. Bouallègue, S. Modeling and Control Design of an Activated Sludge Process: a Multi-Model Approach, Proceedings of the 2022 IEEE 21st International Conference on Sciences and Techniques of Automatic Control and Computer Engineering, pp. 209-214, Sousse, Tunisia, December 19-21, 2022.

[7] Revollar, S., Vilanova, R., Francisco, M., Vega, P. PI dissolved oxygen control in wastewater treatment plants for plant wide nitrogen removal efficiency, IFAC-PapersOnLine, vol. 51, no. 4, pp. 450-455, 2018.

[8] Du, X., Wang, J., Jegatheesan, V., Shi, G. Dissolved oxygen control in activated sludge process using a neural network-based adaptive PID algorithm, Applied Sciences, vol. 8, doi: 10.3390/app8020261, 2018.

[9] Revollar, S., Vega, P., Vilanova, R., Francisco, M. Optimal control of wastewater treatment plants using economic-oriented model predictive dynamic strategies, Applied Sciences, vol. 7, no. 8, 2017.

[10] Xie, Y.B., Wang, D., Qiao, J.F. Dynamic multi-objective intelligent optimal control toward wastewater treatment processes, Science China Technological Sciences, vol. 65, pp. 569-580, 2022.

[11] Khallouq, A., Karama, A., Abyad, M. Observer based robust H∞ fuzzy tracking control: application to an activated sludge process, PeerJ Computer Science, vol. 7, no. 2, pp. 1-22, doi: 10.7717/peerj-cs.458, 2021

[12] Abdul Gaffar, S., Murali Mohan, S., Seshagiri Rao, A. Fuzzy Logic Control of Active Sludge-Based Wastewater Treatment Plants, In Karri, R.R., Ravindran, G., Dehghani, M.H. (Eds.), Soft Computing Techniques in Solid Waste and Wastewater Management, Chapter 25, pp. 409-422, 2021.

[13] Matoug L., Khadir M.T., Dynamic Model Prediction Control for an Activated Sludge Model based on a T-S Multi-Model, In Proceedings of the 3rd International Conference on Control, Engineering & Information Technology, pp. 1-6, Tlemcen, Algeria, 2015.

[14] Mulas, M., Tronci, S., Corona, F., Haimi, H., Lindell, P., Heinonen, M., Vahala, R., Baratti, R. Predictive control of an activated sludge process: An application to the Viikinmäki wastewater treatment plant, Journal of Process Control, vol. 35, no. 1, pp. 89-100, 2015.

[15] Yang, T., Qiu, W., Ma, Y., Chadli, M., Zhang, L. Fuzzy model-based predictive control of dissolved oxygen in activated sludge processes, Neurocomputing, vol. 136, no. 1, pp. 88-95, 2014.

[16] Ballhysa, N., Kim, S., Byeon, S. Wastewater Treatment Plant Control Strategies, International Journal of Advanced Smart Convergence, vol. 9, no. 4, pp. 16-25, 2020.

[17] Chakravarty, S.P., Roy, A., Roy, P. Control of activated sludge treatment process using pre-compensated multi-variable quantitative feedback theory-based controller, Transactions of the Institute of Measurement and Control, vol. 44, no. 2, 2022.

[18] Hansen, L.D., Veng, M., Durdevic, P. Compressor scheduling and pressure control for an alternating aeration activated sludge process: a simulation study validated on plant data, Water, vol. 13, no. 8, pp. 1-30, https://doi.org/10.3390/w13081037, 2021.

[19] Harja, G., Naşcu, I. Control of an activated sludge wastewater treatment process based on a Calibrated and modified BSM1 Model, In Proceedings of the 20th International Carpathian Control Conference, pp. 1-6, doi: 10.1109/CarpathianCC.2019.8765912, Krakow-Wieliczka, Poland, 2019.

[20] Rizwan Azhar, M., Emadadeen, A. Advanced control strategy for wastewater treatment process: a parametric study, International Journal of Chemical Engineering and Applications, vol. 5, no. 4, pp. 335-341, 2014.

[21] Tanaka, K., Wang, H.O. Fuzzy Control Systems Design and Analysis: A Linear Matrix Inequality Approach, John Wiley & Sons, Inc, New York, 2001.

[22] Nagy, A.M., Mourot, G., Marx, B., Ragot, J., Schutz, G. Systematic Multimodeling Methodology Applied to an Activated Sludge Reactor Model, Industrial & Engineering Chemistry Research, vol. 49, no. 6, pp. 2790-2799, 2010.

[23] Henze, M., Leslie Grady Jr, C.P., Gujer, W., Marais, G.R., Matsuo, T. Activated Sludge Model no.1, Technical Report 1, I.A.W.Q., London, UK, 1987.

[24] Derouiche, M.L., Bouallègue, S., Haggège, J., Sandou, G. Advanced Metaheuristics-Based Tuning of Effective Design Parameters for Model Predictive Control Approach, International Journal of Advanced Computer Science and Applications, vol. 10, no. 6, pp. 45-53, 2019.

[25] Derouiche, M.L., Bouallègue, S., Haggège, J., Sandou, G. LabVIEW Perturbed Particle Swarm Optimization Based Approach for Model Predictive Control Tuning, Proceedings of the 4th IFAC International Conference on Intelligent Control and Automation Sciences, pp. 359-364, Reims, June 01-03, 2016.

[26] Derouiche, M.L., Bouallègue, S., Haggège, J., Sandou, G. Rapid Model Predictive Control Prototyping with LabVIEW/CDSim and CompactRIO Target, Proceedings of the 4th International Conference on Control Engineering & Information Technology, Hammamet, December 16-18, 2016.

[27] Ben Khoud, K., Bouallègue, S. Model Predictive Control Design for a convertible Quad Tilt-Wing UAV, Proceedings of the 4th International Conference on Control Engineering & Information Technology, Hammamet, December 16-18, 2016

ISSN: 1737-9334

9th International Conference on Green Energy & Environmental Engineering (GEEE-2023)
Proceedings of Engineering & Technology-PET-Vol 75

Effect of Blocks on Critical Ventilation Velocity in Confined Channels

Hella Adouni[#1], Yoldoss Chouari [#2], Herve Bournot[*3], Wassim Kriaa[#4], Hatem Mhiri [#5]

[#]*LTTPI, National Engineering School of Monastir, University of Monastir, Tunisia*

[1]hella.adouni2@gmail.com

[*]*Aix Marseille University, CNRS, IUSTI, Marseille, France*

***Abstract*— Slug flow occurrence in sewer networks is a key factor causing channel blockage, thus the critical longitudinal ventilation velocity is a key parameter in sewer networks design. Slug occurrence in confined channels with obstacles has rarely been studied. Hence, the main aim of this paper is to study the effect of obstacles on critical ventilation velocity in longitudinally ventilated sewer networks. Numerical investigation was applied. Obstacles were located in the upper wall of the confined channel in three different axial positions. Numerical results show that these blocks have direct effect on the dynamic of the air water flow. The critical ventilation velocity increases with the increase of the axial distance between the channel inlet and the block. Moreover, at first instants, the channel with obstacles showed a smooth flow upstream the block and the occurrence of slugs downstream the block which reduced the flow disturbance near the inlet compared with the original case.**

***Keywords*— sewer network; sewer blockage; air water slug flow; blocks; longitudinal ventilation**

I. INTRODUCTION

In this study we consider to evaluate the effect of the existence of blocks situated in the upper part of a confined sewer systems. In fact, these systems ensure the transport of two phase air water treated flow. In some cases, the upper wall may contain hydraulic pipes for other requirements. Such pipes may affect the dynamic of the transported air water flow and obstruct the channel.

Blockage of sewer networks is considered as one of the most fatal threat to the environment and human being as it is generally of high pressure, contains toxic gases from transported treated wastewater and could damage the infrastructure of sewer system initiating flooding. In fact, sewer networks ensure the transport of treated wastewater and are longitudinally ventilated to aerate the channel and to ensure that toxic gases does not return to the cities. During intense rainy events, the capacity of these networks is overloaded which means that the water level increases until it blocks the whole channel. This blockage is described by the transition from air water stratified flow to slug flow ([1]–[5]). For this reason, slug flow control is important in order to avoid the channel blockage ([4], [5]). Reference [4] studied the effect of air velocity on slugs in a confined channel. Results revealed the dependence of the slug flow occurrence to air velocity. It defined a numerical correlation linking slug occurring time and position to air ventilation velocity. However, there are many reasons that trigger the occurrence of slug flow besides the lack of ventilation: heavy rains, inappropriate pipe sizing and the existence of obstacles in the channel...etc. Obstacles can be submerged or even embedded in the top wall of the channel, such as gas pipes crossing the sewer network. Big attention was given to the case of submerged obstacles due to their importance in coastal areas and resolving the challenging problems in ocean engineering. Reference [6] studied experimentally and numerically the effect of two rectangular submerged obstacles at different heights on the water's free surface. Results show that the more the height of the submerged obstacles increases, the more the wave's height reduction and energy loss increase. Reference [7] numerically investigated the effect of submerged obstacles on a solitary wave. It found that the width of the obstacles has little influence on the characteristics of the wave. Furthermore, it showed that the height of the obstacles has direct effect on the height of the wave. The higher the obstacle is, the lower the wave height is. Few of these studies considered the effect of submerged obstacles on the dynamic of the flow when it comes to confined channels. Moreover, the embedded obstacle to the ceiling of confined channels, to our knowledge, has not been investigated in the literature. For this purpose, the matter of this study is to investigate the existing of blocks in the top wall of the channel. It gives particular interest to the effect of these blocks on the critical ventilation velocity that causes the transition to slug flow which obstructs the channel.

Thus a 3D numerical model of confined horizontal channel, describing actual sewer networks, was developed. The model considers the existence of blocks in the upper channel wall at different axial positions. The developed model was used to visualize the dynamic of the flow with and without these blocks. Then, the study presents the effect of the existence of these blocks on the critical ventilation velocity. The results of the present work will be useful in preventing the transition from stratified to slug flow, in the case of sewer networks with blocks on their ceilings.

ISSN: 1737-9334

II. METHODOLOGY

This section describes the numerical modeling and the simulation methodology. A series of numerical simulations were conducted in rectangular confined horizontal channel with dimensions of 3m x 0.15m x 0.075m (length x height x width). These dimensions are in accordance with the test bench of the IUSTI laboratory at the University of Aix Marseille where the experiments were carried out to validate the developed numerical model ([4]). At one end of the simulated channel, the 1/3 of the channel height H (according the y axis) is given to the water phase and the 2/3 H are given for the air phase. Forced air flow was introduced to generate longitudinal ventilation, as shown in Fig. 1. The original case is an empty channel (with no blocks) and the studied cases are with blocks embedded in the upper wall of the channel in three different axial positions.

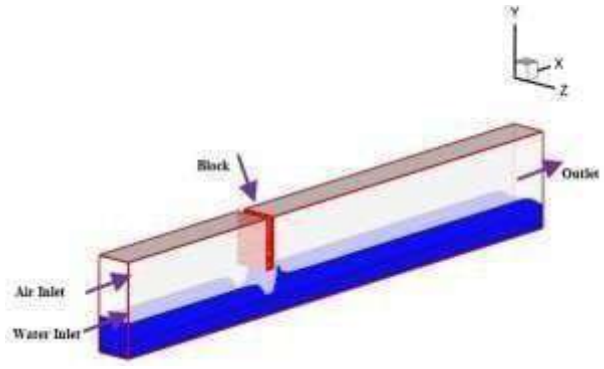

Fig. 1 Schematic representation of the channel with block located at 1 m from the channel inlet

All numerical simulations were conducted using the commercial code fluent. The Volume of Fluid VOF with an "Explicit" scheme was used as the multiphase model. The second order upwind scheme was used for momentum, turbulent kinetic energy and turbulent dissipation rate. The "PISO" pressure-velocity coupling algorithm was used. Simulations were considered as converged when the residuals for the equations of continuity and momentum were less than 10^{-4}. Turbulence was calculated by time-averaging the conservation equations governing the flow to produce the RANS equations (1, 2). The k- s RNG turbulence model was used to solve the additional terms generated by the time-averaging approach. Equations governing the considered two phase flow are solved in each cell of the computational model and are presented as follows:

$$\frac{6\rho}{6t} + \frac{6\rho u_i}{6x_i} = 0 \quad (1)$$

$$\frac{6\rho u_i}{6t} + \frac{6\rho u_i u_j}{6\bar{x}_j} = -\frac{6P}{6x_i} + \frac{6\tau_{ij}}{6\bar{x}_j} + \rho F \quad (2)$$

$$= \left(\frac{6u_i}{6x_j} + \frac{6u_j}{6x_i}\right) - \frac{2}{3}\mu\delta_{ij}\frac{6u_l}{6x_l} \quad (3)$$

Where $u_{i,j}$, u_l are velocity components along the axis of the Cartesian system (x_i, x_j, x_l) with (i, j, l = 1, 2, 3), respectively. Also, t is the time, p is the fluid density, P is the pressure, r_{ij} is the stress tensor, δ i s the Kronnecker delta, μ is the dynamic viscosity and F is the volumetric force due to surface tension. Specific boundary conditions are required to ensure the stability and accuracy of the simulation results. The "Velocity inlet" condition is imposed at the air inlet and at the water inlet. Turbulence quantities were imposed by means of turbulent kinetic energy and turbulent dissipation rate. At the outlet, the "Outflow" condition is imposed. No slip condition is applied at the walls of the channel and the surfaces of the blocks. More boundary condition details are giving in Table 1.

TABLE I
BOUNDARY CONDITIONS

Boundary Conditions		Superficial Velocity [m/s]	Turbulence parameters K [m²/s²] s [m²/ s³]
Air Inlet	**Velocity Inlet**	[0.6-13]	0.01 < K < 1.66 0.02 < s < 59.98
Water Inlet	**Velocity Inlet**	0.16	K=0.001;s =0.001
Outlet	**Outflow**	$\frac{\partial U}{\partial x} = \frac{\partial V}{\partial x} = \frac{\partial W}{\partial x} = 0$	$\frac{\partial K}{\partial x} = \frac{\partial s}{\partial x} = 0$
Channel Walls	**No Slip**	U= V=W=0	K=0; s =0
Block Walls	**No Slip**	U= V=W=0	K=0; s =0

Where U, V, W, are velocities according to x, y, z, respectively.

The plots in all simulations are presented in the symmetry plan, where the x-axis represents the channel longitudinal ventilation and the y-axis represents the height direction.

III. RESULTS

In this section, we numerically studied the effect of blocks on the critical longitudinal ventilation velocity. First we compared the dynamic of the flow in the base case (channel with no blocks) with the channel with a block. Then, we compared the given critical air velocity for the base case with the ones given by the 3 cases of channel with blocks situated at different axial positions. Finally, we depicted the effect of the existence of blocks on the critical air ventilation. Fig.2 presents a comparison between the dynamic of air water flow in confined channel without block (base case) and with block embedded at 1m from the channel inlet for V_{air} =13 m/s and V^s_{air} =0.16 m/s in both cases.

ISSN: 1737-9334

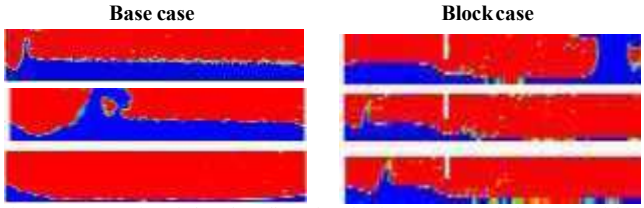

Fig. 2 Dynamic of the slug flow for the base case and the case with a block at the three first instants

It can be seen that a large wave is created near the channel inlet in the base case. At the same time, a large slug is observed near the channel outlet in the case of channel with a block. The slug has already been created and ran the whole channel. This means that the existence of obstacles in confined channels disturbs more the air-water flow and increases the threat created by the occurrence of slug flow. To further investigate the effect of blocks on the dynamic of the flow, a study of the effect of block location was performed and compared with the base case. Three block cases with different axial positions were conducted as follows:

- Case1: block is located at x = 0.2 m from the channel inlet.
- Case2: block is located at x = 0.5 m from the channel inlet.
- Case3: block is located at x = 1 m from the channel inlet.

Fig.3 shows the evolution of the slug flow for each case with its depicted critical air velocity. Unlike the original case, we observe that the slug is created downstream the block in all channel block cases. The flow was kept smooth upstream the block. This means that, for the giving velocities, the existence of blocks ensured the stability of the flow near the inlet which is beneficial to the channel infrastructure and the transport of treated waste water process. Moreover, comparing with the original case, it is clear that the existence of blocks has reduced the critical air ventilation.

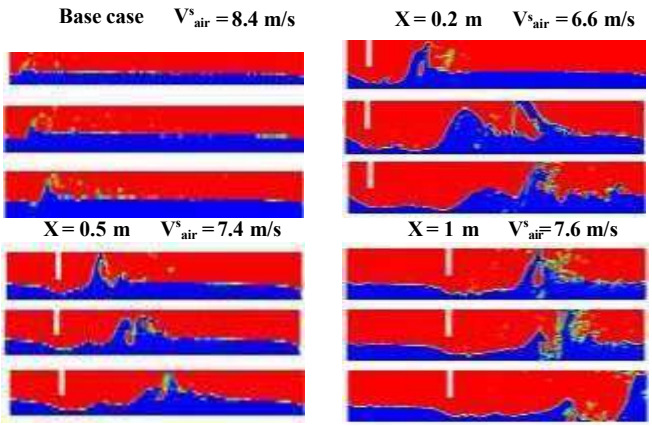

Fig. 3 Dynamic of the slug flow for each case with its depicted critical air velocity at the three first instants

Fig.4 shows the evolution of the critical air velocity in terms of the location of the block in the channel. Numerical results reveal that the critical air velocity is dependent to the block location. The more the block is close to the channel inlet, the less the critical air velocity is. Consequently, a higher ventilation velocity is required to trigger the slug flow in the channel when the block is far away from the channel inlet. Furthermore, it can be seen that the block has less influence on the critical air velocity starting from an axial position equal to 0.5 m from the channel inlet. In such cases, the critical air velocity varies slightly between 11 m/s and 12 m/s.

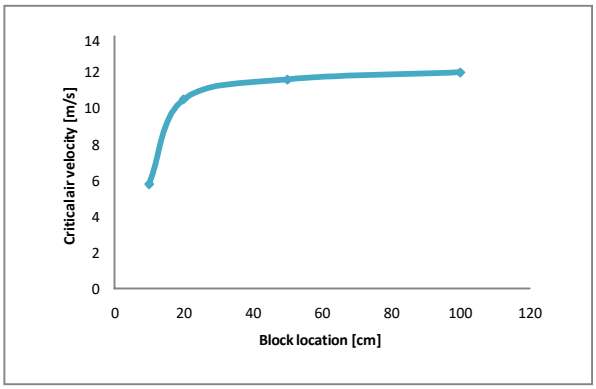

Fig. 4 Evolution of the critical air velocity in terms of the location of the block in the channel

IV. Conclusion

Numerical simulations were conducted to investigate the effect of blockage on critical ventilation velocity in longitudinally ventilated channel with blocks. Blocks were situated on the upper wall of the channel at different axial positions. Results show that the configuration with blocks has major effect on the critical air ventilation comparing with the original case. Major findings are as follows:

- The formation of slugs in the block case is much faster than in the original case.
- In the early stages, the blocks kept the slug formation away from the channel inlet.
- The further the block is from the channel entrance, the higher the critical air velocity.

References

[1] M. G. Conte, G. A. Hegde, M. J. Silva, A. K. Sum, and R. E. M. Morales, "Characterization of slug initiation for horizontal air-water two-phase flow," *Experimental Thermal and Fluid Science.*, vol. 87, pp. 80–92, Oct. 2017.

[2] A. Z. Hudaya, A. Widyatama,O. Dinaryanto,W. E. Juwana, Indarto, and Deendarlianto, "The liquid wave characteristics during the transportation of air-water stratified co-current two-phase flow in a horizontal pipe," *Experimental Thermal and Fluid Science.*, vol. 103, pp. 304–317, May. 2019.

[3] M. Akhlaghi, V. Mohammadi, N. M. Nouri, M. T. khani, and M. Karimi, "Multi-Fluid VoF model assessment to simulate the horizontal air–water intermittent flow," *Chemical Engineering Research and Design.*, vol. 152, pp. 48–59, Dec. 2019.

ISSN: 1737-9334

[4] H. Adouni,Y. Chouari,W. Kriaa, and H. Bournot, "The effect of air velocity on slugs in a confined channel," *Flow Measurement and Instrumentation.,* vol. 81, Oct. 2021.

[5] H. Adouni,Y. Chouari,W. Kriaa, H. Bournot, and H. Mhiri, "A novel ventilation method to prevent obstruction phenomenon within sewer networks," *International Journal of Heat and Mass Transfer.,* vol. 184, Mar. 2022.

[6] A. Ghafari, M. R. Tavakoli, M. N. Ahmadabadi, K. Teimouri, and K. *C.* Kim, "Investigation of interaction between solitary wave and two submerged rectangular obstacles," *Ocean Engineering.*, vol. 237, Oct. 2021.

[7] A Wang J, He. G, You. R, and Liu. P, "Numerical study on interaction of a solitary wave with the submerged obstacle," *Ocean Engineering: An International Journal of Research and Development.*, vol. 158, pp. 1–14, Jun. 2018

ISSN: 1737-9334

IoT and Cloud Computing Integration : A Survey

Sedieg A. Elatab
Engineering Technology College -Surman UniversitySedieg.elatab@sabu.edu.ly

Azdihar A.Ahmed
Faculty of Engineering, Sabratha
ezdihar.alwheshe@sabu.edu.ly

Nashwa E.Zaqout
Faculty Of Economic,University Of Al-Zawiya
n.zaqout@zu.edu.ly

Abdulfatah A. Alfarah
Higher Institute of Marine Science Technologies -Sabratha
Abdufarah26@gmail.com

Thiheebah A. Alwaer
Sabratha University , Economy College ,
Libyadehebaalwaer@gmail.com

Abstract—The integration of Cloud computing and IoT enables thesharing of computing resources and data between devices in a convenient and scalable way. The Cloud provides a platform for storing, processing, and analyzing large amounts of data generated by IoT devices, while IoT enables the collection and sharing of real-time data from various sources. This integration allows for new applications and services such as smart homes, connected cars, and predictive maintenance. However, implementing this integration can also present challenges, such as security and privacy concerns, network connectivity, and data management. This article presents a general background to address these challenges and explore new ways to fully leverage the potential of this integration.

I. Introduction

The security and privacy of cloud and IoT are both a challenge and an open issue that is gaining more attention. The integration of the two technologies in cloud-based IoT creates concerns about privacy, as sensitive data must be protected. Ensuring authorized access to sensitive data is still a challenge and data integrity must be guaranteed. Security remains an issue as the system is vulnerable to different threats from hackers, such as malware injection and information theft. Public key cryptography may not be applicable to all layers due to processing power constraints. There are various challenges, including possible attacks and vulnerabilities, and the lack of trust in service providers, whichrequires attention in order to address the security and privacychallenges in cloud-based IoT [1]–[6].

However, efforts are being made to address these challenges. For example, the use of cryptographic protocols, such as SSL and authentication methods, is helping to improve the security of IoT systems. Additionally, the use of privacy- preserving technologies, such as privelets, is being investigated to enhance the privacy of users. There is also a focus on improving the reliability of data centers and communication channels to reduce the risk of security breaches. Other researchers are investigating the implementation of IPv6 for IoT to improve the interoperability and efficiency of the system. Additionally, research is ongoing in areas such as auditing, flexible and open platforms, and learning and adaptive objects to help address the challenges posed by Cloud-based IoT [7]–[9].

Other security concerns in cloud-based IoT include issues with data privacy and data protection, data sharing, network security, and software security. To mitigate these issues, researchers and practitioners are exploring various security technologies and approaches, such as privacy-preserving datacollection and analysis, data encryption, secure data sharing protocols, firewalls and intrusion detection systems, and secure software development practices [10]–[12]. One of the most promising solutions is to adopt a risk management framework that identifies the security risks and threats associated with cloud-based IoT and provides a systematic approach to address them. This approach involves a combination of policy-based security measures, technical security controls, and organizational processes to ensure the security of the system.

Another important aspect of cloud-based IoT security is the need for transparency and accountability. This requires that the service providers are transparent about their security policies and practices, and that they are accountable for ensuring the security of the data and systems they manage.

This article provides a comprehensive overview of the current state of research on the security and privacy aspects of cloud and IoT integration. It is clear that security and privacy are critical challenges in cloud-based IoT, and a lot of effort is still required to overcome these challenges. The various proposals and solutions presented in the literature demonstrate the ongoing efforts to address these issues. However, it is important to note that these challenges are complex and multifaceted, and more research is needed to find effective and sustainable solutions.

ISSN: 1737-9334

II. Internet of Things

IoT, a term first launched by Kevin Ashton in 1998, is the future of Internet and ubiquitous computing [13]. This technological revolution reflects the good future of connectivity and reachability. In IoT, 'things' refer to any object on the face of the Earth, whether it is a communicating device or a non-communicating dumb object. From a smart device to a leaf of a tree or a bottle of beverage, anything can be part of Internet. The objects become communicating nodes over the Internet, through data communication means, primarily through Radio Frequency Identification (RFID) tags. IoT include smart objects as well. Smart objects can not only physical entities, but also digital ones , and they play some tasks for humans and the habitat. Becausec of this culprit, IoT is not only hardware and software paradigm, but also include interaction and social aspects as well [14]. The architecture of IoT provides a 3-layer, with a Perception layer. Namely, the Network layer, and the Application layer, but some [13], [15] add two more layers: The middle-ware layer and the Business layer. This five-layer architecture is shown in fig.1.

- Perception layer is the lowest layer in the IoT architecture. This means that the purpose is to acquire the

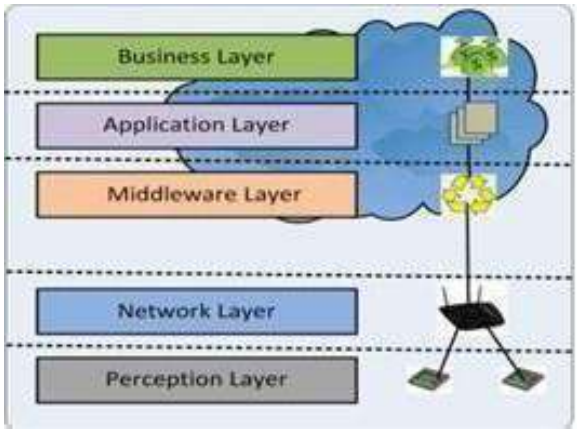

Fig. 1. Internet of Things layers.

information from environment. All the data collection and data sensing part is done on this layer [16]. Sensors, bar code labels, RFID tags, GPS, and camera, lie in this layer. Identifying object/thing and gathering data is the main purpose of this layer.

- Network layer collects the data perceived by the Perception layer. Network layer is like the Network and Transport layer of OSI model. It collects the data from the lower layer and sends to the Internet. Network layer may only include a gateway, having one interface connected to the sensor network and another to the Internet. In some scenarios, it may include network management center or information processing center.
- Middleware layer receives data from Network layer. Its purpose is service management and storage of data. It also performs information processing and takes decisions automatically based on results. It then passes the output to the next layer, the Application layer [15].
- Application layer performs the final presentation of data. Application layer receives information from the Middleware layer and provides global management of the application presenting that information, based on the information processed by Middleware layer. Depending upon the type of devices and their purpose in Perception layer and then on the way they have been processed by the Middleware layer, according to the needs of user, Application layer presents the data in the form of: smart city, smart home, smart transportation, vehicle tracking, smart farming, smart health and other many kinds of applications [15].
- Business layer is all about making money from the service being provided. Data received at the application layer is melded into a meaningful service and then further services are created from those existing services. Furthermore, information is processed to make it knowledge and further efficient means of usage make it wisdom, which can earn a good amount of money to the service provider.

IoT works on the basis of Machine-to-Machine (M2M) communications, but not limited to it. M2M refers to communication between two machines, without human intervention. In IoT, even non-connected entities can becomepart of IoT, with a data communicating device, like a bar-code or an RFID tag, sensed through a device (may even be a smart phone sensing it), which eventually is connected to the Internet. In IoT, non-intelligent objects, known as 'things' in IoT terminology, become the communicating nodes.

III. Cloud Computing

Nowadays, the term "cloud computing" has been an important term in the world of Information Technology (IT). Cloud computing is a kind of computing which is highly scalable and use virtualized resources that can be shared by the users. Users do not need any background knowledge of the services. A user on the internet can communicate with many servers at the same time and these servers exchange information among themselves (Hayes,2008) [17]. Cloud computing is currently one of the new technology trends (virtualization, fast connection and broadband internet). Cloud computing encompasses elements from grid computing, utility computing and autonomic computing, into an innovative deployment architecture. This rapid transition towards the cloud has fuelled concerns on a critical issue for the success of information systems, communication and

ISSN: 1737-9334

information security. The major security challenge with clouds is that the owner of the data may not have control of where the data is placed. This is because if anyone wants to exploit the advantages of using cloud computing, one must also utilize the resource allocation and scheduling provided by clouds. There are numerous security issues for cloud computing as it encompasses many technologies including networks, databases, operating systems, resource scheduling, virtualization, transaction management, load balancing, concurrency control, and memory management. Therefore, security issues for many of these systems and technologies are applicable to cloud computing. As an example, the network that interconnects the systems in a cloud has to be secure [18].

IV. CLOUD COMPUTING ARCHITECTURAL FRAMEWORK cloud computing has been defined by The National Institute of Standards and Technology (NIST) as five essential characteristics, three cloud service models, and four cloud deployment models. They are summarized in visual form in Fig.2 and explained in detail below.

From the researcher's point of view, cloud computing is a model for enabling ubiquitous, convenient, on-demand network access to a shared pool of configurable computing resources (e.g, networks, servers, storage, applications, and services) that can be rapidly provisioned and released with minimal management effort or service provider interaction.

A. Essential characteristics of cloud computing

Cloud services have, in fact, five important characteristics associated with the cloud services which show their relation

Fig. 2. NIST Visual Model of Cloud Computing Definition.

to, and their differences from, conventional computing approaches:

- On-Demand Self-Service A consumer can unilaterally provision computing abilities such as server time and network storage as needed automatically, without requiring human communication with a service provider.
- Broad Network Access If Capabilities are available over the network and accessed through standard mechanisms, this will promote the usage of heterogeneous thin or thick client platforms (e.g., mobile phones, laptops, and PDAs) as well as other conventional or cloud based software services.
- Resource Pooling The provider's computing resources are pooled to serve multiple consumers using a multi-tenant model, with different physical and virtual resources dynamically assigned and reassigned according to consumer demand. Examples of resources include storage, processing, memory, network bandwidth, and virtual machine.
- Measured Service Cloud systems automatically control and optimize resource usage by leveraging a metering capability at some level of abstraction appropriate to the type of service (e.g., storage, processing, bandwidth, or active user accounts). Resource usage can be monitored, controlled, and reported-providing transparency for both the provider and consumer of the service.
- Rapid Elasticity Capabilities can be rapidly and elastically provisioned-in some cases automatically – to quickly scale out; and rapidly released to quickly scale in. To the consumer, the Capabilities available for provisioning often appear to be unlimited and can be purchased in any quantity at any time.

B. Cloud Services Models

Cloud service delivery is divided among three archetypal models and various derivative combinations. The three fundamental classifications are often referred to as the "SPI Model" where "SPI" refers to Software, Platform or Infrastructure (as a Service), respectively – defined thus

- Cloud Software as a Service (SaaS) The capability provided to the consumer is to use the provider's applications running on a cloud infrastructure. The applications running are accessible from various client devices through a thin client interface such as a web browser (e.g., webbased email). The consumer does not manage or control the underlying cloud infrastructure including network, servers, operating systems, storage, or even individual application capabilities, with the possible exception of limited user-specific application configuration setting. • Cloud Platform as a Service (PaaS) The capability provided to the consumer is to deploy onto the cloud infrastructure consumer-created or acquired applications created using programming languages and tools supported by the provider. The consumer could not manage or control the underlying cloud infrastructure including network, servers, operating systems, or storage, but has control over the deployed applications and possibly application hosting environment configurations. • Cloud Infrastructure as a Service (IaaS) The capability provided to the consumer is to provision processing, storage, network, and other fundamental computing resources where the consumer is able to

ISSN: 1737-9334

deploy and run arbitrary software, which can include operating systems and applications. The consumer does not manage or control the underlying cloudinfrastructure but has control over operating systems, storage, deployed applications, and possibly limited control of select networking components (e.g., host firewall).

C. Cloud deployment models

Regarding the service model utilized (SaaS, PaaS, or IaaS) there are four important deployment models for cloud services, with derivative differences that address specific needs.

- Public cloud
  It is very crucial that the cloud infrastructure could be easily reached by the general public or a large company group and is owned by an organization selling cloud services.
- Private Cloud
  The cloud infrastructure is controled only for a single organization. It may be managed by the organization or a third party, and may exist on –premises or off-premises. • Community cloud Many organization has shared the cloud infrastructure and support a specific community that has shared concerns (e.g., mission, security requirements, policy, or compliance considerations). It may be managed by the organizations or a third party and may exist on-premises or off-premises.
- Hybrid cloud
  The cloud infrastructure consists of two or more clouds (private, community, or public) that remain unique entities but are bound together by standardized or proprietary technology that enables information and application portability (e.g., cloud bursting for load–balancing between clouds).

V. CLOUD-BASED INTERNET OF THINGS

III. It is evident that the IoT and Cloud computing are increasingly developing services, and have their own unique characteristics. On the one hand, the IoT approach is based on smart devices which links in a global network and dynamic infrastructure. It enables ubiquitous computing scenarios. The IoT is typically characterised by widely-distributed devices with limited processing capabilities and storage. These devices face issues regarding performance, reliability, privacy, and security [20]. On the other hand, Cloud computing has a significant network with vast spaces abilities and computation power.To add more , it provides a flexible, robust environment which allows for dynamic data integration from various data sources [21]. Cloud computing has partially resolved most of the IoT issues. Indeed, the IoT and Cloud are two differentely challenging technologies, and are being joined in order revoluitionize the current and future environment of internetworking services [22].

The Cloud-based Internet of Things is a platform which allows for the smart usage of applications, information, and infrastructure in a cost-effective way. While the IoT and Cloud computing are different from each other, their features are almost complementary, as shown in table1. This complementarily is the primary reason why many researchers have proposed their integration [20].

TABLE I
Comparison of the IoT with cloud computing

Items	IoT	Cloud Computing
Characteristics	IoT are pervasive (things are everywhere). These are real-world objects.	Cloud is ubiquitous (recourses are available from everywhere). These are virtual resources
Processing capabilities	Limited computational capabilities	Virtually unlimited computational capabilities
Storage capabilities	Limited storage or no storage capabilities.	Unlimited storage capabilities
Connectivity	It uses the internet as a point of convergence.	It is uses the internet for service delivery.
Big Data	It is a source of big data.	It is a means by which to manage big data.

VI. CLOUD- BASED IOT ARCHITECTURE PARADIGM

Cloud Computing services are implemented in many areas related to the IoT, including Genomics Data Processing, Teaching, and Studying, Services for Small and Medium Businesses, E-Learning Method, Augmented Reality, Manufacturing, Emergency Recovery, Smart Cities and others, Remote Forensics, Hospitality Business, E-Government and Human Resource Administration, Internet of Cars [23], [24]. Challenges in cloud computing and the IoT separately and in Application environments that are unique [25]. Critical difficulties in researching how the IoT and Cloud Computing could be integrated yielded inconclusive findings.

Cloud computing and IoT have spread over the world and increased significantly in recent years [26]. The characteristics they show can be outstanding when joined. They are each really special and important for each other [27]. Researchers scheduled a range of applications concerning the Coordination of the Cloud and IoT to develop and accumulate data as it gets assistance from cloud storage and computational capability. In this part, then explain the Cloud-IoT (Cloud and IoT) architecture. The layers of knowledge in Fig 3 are explained below. The application, network, and sensing layers are interconnected.

Objects capable of reading and collecting data via different IoT systems are exhibited through IoT visualization protocols. For easier processing, this knowledge may be processed in the Cloud [28]. The application layer can sense environment data

ISSN: 1737-9334

and send requests to the Cloud simultaneously to process and obtain sensor information results [29]. It is also important to

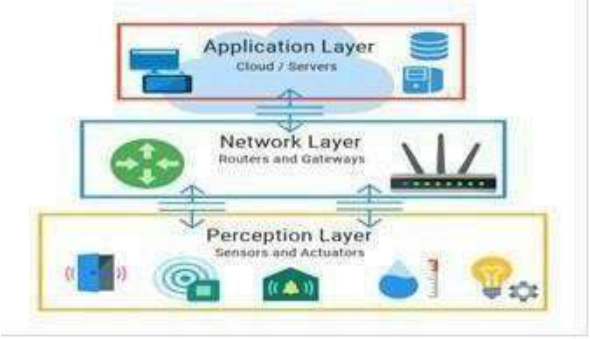

Fig. 3. Cloud-IoT Architecture.

also repost information to the IoT and other IoT objects, data gained from the sensor layer, and data analysis for additional processing [30], [31].

RESTful with Web servers and Simple Object Access Protocol (SOAP) is used for interacting between devices on the Internet. SOAP Web Services works with XML sharing, but most WSS works with an HTTP protocol essential for energylimited resources and computers as shown in Fig.4 [32]. The Constrained Application Protocol (CoAP) program protocol requires using RESTful facilities by computers with minimal resources. For wireless communication between devices with limited resource access [33]. CoAP uses the UDP protocol instead of TCP, which is widely used in HTTP.

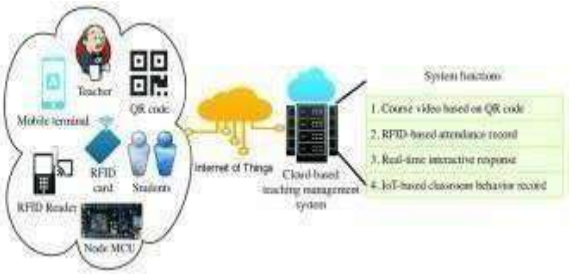

Fig. 4. Cloud-IoT Environment.

VII. SECURITY ISSUES IN IOT AND CLOUD COMPUTING INTEGRATION

There is a quick and independent evolution considering the two words of IoT and Cloud Computing. To start with, the virtually unlimited capabilities and resources of Cloud Computing in order to compensate its technological constrains, such as processing, storage and communication, could be a benefit for the Internet of Things technology [34]. Also, the IoT technology extends its scope to deal with real world things in a more distributed and dynamic manner and by delivering new services in a large number of real life scenarios, might be beneficial for the use of Cloud Computing technology. In many cases, Cloud can give the intermediate layer between the things and the applications, hiding all the difficulty and functionalities necessary to implement the latter. Through the integration of IoT and Cloud Computing could be observed that Cloud Computing can fill some gaps of IoT such the limited storage and applications over internet. Also, IoT can fill some gaps of Cloud Computing such the main issue of limited scope. Based in the important issue of security in both technologies we can consider some drivers for the integration. The security issue of this integration has a serious problem. When critical IoT applications move towards the Cloud in the service provider or the knowledge about service level agreements (SLAs) and knowledge about the physical location of data. Consequently, new challenges need specific attention as mentioned in survey. Multi-tenancy could also compromise security and contribute to sensitive information leakage. Furthermore, public key cryptography cannot be applied at all layers due to the computing power constraints imposed by the things. These are examples of topics that are currently under investigation in order to tackle the big challenge of security and privacy in Cloud Computing and IoT integration. Subsequently, some challenges about the security issue in the integration of two technologies are listed [35].

- Heterogeneity: A big problem in Cloud Computing and IoT integration is related to the wide heterogeneity of devices, operating systems, platforms, and services available and possibly used for new or improved applications. • Performance: Often Cloud Computing and IoT integration's applications introduce specific performance and QoS requirements at several levels (i.e. for communication, computation, and storage aspects) and in some particular scenarios meeting requirements may not be easily achievable.
- Reliability. When Cloud Computing and IoT integration is adopted for mission-critical applications, reliability concerns typically arise e.g., in the context of smart mobility, vehicles are often on the move and the vehicular networking and communication is often intermittent or unreliable. When applications are deployed in resource constrained environments a number of challenges related to device failure or not always reachable devices exists.
- Big Data. With an estimated number of 50 billion devices that will be networked by 2020, specific attention must be paid to transportation, storage, access, and processing of the huge amount of information they will produce. The ubiquity of mobile devices and sensor pervasiveness, indeed call for scalable computing platforms.
- Monitoring. As largely documented in the literature, monitoring is an essential activity in Cloud environments

ISSN: 1737-9334

for capacity planning, for managing resources, SLAs, performance and security, and for troubleshooting.

VIII. OPEN ISSUES AND FUTURE DIRECTIONS

This section will address some of the open issues and future research directions related to Cloud-based IoT, and which still require more research efforts. These issues include:

1) Standardization Many studies have highlighted the issues of lack of standards, which is considered critical in relation to the Cloudbased IoT paradigm [36]. Although a number of proposed standardizations have been put forth by the scientific society for the deployment of IoT and Cloud approaches, it is obvious that architectures, standard protocols, and APIs are required to allow for interconnection between heterogeneous smart things and the generation of new services.
2) Fog Computing
   Fog computing is a model which extends Cloud computing services to the edge of the network. Similar to the Cloud, Fog supply communicates application services to users. Fog can essentially be considered an extension of Cloud Computing which acts as an intermediate between the edge of the network and the Cloud; indeed, it works with latency-sensitive applications that require other nodes to satisfy their delay requirements [6]. Although storage, computing, and networking are the main resources of both Fog and the Cloud, the Fog has certain features, such as location awareness and edge location, that provide geographical distribution, and low latency; moreover, there are large nodes; this is in contrast with the Cloud, which is supported for real-time interaction and mobility [37], [38].
3) Cloud Capabilities As in any networked environment, security is considered to be one of the main issues of the Cloud-based IoT paradigm. There are more chances of attacks on both the IoT and the Cloud side. In the IoT context, data integrity, confidentiality and authenticity can be guaranteed by encryption. However, insider attacks cannot be resolved and it is also hard to use the IoT on devices with limited capabilities [37].
4) SLA enforcement
   Cloud-based IoT users need created data to be conveyed and processed based on application-dependent imitations, which can be tough in some cases. Ensuring a specific Quality of Service (QoS) level regarding Cloud resources by depending on a single provider raises many issues. Thus, multiple Cloud providers may be required to avoid SLA violations. However, dynamically choosing the most appropriate mixture of Cloud providers still represents an open issue due to time, costs, and heterogeneity of QoS management support [38].
5) Big data
   Although a number of contributions have been proposed, Big Data is still considered a critical open issue, and one in need of more research. The Cloud-based IoT approach involves the management and processing of huge amounts of data stemming from locations and from heterogeneous sources; indeed, in the Cloud-based IoT, many applications need complicated tasks to be performed in real-time [39].
6) Security and privacy security and privacy are both critical research issues which have received a great deal of attention although they are still open issues which require more efforts. Hence,adapting to different threats from hackers is still a problem [40]. In addition, another problem is providing the appropriate authorization rules and policies while ensuring that only authorized users have access to sensitive data; this is crucial for preserving users' privacy, specifically when data integrity must be guaranteed.
7) Energy efficiency
   Recent Cloud-based IoT applications include frequent data that is transmitted from IoT objects to the Cloud, which quickly consumes the node energy.Hence , generating efficient energy when it comes to data processing and transmission remains a significant open issue. Several directions have been suggested to get rid of this issue, such as compression technologies, efficient data transmission; and data caching techniques for reusing collected data with time-insensitive application [40].

IX. CONCLUSION

This paper surveyed the literature on the integration of Cloud Computing and IoT, focusing on the complementary aspects and main drivers of their integration. The main focus is on identifying the security issues that arise when combining these technologies and how they can be addressed. The paper highlights the benefits of integrating Cloud Computing and IoT, such as increased scalability and flexibility, improved data management, and enhanced security. Additionally, the paper proposes an algorithm model to address the security challenges and examines how encryption algorithms can contribute to the integration of IoT and Cloud Computing. The paper also suggests that further research is needed in this field, as the rapid development of both technologies requires a better integration model with reduced security issues. Overall, the integration of Cloud Computing and IoT is seen as a major step forward for the future Internet.

REFERENCES

[1] Le, X. H., Lee, S., True, P. T. H., Khattak, A. M., Han, M., Hung, D. V., Hassan, M. M., Kim, M., Koo, K.-H., Lee, Y.-K., et al., 2010. Secured wsn-integrated

ISSN: 1737-9334

cloud computing for u-life care. In: Proceedings of the 7th IEEE conference on Consumer communications and networking conference. IEEE Press, pp. 702–703.

[2] Kapadia, A., Myers, S., Wang, X., Fox, G., 2011. Toward securing sensor clouds. In: Collaboration Technologies and Systems (CTS), 2011 International Conference on. IEEE, pp. 280–289.

[3] G. Suciu A. Vulpe S. Halunga O. Fratu G. Todoran V. Suciu "Smart Cities Built on Resilient Cloud Computing and Secure Internet of Things" 19th Int. Conf. Control Systems and Computer Science (CSCS) 2013, pp. 513518.

[4] A. Alenezi, N. H. N. Zulkipli, H. F. Atlam, R. J. Walters, and G. B. Wills, "The Impact of Cloud Forensic Readiness on Security," in 7st International Conference on Cloud Computing and Services Science, 2017, pp. 1–8.

[5] K. S. Dar, A. Taherkordi and F. Eliassen, "Enhancing Dependability of Cloud-Based IoT Services through Virtualization," 2016 IEEE First International Conference on Internet-of-Things Design and Implementation (IoTDI), 2016, pp. 106-116.

[6] C. Doukas and I. Maglogiannis, "Bringing IoT and cloud computing towards pervasive healthcare," Proc. - 6th Int. Conf. Innov. Mob. Internet Serv. Ubiquitous Comput. IMIS, 2012, pp. 922–926.

[7] Dimosthenis Kyriazisa, Theodora Varvarigou, "Smart, autonomous and reliable Internet of Things", The 4th International Conference on Emerging Ubiquitous Systems and Pervasive Networks, Volume 2, 2013, pp 442- 448, DOI: 10.1016/j.procs.2013.09.059.

[8] Xiao Ming Zhang, Ning Zhang, "An Open, Secure and Flexible Platform Based on Internet of Things and Cloud Computing for Ambient Aiding Living and Telemedicine", International Conference on Computer and Management, 19-21 May 2011, Wuhan, pp 1-4, DOI: 10.1109/CAMAN.2011.5778905.

[9] Yifan Bo, Haiyan Wang, "The Application of Cloud Computing and The Internet of Things in Agriculture and Forestry", International Joint Conference on Service Sciences, 25-27 May 2011, Taipei, pp 168-172, DOI: 10.1109/IJCSS.2011.40.

[10] T. Bhattasali, R. Chaki, N. Chaki, Secure and trusted Cloud of Things, in: India Conference (INDICON), 2013 Annual IEEE, IEEE, 2013, pp. 1–6.

[11] Y. Simmhan, A.G. Kumbhare, B. Cao, V. Prasanna, An analysis of security and privacy issues in smart grid software architectures on Clouds, in: Cloud Computing (CLOUD), 2011 IEEE International Conference on, IEEE, 2011,pp. 582–589.

[12] S. Subashini, V. Kavitha, A survey on security issues in service delivery models of Cloud computing, J. Netw. Comput. Appl. 34 (1) (2011) 1–11.

[13] Miao Wu et. al., "Research on the architecture of Internet of things", in the proceedings of 3rd International Conference on Advanced Computer Theory and Engineering, 20-22 August, 2012,Beijing, China.

[14] Gerd Kortuem, Fahim Kawsar, Daniel Fitton, and Vasughi Sundramoorthi, "Smart Objects and Building Blocks of Internet of Things", IEEE Internet Computing Journal, volume 14, issue 1, pp. 44-51, Jan.-Feb., 2010.

[15] Rafiullah Khan, Sarmad Ullah Khan, Rifaqat Zaheer, and Shahid Khan, "Future Internet: The Internet of Things Architecture, Possible Applications and Key Challenges", in the proceedings of 10th International Conference on Frontiers of Information Technology, Islamabad, Pakistan, 17-19 December, 2012.

[16] Dieter Uckelamann, Mark Harrison, and Floria Michahelles, "Architecting the Internet of Things," Springer-Verlag Berlin Heidelberg, 2011.

[17] Peter Mell,Timothy Grance , The NIST Definition of Cloud Computing ,The National Institute of Standard and Technology, U.S.Department of Commerce ,Special Publication 800-145

[18] Security Issues for Cloud Computing , Technical Report UTDCS-0210, Department of Computer Science, The University of Texas at Dallas, February 2010, (Kevin Hamlen, Murat Kantarcioglu, Latifur and Bhavani Thuraisingham).

[19] Sedieg A.Elatab , Rabeah H.Ghareb , "Security Issues for Cloud Computing" in the proceedings of 5th International Conference on Automation, Control Engineering and Computer Science (ACECS-2018).

[20] A Botta, W. De Donato, V. Persico, and A. Pescape, "Integration´ of Cloud computing and Internet of Things: A survey," Futur. Gener. Comput. Syst., vol. 56, 2016, pp. 684–700.

[21] J. Zhou et al., "CloudThings: A common architecture for integrating the Internet of Things with Cloud Computing," Proceedings of the 2013 IEEE 17th International Conference on Computer Supported Cooperative Work in Design (CSCWD), 2013, pp. 651-657.

[22] S. M. Babu, A. J. Lakshmi and B. T. Rao, "A study on cloud based Internet of Things: CloudIoT," 2015 Global Conference on Communication Technologies (GCCT), 2015, pp. 60-65.

[23] M. Sadeeq, A. I. Abdulla, A. S. Abdulraheem, and Z. S. Ageed, "Impact of Electronic Commerce on Enterprise Business," Technol. Rep. Kansai Univ, vol. 62, pp. 2365-2378, 2020.

[24] A. M. Abdulazeez, S. R. Zeebaree, and M. A. Sadeeq, "Design and Implementation of Electronic Student Affairs System," Academic Journal of Nawroz University, vol. 7, pp. 66-73, 2018.

[25] H. Shukur, S. Zeebaree, R. Zebari, D. Zeebaree, O. Ahmed, and A. Salih, "Cloud computing virtualization of resources allocation for distributed systems," Journal of Applied Science and Technology Trends, vol. 1, pp. 98-105, 2020.

[26] L. M. Haji, S. Zeebaree, O. M. Ahmed, A. B. Sallow, K. Jacksi, and R. R. Zeabri, "Dynamic resource allocation for distributed systems and cloud computing," TEST Engineering & Management, vol. 83, pp. 2241722426, 2020.

[27] A. Hosseinian-Far, M. Ramachandran, and C. L. Slack, "Emerging trends in cloud computing, big data, fog computing, IoT and smart living," in Technology for smart futures, ed: Springer, 2018, pp. 29-40.

[28] J. Ren, H. Guo, C. Xu, and Y. Zhang, "Serving at the edge: A scalable IoT architecture based on transparent computing," IEEE Network, vol. 31, pp. 96-105, 2017. 7

[29] M. Aazam, I. Khan, A. A. Alsaffar, and E.-N. Huh, "Cloud of Things: Integrating Internet of Things and cloud computing and the issues involved," in Proceedings of 2014 11th International Bhurban Conference on Applied Sciences & Technology (IBCAST) Islamabad, Pakistan, 14th18th January, 2014, 2014, pp. 414-419.

[30] R.Gravina, P. Alinia, H. Ghasemzadeh, and G. Fortino, "Multi-sensor fusion in body sensor networks: State-of-the-art and research challenges," Information Fusion, vol. 35, pp. 68-80, 2017.

[31] P. Tan, H. Wu, P. Li, and H. Xu, "Teaching management system with applications of RFID and IoT technology," Education Sciences, vol. 8, p. 26, 2018.

[32] S. R. Zeebaree, K. Jacksi, and R. R. Zebari, "Impact analysis of SYN flood DDoS attack on HAProxy and NLB cluster-based web servers," Indones. J. Electr. Eng. Comput. Sci, vol. 19, pp. 510-517, 2020.

[33] C. Stergiou, K. E. Psannis, B.-G. Kim, and B. Gupta, "Secure integration of IoT and cloud computing," Future Generation Computer Systems, vol. 78, pp. 964-975, 2018.

[34] N. Park, et al., Symmetric key-based authentication and the session key agreement scheme in IoT environment, in: Computer Science and its Applications, three hundred and thirtyth ed., Springer Berlin, Heidelberg, Berlin, 2015, pp. 379–384.

[35] Sedieg A.Elatab., Integration of IoT and Cloud Computing and its Security Issues, 6th International Conference on Control & Signal Processing (CSP - 2019). Hammamet-Tunisia , 30-31 March 2019,p8.

[36] G. Suciu A. Vulpe S. Halunga O. Fratu G. Todoran V. Suciu "Smart Cities Built on Resilient Cloud Computing and Secure Internet of Things" 19th Int. Conf. Control Systems and Computer Science (CSCS)2013, pp. 513-518.

[37] A. Botta, W. de Donato, V. Persico and A. Pescape, "On the Integration´ of Cloud Computing and Internet of Things," 2014 International Conference on Future Internet of Things and Cloud, Barcelona, 2014,pp. 23-30.

[38] S. M. Babu, A. J. Lakshmi and B. T. Rao, "A study on cloud basedInternet of Things: CloudIoT," 2015 Global Conference onCommunication Technologies (GCCT), 2015, pp. 60-65.

[39] Diaz, Manuel, Cristian Martin, and Bartolome Rubio. "State-of-the-´ art,challenges, and open issues in the integration of Internet of things and cloud computing." Journal of Network and Computer Applications, 2016, pp. 99-117.

[40] H. F. Atlam, A. Alenezi, R. J. Walters, and G. B. Wills, "An Overview of Risk Estimation Techniques in Risk-based Access Control for the Internet of Things," in 2nd International Conference on Internet of Things, Big Data and Security, 2017, pp. 1–8.

ISSN: 1737-9334

Data Anonymization Techniques To Enhance Privacy

Sedieg A. Elatab
College of Technology Engineering **Surman**
Sedieg.elatab@sabu.edu.ly

Rabeea H. Ghareeb
Sabratha University , Economy College , Libya
Rabee7878@gmail.com

Hamida A. Oushah
Faculty of Engineering, Sabratha University
E_hamida@yahoo.com

Lamia Gweder
Surman College for Science and Technology
lamiagweder@yahoo.com

Samira A.Alshfah
Faculty of education,University of Zawia
Samira_7_8@yahoo.com

***Abstract*—**The privacy of indivisual information is a very significant issue these days. How to process the data and use it for analysis without compromising the individual's identity is a critical task and must be done in order to ensure the anonymity of this data. To try to unanimously unify this anonymity, laws and regulations such as GDPR were created. In this paper, GDPR will be described and the concepts of anonymization and pseudonymization will be explained. We show some of the main anonymization techniques and efficient software to support the application of these techniques. The main objective is to understand which techniques offer a higher level of anonymization, the positive and negative of each one and the benefit in its use.

1. INTRODUCTION

Recentally, the exponential growth of digital information has improved more than expected with technological development. Nowadays, about 53% (ONU News, 2019) of the world population has access to Internet and, for this reason, their personal data is spread out and accessible. Now, a technological area in great expansion, precisely due to the large volume of data available, is the area of data analysis.
What happens in large organizations and which has also been growing in smaller ones is that they carry out analyzes on their data in order to find patterns, trends and customer profiles. This would not be a problem if these data were processed internally within the organization. But what is happening is that a lot of data is sold to other organizations or made available to the public for research purposes as a consultation service. These personal data may contain information that allows to identify the individual and being made public may violate privacy. By doing this, a very debated question has been how to keep the privacy of this data without rendering it useless for analysis.

To provide a soultion to this question , data protection rules and regulations have joined over the world, such asGDPR (General Data Protection Regulation , s.d.), and with them the concept of data anonymization that allows the removal of personal identity from data through anonymization techniques. But can these techniques be reversible? Will it be possible to identify the individual again after its application? What data should or should not be anonymized? Such these questions are found in research topics nowdays.

In this article , many ideas about data anonymization will be demonstrated, some of the techniques used for this anonymization will be studied, which are the risks of re-identification related to the analysys of some software tools that allows to play these techniques.
The other sections of this paper will be divided as follows. Section 2 iullstrates the concepts of GDPR, anonymization and pseudonymization. In Section 3, the main techniques used for anonymizing data are presented. Section 4 report the risks associated with the re-identification of each technique. Then, in Section 5, some software is presented that allows applying the techniques described in section 3. Finally, section presents the conclusions of the study and future work.

2. DEFINITIONS AND CONCEPTS

Data anonymization refers to the method of preserving private or confidential information by deleting or encoding identifiers that link individuals to the stored data. It is done to protect the private activity of an individual or a corporation while preserving the credibility of the data collected and exchanged as shown in figure 1 .

Figure 1 - Data anonymization concept

To better understand the framing of this topic, it is necessary to clarify some of the concepts. In this section, we give an understanding what the GDPR consists of and what it means to anonymize data.

GDPR

ISSN: 1737-9334

The GDPR – General Data Protection Regulation – is an official European regulation that aims to harmonize privacy and data protection laws in all member states. It has been applied since May 25th, 2018 (General Data Protection Regulation , s.d.). Generally , this regulation consists of clauses and requirements on how indivisual information and data are treated and is avaliable to all companies operating in the European Economic Area, regardless of their country of origin. The neccessity of stored data have to be anonymized or pseudonymised in such a way that they do not permit to identify any individual again.

Pseudonymization vs. Anonymization

The GDPR has many requirements about how data is treated and differentiates personal data from anonymized and seudonymised data. Therefore, according to article 4 of the GDPR:

- Personal data is "any information relating to an identified or identifiable natural person ('data subject');
- Pseudonymised data is processed personal data that can no longer be attributed to a specific holder without the use of additional information;
- Anonymized data is personal data treated in such a way that it is impossible to re-identify or deduce information about a specific individual.

So, if there is any way to identify the individual data subject, the data were not anonymous but pseudonymized.

Anonymization is important because these data can be used for analysis by companies and does not offer great risks to the data subject because, according to Recital 26, "the principles of data protection should therefore not apply to anonymous information, namely information which does not relate to an identified or identifiable natural person or to personal data rendered anonymous in such a manner that the data subject is not or no longer identifiable." That is, when a dataset is correctly anonymized, GDPR is no longer applicable.

Hence , it is essential to know the data anonymization techniques and how they can be applied

I. DATA ANONYMIZATION TECNHIQUES

If we have to choose the anonymization techniques to be implemented , we must know what is the purpose of this anonymization because the different techniques have different characteristics and may be more or less suitable for certain purposes. The three most used ways to change data are to replace, modify or remove an attribute or a record.

Note that it is important to be able to maintain the usefulness of the data and at the same time respect the privacy terms.

In this section, we describe some of the data anonymization techniques and in what situations they should be applied.

Data swapping

known as shuffling and permutation, a technique used to rearrange the dataset attribute values so they don't correspond with the original records. Swapping attributes (columns) that contain identifiers values such as date of birth, for example, may have more impact on anonymization than membership type values.

Before Anonymization:

Person	First name	Account type	Subscription date	Tickets submitted
1	Luke	Pro	13 May 2017	2
2	John	Enterprise	25 Feb 2016	3
3	Nathan	Free	17 Sep 2014	5
4	Aaron	Free	2 May 2018	2
5	Daniel	Pro	13 Aug 2018	0
6	Michael	Pro	13 Dec 2018	1

In this example, values for all attributes have been swapped:

Person	First name	Account type	Subscription date	Tickets submitted
1	Daniel	Free	13 Dec 2018	1
2	Nathan	Pro	2 May 2018	0
3	Michael	Free	25 Feb 2016	2
4	Luke	Pro	17 Sep 2014	3
5	Aaron	Pro	13 May 2017	5
6	John	Enterprise	13 Aug 2018	2

Remove Attributes (Suppression)

In this technique, an attribute is removed from the dataset. This should happen whenever an attribute is not relevant or necessary for analysis or whenever it is impossible to anonymize it in any other way. In the example given in the Guide to Basic Data Anonymization Techniques (Personal Data Protection Commission Singapore, 2018) for this technique, in which it was intended to analyse students' grades in an assessment test, the dataset was composed of three attributes: student name, trainer and grade. Table 1 shows an example of the original dataset.

Before anonymisation:

Student	Trainer	Test Score
Mohmed	Fatima	93
Saied	Ali	86
Akrm	Ali	54
Ameer	Fatima	78

Table 1: Suppression – Original dataset.

ISSN: 1737-9334

In order to anonymize the data, the attribute “student name” was removed using the technique of removing attributes, according to the table below.
After suppressing the "student" attribute:

Trainer	Test Score
Fatima	93
Ali	86
Ali	54
Fatima	78

Table 2: Suppression – Anonymized dataset.

Suppression can also occur for a complete dataset record affecting several attributes.

The main advantage of this technique is that, when permanently deleting an attribute or record, it becomes impossible to retrieve the information.

Character Replacement

The substitution of characters consists of covering up characters of an attribute or value of the data by replacing those characters with a predefined symbol (for example, by X or *). This substitution can be partial, partially hiding a text or attribute, which may be sufficient to anonymize its content.

Also, in the Guide to Basic Data Anonymization Techniques (Personal Data Protection Commission Singapore, 2018), an example can be found in which to make an analysis of a dataset where the post code was identified, the last 4 digits of the post code were replaced by the character ‘X’. Table 3 shows the original dataset and the anonymized dataset.

Before anonymisation:

Postal code	Average No.of Orders/month
100111	2
200222	8
300333	1

After suppressing the"student"attribue:

Postal code	Average No.of Orders/month
10xxxx	2
20xxxx	8
30xxxx	1

Table 3: Example of replacing characters.

Shuffling

In this technique, the data is randomly mixed or reorganized and the values of the original attributes remain in the dataset but can be associated with another record. This technique can be used when it is intended to analyse only one attribute and it is not necessary to relate it to the others.

For instance , if we want to analyse the amount of sales in a given region, it is only necessary to use the attribute ‘region’ and the permutation does not influence the results because a certain region will occur the same number of times before and after the permutation.

However, this technique does not always provide anonymization of the data and it may be possible to reorganize it to its original form. Therefore, it must be used in conjunction with other techniques.

Noise Addition

The addition of noise is one of the most used data anonymization techniques, being applied by several technological “giants” such as Google (Google, s.d.). The technique is to slightly modify the attributes of the dataset making them less accurate. An application of this technique is, for example, to add or subtract days or months to a date. Although this technique allows to hide the authentic values, it is necessary to understand the level of noise that must be applied in order to have small impact on data analysis and individuals’ privacy.

Generalization

Generalization is another approach used by Google (Google, s.d.) and consists of generalizing the attributes in order to change the respective scale or order of magnitude.

An example of this is to change the “date”attribute (day/month/year) with the “year” attribute, removing the day and month.

Like the addition of noise, this approach may provoke the individual from being identified, but it may not result in effective anonymization.

There are two techniques that can be considered generalization: K-Anonymity and L-Diversity, described in the following subsections.

K-Anonymity

This technique consists of grouping the records of K individuals into categories making them fall under the same combinations. Thus, each record in the dataset “is similar to at least K-1 other records” (El Emam, 2008).

For example, if the identifying attributes are age and disease and K=3, the dataset anonymized by this method will have at least 3 records for each combination of the identifying attributes. Considering the two individuals in the example illustrated in table 4, the result of k-anonymity with K=3 would be the one illustrated in table 5.

Ali	
Age	Disease
21	Heart Disease

Omar	
Age	Disease
38	Cancer

Table 4: K-Anonymity: original dataset.

Age range	Disease

ISSN: 1737-9334

20-30	Heart Disease
20-30	Heart Disease
20-30	Heart Disease
30-40	Cancer
30-40	Cancer
30-40	Cancer

Table 5: K-Anonymity: original dataset.

After the application of K-Anonymity, the probability of identifying an individual is equal to or less than 1/K. Therefore, the higher the K, the lower the probability of identification.

L-Diversity

Based on Machanavajjhala et al. (2007), L-Diversity is an evolution of K-Anonymity in which at least L distinct values must exist for each equivalent group and sensitive attribute (identifier). That is, it is guaranteed that in each equivalent group each attribute has at least L different values.

The objective of this technique is to limit the occurrence of equivalence classes with low variability of the attribute. Thus, an intruder who has access to data for specific individual always remains with a degree of uncertainty.

However, this technique is susceptible to attacks of probabilistic inference.

2. DATA ANONYMIZATION TOOLS

As mentioned earlier, there is anonymization software that allows to systematically apply the techniques described.

Based on the work developed in 2014 by Bergeat et al. (Maxime Bergeat, 2014) and in 2017 by Pinho (Pinho, 2017), software for these purposes are presented below.

ARX

ARX is an open source framework developed in Java (ARX, s.d.). It allows to implement several of the techniques described, such as K-Anonymity and LDiversity, and also to implement a set of metrics to assess the loss of information.

This software has a graphical tool with a simple and intuitive interface, shown in Figure 2, which supports the import and cleaning of data, wizards for creating transformation rules, intuitive ways to adapt the anonymized dataset to the requirements and visualizations of risks and re-identification.

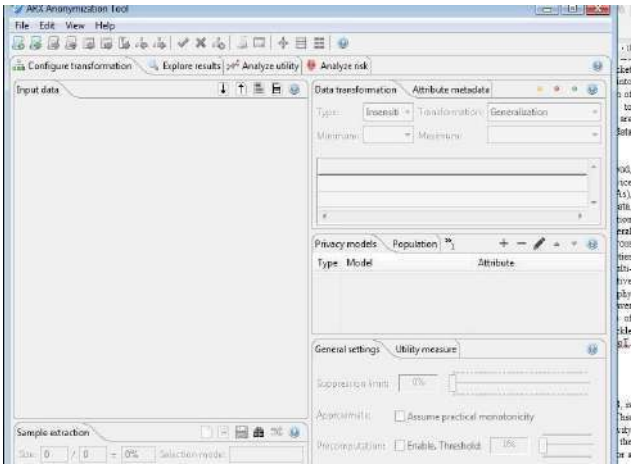

Figure 2: ARX Interface.

ARX is also available as a library with an API that provides data anonymization capabilities for any Java program. ARX is compatible with SQL databases, Microsoft Excel and CSV files.

Succinctly, to perform anonymization, we start by importing the dataset, defining the indicators and sensitive variables and defining the generalization hierarchies. At the end, the transformations are extracted.

µ-Argus

Argus stands for 'Anti Re-identification General Utility System' and is a software developed to create safe microdata files (MU-Argus, s.d.). It is based on R programming language and uses different statistical methods of anonymization such as noise addition and suppression. It can also be used to generate synthetic data. Its interface can be seen in Figure 3.

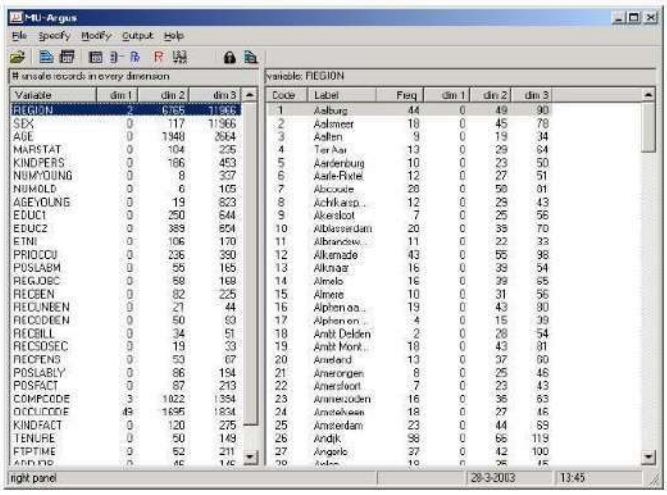

Figure 3: µ-Argus Interface.

Anonymization steps involve defining sensitive indicators and variables, estimating the risk of disclosure and re-identification, implementing methods that reduce this risk and exporting microdata.

SDCMicro

SDCMicro is a free open source package for researchers and public use (International Household Survey Network, s.d.).

ISSN: 1737-9334

Can be used to generate anonymous data by creating files that can be used by the public and scientific researchers.

This tool allows to apply various anonymization techniques such as suppression, adding noise and shuffling and includes functions to measure the risk throughout the process.

It is provided as a user-friendly GUI in which users unfamiliar with R can implement anonymization methods. Supports the import and export of microdata in various formats such as STATA, SAS, SPSS, CSV and R.

Figure 4 shows its interface.

Figure 4: SDCMicro Interface.

One of the advantages of this tool is that it includes functions to measure, visualize and compare risk and utility during the anonymization process, helping organizations to prepare reports.

3. Software vs Techniques

Table 6 shows the software listed above and which is usually used for the application of the studied techniques.

Table 6: Software vs Techniques.

Software/Tool	Techniques
ARX	Generalization K-Anonymity L-Diversity Suppression
μ-Argus	Noise Addition; Suppression
SDCMicro	Noise Addition Suppression Shuffling

4. CONCLUSIONS AND FUTURE WORK

Privacy is very important to the sensitive data from the attacker. To provide privacy to the data anonymization methods can be used. In this paper anonymization is done by using K-anonymity method in arx tool. The experimental results show the difference between the original and the anonymized data. On this anonymized datamining applications can be applied using the weka tool.

Anonymization is an important issue that has been increasingly demanding the attention of the community. With the large volume of personal data available for analysis and treatment there is a need to ensure the privacy of individuals.

Anonymization is an important issue that has been increasingly demanding the attention of the community. With the large volume of personal data available for analysis and treatment there is a need to ensure the privacy of individuals.

As future work, we intend to test each of these tools with real datasets and evaluate the anonymization performance of each one.

REFERENCES

- *UN study reveals world has gender digital divide*. (2019, November 9). Retrieved from ONU News: https://news.un.org/pt/story/2019/11/1693711
- *General Data Protection Regulation* . (n.d.). Retrieved from Intersoft Consulting: https://gdpr-info.eu/
- Recital 26 - EU GDPR https://www.privacy-regulation.eu/en/recital-26-GDPR.htm
- Personal Data Protection Commission Singapore. (2018, January 25). Guide to Basic Daa Anonymisation Techniques. pp. 12, 13.
- El Emam, K. &. (2008). Protecting Privacy Using KAnonymity. *Journal of the American Medical Informatics Association*, pp. 627-637.
- Maxime Bergeat, N. C.-B. (2014). A French Anonymization Experiment with Health Data. *Privacy in Statistical Databases.* Eivissa, Spain.
- MU-Argus. (n.d.). Retrieved from http://neon.vb.cbs.nl/casc/mu.htm
Personal Data Protection Commission Singapore. (2018, January 25). Guide to Basic Daa Anonymisation Techniques. pp. 12, 13.

ISSN: 1737-9334

Modeling and Performance Investigation of 16-QAMModulation with and without Applying TCM CodingTechnique over Different Communication Channels

Sana Ahmed Abdaljlil
Faculty of Engineering,Sabartha University
Sabratha, Libya
sana.abdaljlil@gmail.com
ORCID 0000-0003-1504-3647

Amer R. Zerek
Libya Open University
Tripoli, Libya
a.zarieg@staff.ou.edu.ly
ORCID **0000-0002-4095-8171**

Ol Olga Boiprav
Information Protection Deprt.
Belarusian State University
of Informatics and Radioelectronics
Minsk, Belarus
smu@bsuir.by
ORCID 0000-0002-9987-8109

Abstract— **Wireless communication technologies are modern technology that requires improved speed, reliability, higher data rates, and spectral efficiency that achieve better channel capacity requirements. Multi input multi output (MIMO) systems with multiple antenna elements at both link ends are an efficient solution to enhance the system performance under the constraints of limited bandwidth and transmit power by using orthogonal space-time block code (OSTBC). Modulation schemes and coding techniques were evaluated and compared in terms of the Bit Error Rate (BER).**

In this project it will investigate the evaluation of the BER performance of unencoded and Trellis Coded Modulation (TCM) encoded OSTBC 2×2 and 3×3 MIMO systems consecutive with 16-QAM over AWGN and fading channels.

The simulated results indicate that the more Eb/No power is required for unencoded 16-QAM to achieve the same BER compared to coded 16-QAM Therefore, the application of the coding technique improved and enhanced the overall performance . Also, in both cases with or without coding technique over the AWGN channel, it gives better performance compared to the Rician and Rayleigh channels.

Keywords—TCM, OSTBC , bit error rate and QAM

I. INTRODUCTION

Digital modulation offers many advantages over analog modulation and greatly improves the performance of the communication systems. Many types of digital modulation schemes are possible, and the choice of which one to use depends on spectral efficiency, power efficiency, and bit error rate performance[1]. There are three main types of digital modulation schemes such as a Binary Amplitude Shift Keying (ASK), , Phase Shift Keying (PSK) and Frequency Shift Keying (FSK) as well as an M-ary QAM, M-ary FSK and M-ary PSK . In this work the 16- QAM modulation [2]. with and without Applying TCM coding technique over AWGN and fading channels scheme will be considered. [1, 2].

16 QAM scheme is one of most efficient digital data transmission systems as it achieves better bandwidth efficiency than other modulation techniques and gives higher data rate. In an sixteen level signaling scheme, one of 1 possible signals $s_1(t),s_2(t)\ldots s_{16}(t)$ can be transmitted, during each signaling interval of duration T_s. For almost all applications, the number of possible signals: $M = 2^4$.

TCM modulation is channel coding (TCM modulation was invented by Gottfried Under back 1982). TCM employed to improve coding gain which allows efficient transmission over limited wireless channel bandwidth. The functions of convolutional coder and mapper in TCM with rate of k/(k+1), where k is integer number and M-array mapper with $M=2^k$ provides large constellation of $M=2^k+1$, Constellation diagram.

An M-ary digital modulation technology plays an important role in transmission of signals over various of, communication channels in all communication systems. M-ary QAM types of modulation that can be used to improve the performance of the communication system in various environment e.g for M=16 , although a price is paid by injecting more signal energy to maintain an acceptable level of BER . However by applying the TCM coding technique over AWGN and fading (, Rayleigh and Rician) channels using Multi Input Multi Output (MIMO) system hopefully improve 16-QAM system performance and give an acceptable BER performance compared with system without applying TCM. [3-5],

II. WIRELESS COMMUNICATIONS SYSTEM

Nowadays, the demand for usage and capacity of wireless networks has grown effectively due to the rapid development and advancement in technology. Wireless communication at high transmission speed has become one of the most exciting areas of modern engineering. Therefore, to deal with the ever-

ISSN: 1737-9334

increasing bandwidth to meet the high demand, multiple antennas at the sending and receiving ends can help solve this problem by making high data rate possible [1]. Wireless network efficiency can be improved by deploying more compact wireless access points as well as using more spectrum. We can also increase the spectral efficiency allowing to improve the number of bits per second that can be transmitted per unit of bandwidth. Potential wireless networks and technologies could use an increasing density of access points, including the use of different spectral information. However, the necessity to improve the spectral efficiency in each band will always be the main objective. Fig.1 is showing the wireless communication system. [3].

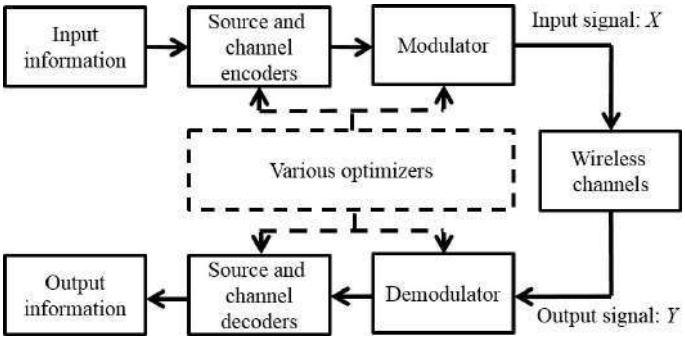

Fig. 1. Block-Diagram-of-a-Wireless-Communication-System

III. MIMO - OSBTC SYSTEM

A channel with multiple antennas at the transmitter and multiple antennas at the receiver is called a multiple-in-multiple-out (MIMO) channel, whereas the SISO channel has a single antenna at the transmitter and a single antenna at the receiver. The data rate in MIMO can be improved by using special coding schemes such as TCM with quadrature phase-shift keying (QPSK) while reliability is further enhanced by OSTBC diversity technology on fading wireless communication and limited bandwidth channels. OSTBC was used in MIMO using MLE technology with TCM technique. [5-8].

The OSTBC contains two types, a generic and a simple layout. MIMO techniques can be defined as antenna technologies for wireless communications in which multiple antennas are operated at both Transmitter (Tx) and Receiver (Rx) sides. That system uses m^{th} antennas at the transmitter (m_T) and n^{th} antennas at the receiver (n_R) i.e. ($m_T \times n_R$).

MIMO systems are mainly used to get a higher overall data rate for a wireless link. However, different kinds of multi-antenna systems can be used namely, Multi Input Single Output (MISO), Single Input Multi Output (SIMO), and Single Input Single Output (SISO). MIMO techniques provide several benefits including minimizing the effects of fading, improving the quality of service with enhanced spectral efficiency, increasing data rates, and reaching a reduced BER. Nevertheless, it suffers from a few disadvantages such as increased cost, hardware complexity growth, and higher power consumption of hardware while the battery gets depleted quickly because of complex computations processing [7, 9].

The generalized OSTBC uses more than two antennas and the code rate is less than one. With a fixed number of receiving antennas and increasing the number of antennas at the transmitter. In Alamouti the symbols are sent in two groups. The Tx in Alamouti matrix code which is allocated along time and space is viewed as a special case of generic OSTBC at a certain rate. Figure (2.4) shows the OSTBC model.

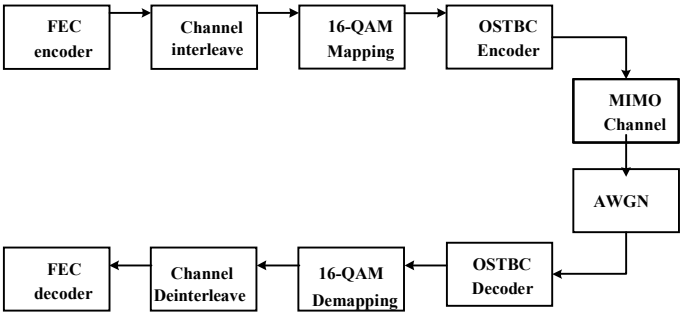

Fig. 2 OSTBC system model

In this paper, a 2x2 and3 3x3 MIMO systems are clarify in the following points:

A) 2x2 MIMO Model

The MIMO scheme of two antennas on both sides Tx and Rx, i.e., 2×2 is considered as illustrated in Fig.3.

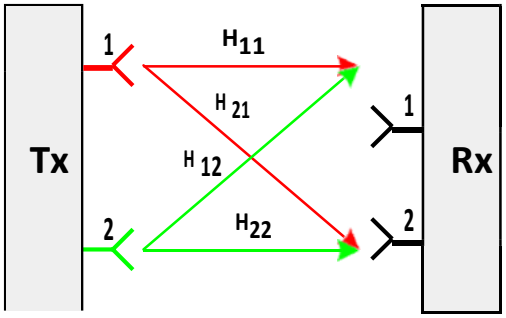

Fig. 3 2x2 MIMO system Model

Referring to the ref [}, for the 2 for both transmitting and receiving antennas, the general equation for received signal (R) at the input of the receiver is given by

$$R_i = H_{mn}.S_i + N_i \quad (1)$$

Where

i, m and n =1,2,…

R is the received signal matrix

'S is the transmitted signal matrix

H is the channel matrix, and N is the noise vector

The following matrix represents the above-mentioned equation for 2x2 MIMO.

$$\begin{bmatrix} R_1 \\ R_2 \end{bmatrix} = \begin{bmatrix} H_{11} & H_{12} \\ H_{21} & H_{22} \end{bmatrix} \begin{bmatrix} S_1 \\ S_2 \end{bmatrix} + \begin{bmatrix} N_1 \\ N_2 \end{bmatrix} \quad (2)$$

Where

ISSN: 1737-9334

R_1 *and* $R_2$are the Received signals.

H_{nm} is 2x2 channel matrix

S_1 *and* S_2 are the transmitted signals and N_1 and N_2 are the noise signals

For n and m=1and 2

B) 3x3 MIMO Model

The MIMO scheme of three antennas on both sides Tx and Rx, i.e. 3x3 is considered as illustrated in Fig.4. 0

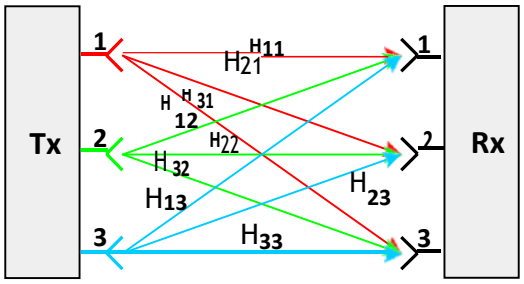

Fig.4 3x3 MIMO system Model

The following matrix represents the equation (1) for 3x3 MIMO.

$$\begin{bmatrix} R_1 \\ R_2 \\ R_3 \end{bmatrix} = \begin{bmatrix} H_{11} & H_{12} & H_{13} & H_{14} \\ H_{21} & H_{22} & H_{23} & H_{24} \\ H_{31} & H_{32} & H_{33} & H_{34} \end{bmatrix} \begin{bmatrix} S_1 \\ S_2 \\ S_3 \end{bmatrix} + \begin{bmatrix} N_1 \\ N_2 \\ N_3 \end{bmatrix} \quad (3)$$

Where

R_1, R_2 *and* R_3 are the Received signals.

H_{nm} is 3x3 channel matrix

S_1, S_2 *and* S_3 are the transmitted signals and N_1, $N_2$and N_3 are the noise signals

For n and m=1,2and 3

IV. Quadrature Amplitude Modulation

Quadrature Amplitude Modulation, QAM is a signal in which two carriers shifted in phase by 90 degrees (i.e., sine and cosine) are modulated and combined. As a result of their 90° phase difference, they are in quadrature and this gives rise to the name. Often one signal is called the In-phase or "I" signal, and the other is the quadrature or "Q" signal. The resultant overall signal consisting of the combination of both I and Q carriers contains of both amplitude and phase variations. In view of the fact that both amplitude and phase variations are present it may also be considered as a mixture of amplitude and phase modulation. The mathematical formula of M-ary QAM is given by [4].

$$s_i(t) = a_i \cos(2\pi f_c t) + b_i \sin(2\pi f_c t)$$

Where $0 \le t \le T$; $i = 1, 2, \ldots M$ (4)

In M-ary QAM modulation, data is transmitted through a signal created by adding carrier signal amplitude and phase modulations such as a sine wave and a modulated sine wave or square wave. Moving more bits per position change can be achieved because there are still a lot of shift points. The constellation points are arranged in a square grid with horizontal and vertical equal distances on a constellation chart (other configurations can also be made). Since data is binary in digital communications, the number of points in the grid will typically be a function of the power of 2, $M = 2^n$. , where n = 1,2,3,…. Because the modulation of the quadratic amplitude is usually square. Fig. 5 illustrated the constellation diagram of 16-QAM .[10, 11].

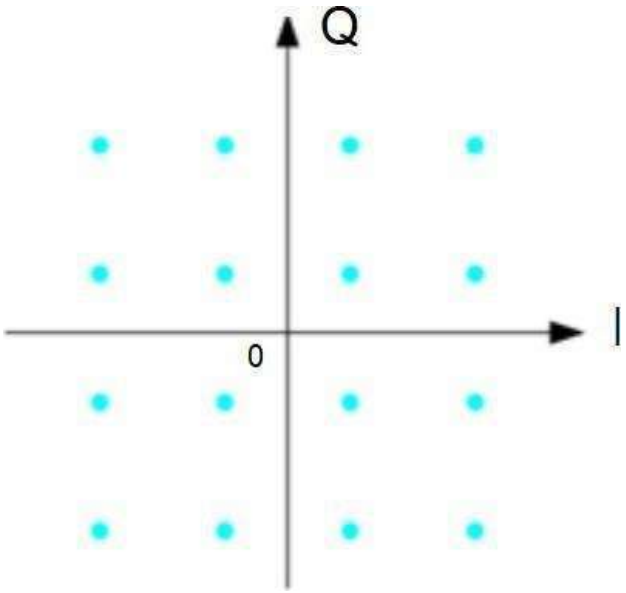

Fig. 5 Constellation diagram of 16-QAM

V. Trellis Coded Modulation

Interferometrycode modulation (TCM) is one of the coding techniques used in digital communications. It combines the choice of modulation scheme and the choice of convolutional code together for the purpose of gaining noise immunity over uncoded transmission without extending the signal bandwidth or increasing the transmitted power.

In a power-limited communication system, the required system performance must be achieved at the smallest possible transmitted power. One solution is to use error-correcting codes, which increase energy efficiency by adding redundant bits to the transmitted sequence. This procedure requires the modulator to operate at a higher data rate and therefore an extended bandwidth. In a band-limited system, an increased frequency utilization efficiency can be obtained by choosing higher order modulation schemes, but greater signal power will be required to maintain the same separation distance between signals, and thus the same error probability. The TCM solution combines the selection of a highly ordered modulation scheme with a convolutional code system. It can reap the benefits of coding without increasing the bandwidth. Fig. 5 illustrated the TCM modulation. [12-14].

ISSN: 1737-9334

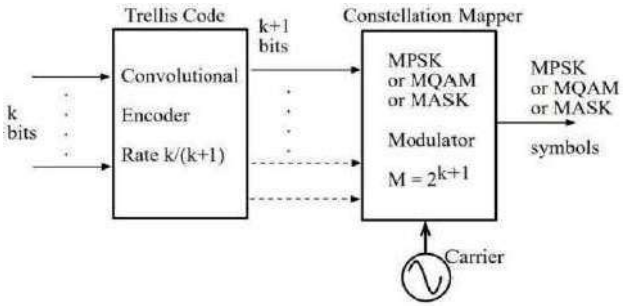

Fig. 6 Trellis coded Modulation

VI. OSTBC WITH TCM

OSTBCs are possibly the most popular and broadly used space-time (ST) codes and are an attractive technique for MIMO wireless communications. That OSTBC has several advantages such as It achieves full spatial diversity, optimal maximum likelihood decoding can be performed symbol-by-symbol quite easily and extract all array gain at the receiver side …etc. but it suffers from some draw backs such as the multiplexing gain for OSTBCs accords with the code rate is limited to 1. [11, 12].

In a MIMO communication system, OSTBC and TCM aim for full diversity gain with cipher gain over Rayleigh and Rician communication channels, with a relatively easy-to-use but complex encoder and decoder designed with the advantage of transmitting higher rate data without the requirement for increased bandwidth. The OSTBC model sequential with TCM structure is illustrated in Fig.7 .[7-10].

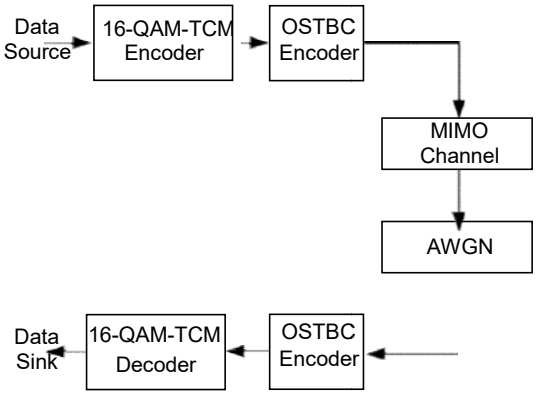

Fig. 7. OSTBC with TCM model

VII. SIMULATING A 2X2 AND 3X3 MIMO SYSTEM COUPLED TO 16- QAM WITHOUT AND WITH TCM OVER THE DIFFERENT COMMUNICATION CHANNELS

The typical 16-QAM without and with TCM are constructed using Simulink as shown in Fig 8, over the AWGN, Rayleigh, and Rician communication channels. Fig. 8 represents the simulation model for 16-QAM and 16-QAM-TCM systems. That model includes the following components:

Binary data source to generate random binary numbers using a Bernoulli distribution, 16-QAM modulator to generate the modulated signal, OSTBC encoder to encode an input symbol sequence using space-time OSTBC, communication channels is used to pass the information through it, OSTBC combiner which combines the input signal from all of the receive antennas and the channel estimate signal to take out the soft information of the symbols that were encoded using an OSTBC, Rectangular QAM Demodulator which demodulates a signal that was modulated using 16-QAM modulator and error rate calculation is used to compute the BER.

The 16-QAM -TCM model is similar to the 16-QAM model shown in Fig. 8 just replace 16-QAM modulator/demodulator by 16-QAM -TCM blocks . Where the Rectangular QAM-TCM Encoder block implements TCM by convolutionally encoding the binary input signal and mapping the result to a 16-QAM signal constellation. In contrast, the Rectangular QAM TCM Decoder block uses the Viterbi algorithm to decode a trellis-coded modulation (TCM) signal that was formerly modulated using a QAM signal constellation. These blocks have largely replaced ones. [10, 12].

After construction and setting all simulation parameters for each box of the 16-QAM and 16-QAM-TCM models illustrated in Fig. 8, the obtain simulation results will be explained in the following section.

VIII. SIMULATION RESULTS

The obtained simulation results demonstrated the relationship between the Eb/No and BER of the 16-QAM without and with TCM model which shown in Fig. 8 for 2x2 and 3x3 MIMO system over AWGN, Rican and Rayleigh channels. That simulation results are presented in the following points:

A. AWGN channel

After constructing and arranging the simulation model settings shown in Fig. 6, the simulation result for BER vs. Eb/No performance is shown in Fig. 9.
Referring to the achieved results, 16- QAM-TCM out performs 16- QAM when BER=10^{-5} by about 3.9 and 5.7 dB in energy savings on average for 3x3 and 2x2 MIMO systems, respectively.

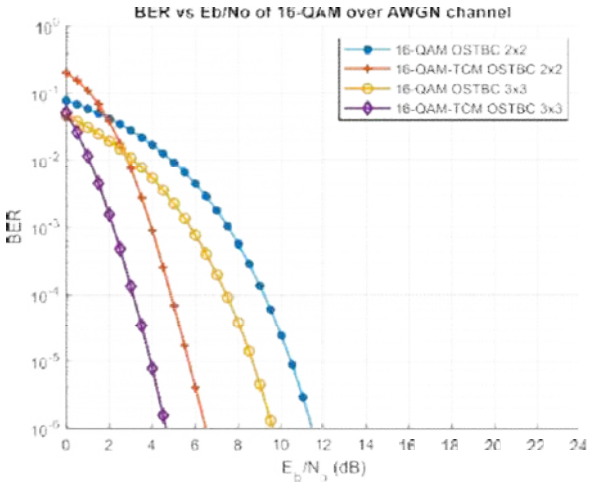

Figure 9 . E_b/N_o v.s. BER for 16-QAM without and with TCM MIMO 2x2 and 3x3 over AWGN Channel

ISSN: 1737-9334

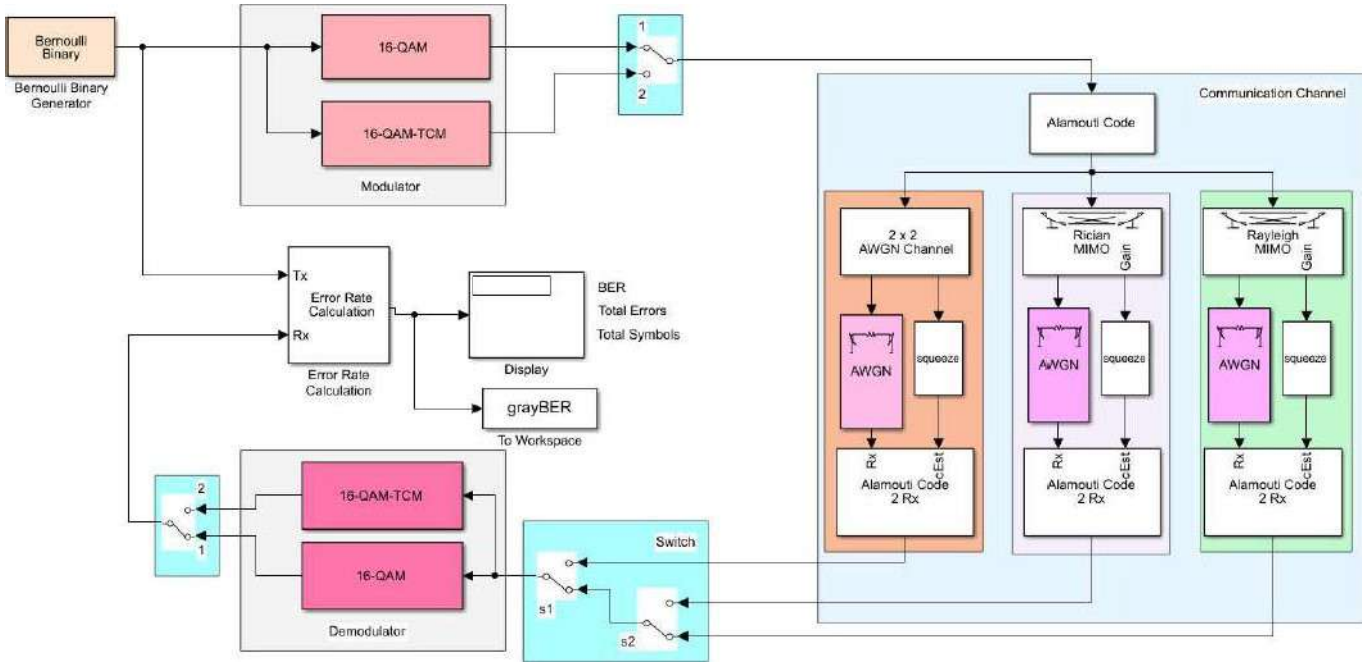

Fig. 8. QAM without and with TCM Model Over AWGN and Fading Channels

B. *Rican Channel*

In this case using the same producer in point A just replacing the AWGN channel by Rician , furthermore the reached result is characterized the relation between the Eb/No v.s BER of 16-QAM without and with TCM for 2x2 and 3x3 MIMO systems as illustrated in fig.10.

From the reached simulation results, it noted that-QAM-TCM has better BER performance with respect to 16-QAM without TCM.

when BER=10^{-5} by about 10.5 and 13.5 in energy savings on average for 3x3 and 2x2 MIMO systems respectively.

C. *Rayleigh channel*

This case is similar to the case in points A and B just using the Rayleigh channel instead of AWGN and Ricia, moreover the gotten simulation result is categorized the relation between the Eb/No and BER of 16-QAM without and with TCM for 2x2 and 3x3 MIMO systems as illustrated in fig.11.

From the achieved results it observes that 16-QAM with TCM appeared better BER performance compared with 16-QAM by about 18 and 12.5 dB in saving average power for 2x2, and 3x3 OSTBC MIMO system respectively

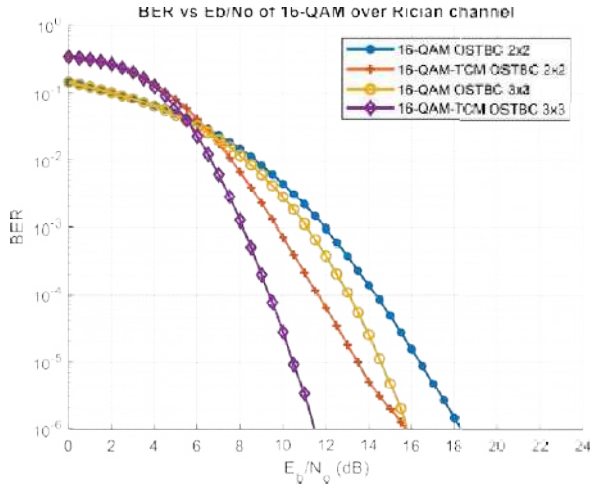

Fig 10 . BER vs. E_b/N_o for 16-QAM without and with TCM MIMO 2x2 and 3x3 over Ricain Channel

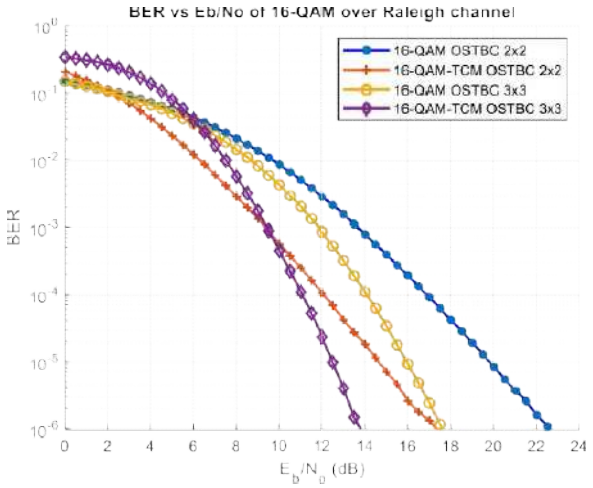

Fig 11. E_b/N_o v.s. BER of 16-QAM and 16-QAM-TCM MIMO 2x2 and 3x3 MIMO over Rayleigh Channel

ISSN: 1737-9334

VIIX CONCLUSION

This paper constructed and simulated model of using 16-QAM without and with TCM over the three different communication channels such as AWGN, Rician, and Rayleigh.

The simulation results obtained confirmed the BER performance when these three different communication channels were considered. It was very clear that in order to achieve better BER performance, a more signal energy (Eb/No) was required. Mainly when it's 16-QAM compared to 16b-QAM-TCM

Moreover, the system model performs better in terms of BER in both 16-QAM without and with TCM situations when the transmitted signal is transmitted over an AWGN channel instead of the Rician and Rayleigh channels.

REFERENCES

[1][2] L. W. Couch, II, " Digital and Analog Communication Systems ", 8th Edition , 2013.

[2][3] A. Carlson Bruce, Communication Systems ",An introduction to Signal and Noise in Electrical Communication , -Hall, New York, 5th edition, 2018.

[3]T., David, and Pramod Viswanath. Fundamentals of wireless communication. Cambridge university press, 2005.

[4]K.. F. Alhaddar , A. M. Daeri and A. R. Zerek, "Modelling and Performance Analysis of RF Satellite Link System Using 16 QAM ", 5th International Conference on Green Energy & Environmental Engineering (GEEE – 2018), , Sousse – Tunisia, April 28 – 30, 2018.

[5]J. K. Daksh, R. Mohan, and S. Sharma, "Performance analysis with space-time coding in MIMO-OFDM Systems with multiple antennas", Int. J. of Adv. Comp. Res., vol. 3, no. 2, issue 10, 2013 [Online]. Available: https://www.accentsjournals.org/PaperDirectory/Journal/ IJACR/2013/6/17.pdf.

[6]R. Vithiya, V. Karthika, P. Samundeeswari, and S. Mohanraj, "Trellis coded modulation for MIMO wireless communication system", Int. J. of Engin. Res. and Technol., vol. 2, no. 12, pp. 2577–2583, 2013 [Online]. Available: https://www.ijert.org/research/ trellis-coded-modulation-for- mimo-wireless-communication-system-IJERTV2IS120927.p

[7]A. A. Kreshchuk and V. V. Zyablov, "Generalized concatenated system with embedded space-time codes for MIMO systems", J. of Commun. Technol. and Electron., vol. 59, no. 12, pp. 1489–1500, 2014 (DOI: 10.1134/S1064226914120109).

[8]S. A. K. Alrufaiaat and A. Q. J. Althahab, "Robust decoding strategy of MIMO-STBC using one source Kurtosis based GPSO algorithm", J. of Ambient Intell. and Human. Comput., 2020 (DOI: 10.1007/s12652-020-02288-1).

[9]S. R. Chopra, A. Gupta, and H. Monga, "Performance analysis of space time trellis codes in Rayleigh fading channel", in Harmony Search and Nature Inspired Optimization Algorithms, N. Yadav et al., Eds. Advances in Intelligent Systems and Computing, vol. 741, pp. 957–967. Springer, 2019 (DOI: 10.1007/978-981-13-0761-4 90).

[10] S.A. Abdaljlil, H. Almqadim,A. R. Zerek and Y. Jaradat, " BER Performance Investigation of OSTBC-MIMO Systems Concatenated with QAM-TCM Over AWGN and Fading Channels", 2022 IEEE 21st international Ccnference on Sciences and Techniques of Automatic Control and Computer Engineering (STA) , December 19-21, 2022, Sousse-Tunisia, 2022.

[11] . *M. Hamdona , A. O. Althini,* A. M. Daeri *and* A. R. Zerek," *Performance Assessment and Computer Simulation of the M-ary QAM Modulation Schemes".",* 2020 17th International Multi-Conference on Systems, Signals & Devices (SSD). Julyu 20-23, 2020, Sfax, Tuinisia, 2020.

[12] Q. Jing and J. Wu, "Performance comparison of space-time block and trellis codes in the MIMO land mobile satellite channels", Radio electron. and Commun. Syst., vol. 60, no. 1, pp. 3–17, 2017 (DOI: 10.3103/S0735272717010010).

[13] L. R. Krushnarao1 , Akhila S2 "Performance Analysis of MIMO Systems for Wireless Communication using Adaptive Modulation Technique" International Journal of Science and Research (IJSR) Volume 5 Issue 8, August 2016.

M.V. Dave, Dr. P. Dholakia and Dr. D. Kamdar, "Performance Analysis of TCM OSTBC MIMO System in Different Fading Environment", International Journal on Future Revolution in Computer Science & Communication Engineering Vol: 4 Issue: 4 April 2018.

ISSN: 1737-9334

Intelligent Protection of the Electrical Power Transmission Network

Nejib Khalfaoui
ISET Jendouba
LR SITI - ENIT
nejibkhalfoui@gmail.com

Mohamed Salah Salhi
National Engineering School of Tunis
LR SITI - ENIT
msalah.salhi@gmail.com

Tahar Bahi
Badji Mokhtar University
Department of Electrical
tbahi@hotmail.fr

***Abstract*—**This article presents an intelligent strategy using the technique of remote distance protection, which is perfectly adapted to very fast intelligent reclosing applications, for the protection of an electricity transmission line. It accredits mathematical modeling of the electrical energy transmission network. This approach thus makes it possible to identify the most important faults and phenomena that can disturb a high-voltage electrical transmission network. It also ensures the submission of measurements of frequent faults on the network in real time.

Key words: transmission line, electrical network, smart protection,short circuit, fluctuation.

I. INTRODUCTION

Electricity-producing power stations are often far from majorconsumptioncities. Their location depends either on geographical conditions, on the supply of fuel, on the supply of cooling water, or on environmental requirements.

However, the kilowatt-hours obtained must reach their users and must therefore cover long and complex journeys.

The electricity transmission network provides a permanent link between production centers and places of consumption. Such a network is mainly made up of HTB/HTB or HTB/HTA transformer stations connected by transmission lines [1,2].

An electrical network must also ensure the dynamic management of the entire production, transport and distribution by making adjustments aimed at ensuring the stability of the system (the frequency, the supply voltage must be stable and the concordance of the phases (synchronism)). [3,4].

Large-scale protection systems for transmission and primary distribution circuits suitable for automatic resetting of circuit breakers are regularly developed.Figure 1 below provides us with a representative sample of an electric power transmission diagram [5].

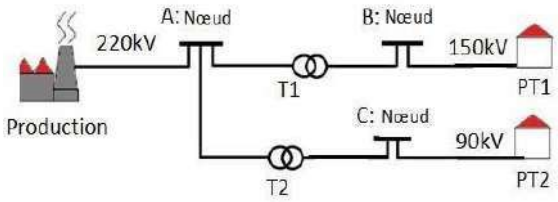

Figure 1. Diagram of electric power transmission

II. MODELINGOF THE TRANSPORT NETWORK

An electricity transmission network can be represented according to the following architecture, figure 2.

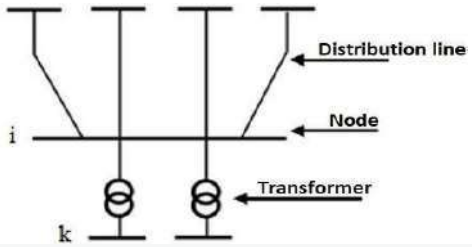

Figure 2.Synopticdiagram of a transport network

High-voltage transformers start at the power plant. They must be of the step-up type in order to neglect voltage drops and losses in the lines [5,6,12]. They can be coupled in parallel or individually in order to provide the subscribers with the necessary energy.

III. ELECTRICAL STATE OF THE NETWORK

Knowledge of the electrical state of the network is essential to determining the power balance in view of carrying out the load distribution. In order to standardize the notations and the representations, we consider both the transformer and a line diagram in (pi) as shown in figure 3.

ISSN: 1737-9334

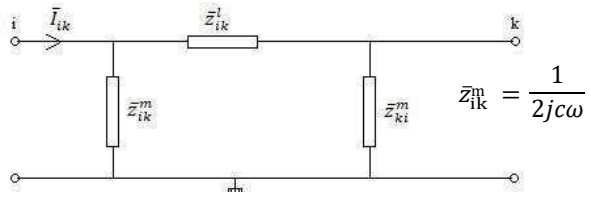

Figure 3.Equivalent diagram of the link between node i and k.

$$\bar{V} = \bar{Z}\bar{I} \quad \text{ou} \quad \bar{I} = \bar{Y}V \tag{1}$$

In the case of a line,we adopt the following expressions:

$$\bar{y}^{l}_{ik} = G_{ik} + jB_{ik} \tag{2}$$

Having: $_{ik} = \frac{R_{ik}}{z^2_{ik}}$; $B_{ik} = -\frac{K_{ik}}{z^2_{ik}}$ and $\bar{y}^{m}_{ik} = \bar{y}^{m}_{ki} = 2jcw$

A. Transited power and losses

The power transmitted on the linksi and k is the quantity expressed as follows:

$$\bar{S}_{ik} = \bar{v}_i \bar{I}^{*}_{ik} \tag{3}$$

This quantity is calculated, during the losses in active and reactive parts of the connection, by the algebraic sum of the transited powers as follows:

$$\bar{S}_{ik} = \bar{S}_{ik} + \bar{S}_{ki} = P_{ik} + jQ_{ik} \tag{4}$$

$$S_{ki} = S_{ki} + S_{ik} = P_{ki} + jQ_{ki} \tag{5}$$

$$\bar{I}_{ik} = \bar{y}^{m}_{ik}\bar{v}_i + \bar{y}^{l}_{ik}(\bar{v}_i - \bar{v}_k) \quad , \quad \bar{S}_{ik} = \bar{v}_i[(\bar{y}^{m}_{ik} + \bar{y}^{l}_{ik})\bar{v}^{*}_{i} - \bar{y}^{l*}_{ik}\bar{v}^{*}_{k}] \tag{6}$$

let's put :$\bar{y}^{m}_{ik} = G^{m}_{ik} + jB^{m}_{ik}$

$$\bar{y}^{l}_{ik} = G^{l}_{ik} + jB^{l}_{ik} \quad ; \; \bar{v_i} = v_i \angle \alpha i$$

So, the equation becomes as:

$$S_{ik} = P_{ik} + jQ_{ik} = v^2_i[(G^{m}_{ik} + G^{l}_{ik}) - j(B^{m}_{ik} + B^{l}_{ik})] - v_i v_k[\cos(\alpha i - \alpha k) + j\sin(\alpha i - \alpha k)][G^{l}_{ik} - B^{l}_{ik}]$$

$$P_{ik} = v^2_i(G^{m}_{ik} + G^{l}_{ik}) - v_i v_k[G_{ik}\cos\alpha_{ik} + B^{l}_{ik}\sin\alpha_{ik}] \tag{7}$$

Having: $\alpha = -\alpha_i$

$$_{ik} = -v^2(B^{m} + B^{l}) - v\,v\,[G^{l}\sin\alpha \quad -B^{l}\cos\alpha] \tag{8}$$
$$_{ik} \quad _{i} \quad _{ik} \quad _{ik} \quad _{i}\,_{k} \quad _{ik} \quad _{ik} \quad _{ik} \quad _{ik}$$

To find P_{ki}, and Q_{ki}, it suffices to permute i and k in the expressions (7) and (8).Thus we find the following relations.

$$P_{ki} = v^2_k(G^{m}_{ki} + G^{l}_{ik}) - v_i v_k[G^{l}_{ik}\cos\alpha_{ik} - B^{l}_{ik}\sin\alpha_{ik}] \tag{9}$$

$$Q_{ki} = -v^2_k(B^{m}_{ki} + B^{l}_{ik}) - v_i v_k[-G^{l}_{ik}\sin\alpha_{ik} - B^{l}_{ik}\cos\alpha_{ik}] \tag{10}$$

According to the notations ($\bar{y}_{ij}, \theta_{ik}$)the injected current is written as follows:

$$\bar{I}_i = \sum^{n}_{k=1} \bar{y}_{ik} v_k = \sum^{n}_{k=1} y_{ik} v_k e^{j(\alpha_k + \theta_{ik})} = I_{Ai} + jI_{Ri} \tag{11}$$

$$S_i = \sum^{n}_{k=1} y_{ik} v_k v_i e^{j(\alpha_i - \alpha_k - \theta_{ik})} = P_i + jQ_i \tag{12}$$

This allows us to write equations 1 and 2 on the new form:

$$P_i = \sum^{4}_{k=1} y_{ik} v_i v_k \cos(\alpha i - \alpha k - \theta_{ik}) = R(S_i) = R(v_i I_i) \tag{13}$$

$$Q_i = \sum^{4}_{k=1} y_{ik} v_i v_k \sin(\alpha i - \alpha k - \theta_{ik}) = I(S_i) = I(v_i I_i) \tag{14}$$

We noticed that the expressions (13) and (14) are recurrent relations.

IV. DEFECTS AND PHENOMENA ON THE TRANSMISSION NETWORKS

During the transmission of electrical energy, several factors can affect the proper functioning of the electrical network. The causes of failures are:

- External attacks
- Weather hazards
- Failures linked to the humanfactor.

The most important faults and phenomena that can disturb a high-voltage electrical network are:

- Short circuits
- Power surges
- Overloads
- The swings

V. PROTECTION OF ELECTRICITY TRANSMISSION LINES

The objective of the protection is to permanently monitor the elements of the transport network and to switch off (by opening the circuit breakers) the elements that are the source of a malfunction, whatever their origin. Such as distance protection based on the impedance measurement, which permanently takes into account the electrical quantities, namely the voltage V and the current I of the same phase, to evaluate the impedance of the network on this phase (15), seen from the point where the measurement relay is located.

This impedance evaluation is generally carried out on the three phases, either between phase and neutral or between phases. See figure 4 below.

$$Z = \frac{V}{I} \tag{15}$$

ISSN: 1737-9334

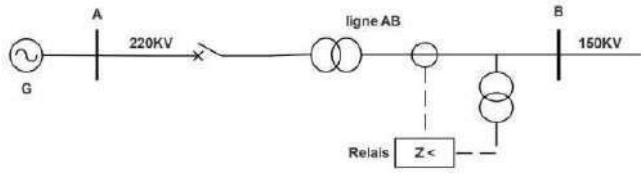

Figure 4. Schéma de principe de la protection de distance.

Distance protection measures attempt to differentiate between fault impedance and load impedance.

The distance protection, in its basic structure, is a protection device without sections that delivers appreciable economic and technical favors. Contrary to the phase and neutral overcurrent protection shown in figure , the most important advantage of distance protection lies in the fact that the monitoring of the equipment is almost independent of the fluctuation of the source impedance.

To find P_{ki}, and $Q_{ki,}$ it suffices to permute i and k in the expressions (9) and (10).

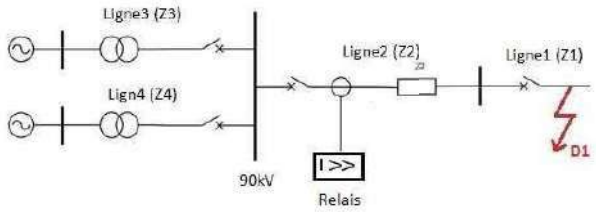

Figure 5: Overcurrent protection AC fault in line1

With, $Z2 = 5\Omega$; $Z3=12\ \Omega$; $Z4=12\ \Omega$

The fault current I_{D1}:

$$I_{D1} = \frac{90.10^3}{\sqrt{3}.(5+6)} = 4\ 723{,}774\ \text{A}$$

Relay current setting> 4 723,774 A

VI. MEASUREMENT OF INFLUENTI L QUANTITIES

The measurement results of the electrica quantities following faults on the transport network are represented by figures 6 and 7.

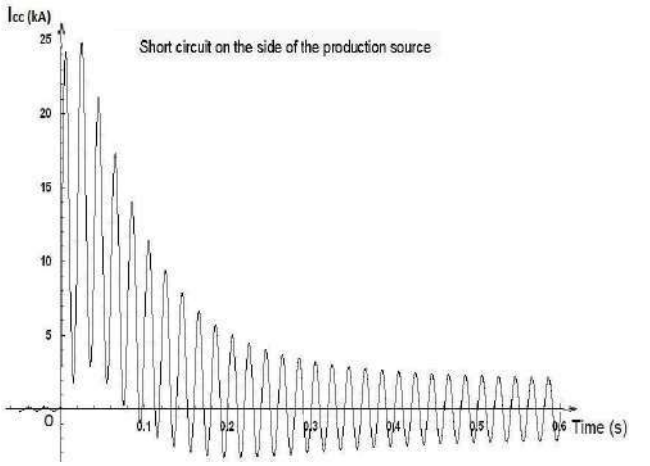

Figure 6. Current in a li ne following a short circuit

The curve above represent the peak of the short-circuit current manifesting itself in a line for a brief moment.

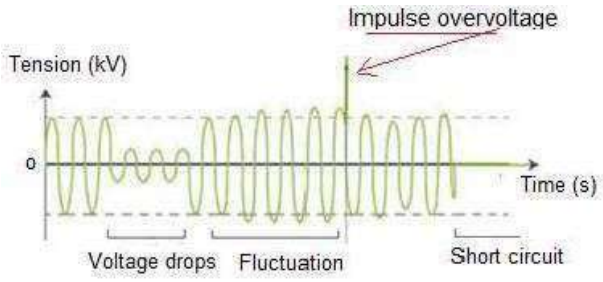

Figure 7.Representative of line voltage affected by faults

The measurement of the vol age carried out on a line shows that the signal presents four types of faults with different frequencies.

VI. CONCLUSION

Distance protection is virtually easy to use and instantaneous in detecting faults throughout the equipment to be protected. In addition, it can transmit fundamental and remote backup data in the same pattern. Thus, it can be quickly harmonized to realize an intelligent unit protection model when implemented with a sign ling sector and a teleaction structure.

This solution is ideal for very fast intelligent reclosing applications for the protectio of critical transmission lines. Therefore, for the protection to be total, the electrical network must be divided into zones demarcated by the circuit breakers. All areas should be effectively protected. Thus, the

ISSN: 1737-9334

zones overlap to tolerate no place in the network without protection.

REFERENCES

[1]. lignes et réseaux électriques - volume 1,2,3,4, Collection sciences et technologies de l'énergie. Auteur : Jean-Claude Sabonnadière. Editeur(s) : Hermès Lavoisier, 2007

[2]. lignes et réseaux électriques - volume 1,2,3,4. Collection sciences et technologies de l'énergie. Auteur : Jean-Claude Sabonnadière. Editeur(s) : Hermès Lavoisier, 2007

[3]. D Maillard Revue de l'Energie – 2010 « a modern electricity transportation grid, central french economy.RTE.

[4]. Ismail El Kafazi, Rachid Bannari, A Abouabdellah « La modélisation et l'optimisation des systèmes de production complexes ; application aux réseaux énergétiques » Xème **Conférence CCSD** 2015.

[5]. R. Caire, « Gestion de la production décentralisée dans les réseaux de distribution », Thèse de doctorat en Génie électrique, INPG, 2004. Et al. « Dynamic réactive load model », IEEE Trans. On Power System, Vol.13,No.4, pp 1365-1372, November 1998.

[6]. la distribution d'énergie électrique en présence de production décentralisée .Collection traité EGEM. Auteur : Jean-Claude Sabonnadière, NouredineHadjsaïd. Editeur(s) :HermèsLavoisier.Editeur(s) :Hermès Lavoisier, 2012

[7]. M. Eremia, J.Trecat, A.Germond, « Réseaux électriques – Aspects actuels », L'Editeur technique , Bucarest, ISBN :973 - 31-1526-6, 2000.

[8]. J.F Canard, « Impact de la génération d'énergie dispersée dans les réseaux de distribution », Thèse de Doctorat INPG, 2000.

[9]. Coreso, site internet :http://www.enerzine.com/15/7015+coreso,-centre-de-coordinationpour-les-grt-europeens+.html.

[10]. European Network of transmission System Operations For Electricity (ENTSOE), site internet, http://www.entsoe.eu.

[11]. Réseau de transport d'électricité (RTE), site internet : http://www.rte-france.com.

[12]. A.Doulet, « Réseaux de distribution d'électricité »,Techniques de l'ingénieur, D4200.

[13]. P.Bornard, « Conduite d'un système de production-transport »,Techniques de l'ingénieur.

[14]. J.-L.Fraise, J.-P.Horson, « Raccordement de la production décentralisée aux réseaux de distribution », Techniques de l'ingénieur, D4241.

ISSN: 1737-9334

Analysis and Modeling of a Microgrid using the language SysML

Naziha Labiadh*[1], Imen Amdouni*[2], Lilia El Amraoui*[3]

* *Research Laboratory Smart Electricity & ICT, SEICT, LR18ES44,*
National Engineering school of Carthage, University of Carthage, Tunisia

[1]nlabiadh0@gmail.com
[2]amdouniimen@yahoo.fr
[3]lilia.elamraoui@gmail.com

***Abstract*— This paper presents an analysis and modeling of a microgrid using the SysML (Systems Modeling Language). All over the world, there are a large number of environmental problems associated with energy production. However, global warming, greenhouse gases, carbon dioxide emissions and climate change are the most the significant effects of damages resulting from energy generation. solve these environmental issues, in the context of improving our resources and to develop in a more sustainable way, that would be great challenge. This challenge calls for the introduction of renewable energy sources. Therefore, smart grid deployment can provide a very interesting answer for renewable energy use targets energies.**
In this work, we start with presentation of smart grid. Next, we describe the SysML. Subsequently, a graphical description of the functionality of a microgrid system based on SysML diagrams are shown here. Finally, concludes this paper with some prospects.

Keywords*— *Microgrid, decentralized production, renewable energy, systemic approch, control, SysML.

I. INTRODUCTION

Fossil fuels (coal, oil, gas) remain essential for transport, electricity production, heating, the operation of factories... But they are the main cause of CO2 emissions and their reserves, also they're to blame for more than 80 percent of greenhouse gas emissions and 98 percent of CO2 emissions alone. That number will rise dramatically if we don't effectively transform the ways in which we produce and consume energy to further help prevent the worst consequences of environmental damages. Even if they are still vast, are not inexhaustible, unlike renewable energies.

Renewable energies (EnR) are supplied by the sun, the wind, the heat of the earth, the waterfalls, the tides... They make it possible to produce electricity, heat, cold, gas, fuel, fuel. These energy sources, considered inexhaustible on a human time scale, generate little or no waste or polluting emissions. They differ from fossil fuels, which pollute and whose stocks are diminishing. Finally, renewables are more resilient, especially in the event of a crisis.

It is undoubtable that in the future a large proportion of energy used by the human will be derived from a diverse range of renewable sources not only because they are, from an environmental standpoint, inexhaustible, clean and they can be used in a decentralized way (they can be used in the same place as they are produced), but also because they have the additional advantage of being complimentary, the integration between them being favorable [1].

Rapidly advancing technologies can also achieve the energy transition [2]. Indeed, one of the major problems for the integration of renewable energies comes from the intermittence of these sources; therefore, energy generation and demand become two variable factors and adjusting them becomes complex. The contribution of the technology provided by the smart grid has captivated the interest of operators which always seeks to ensure the supply-demand balance.

In this paper we propose a high-level graphical description based on SysML diagrams to understand the overall architecture of future energy systems.

II. PRESENTATION OF SMART GRID

A smart grid is a technology that divides the electricity grid into a two-way flow of data and electricity. The technology includes energy measures ad operations such as smart appliances, smart meters, energy-efficient resources, and more. The technology of the smart grid aims to support and integrate renewable energy into the conventional energy source. Not only does it use alternative energy sources, but the smart grid technology also allows consumers to monitor energy consumption.

The essential part of the smart grid is the two-way electricity and data flow. This technology allows information and data flow to various stakeholders. This data and information are essential to optimize the grid, respond faster to error, foresee possible issues, and more. In addition, the smart grid has several capabilities in which the conventional method does not have. The smart grid can repair itself. The system also ensures premium-quality and consistent power supply with power leak-proof ability. Thus, the electricity can be distributed more efficiently.

Smart grids can be defined according to four characteristics in terms of: [3],[4]

- Flexibility: they make it possible to manage the balance between production and consumption more finely.
- Reliability: they improve the efficiency and security of networks.

ISSN: 1737-9334

- Accessibility: they promote the integration of renewable energy sources throughout the network.
- Economy: they bring, thanks to better management of the system, energy savings and lower costs.

The figure 1 below shows how the structure of the smart grid.

Fig.1 Smart grid architecture [5]

The smart grid will consist of millions of pieces and parts: controls, computers, power lines, and new technologies and equipment. Hence, the complexity and size of the existing power grid will make the development of smart grids very expensive, difficult and it will take some time for all the technologies to be perfected, equipment installed, and systems tested before it comes fully on line. For this, the idea to create micro smart grid interconnected and connected to public networks would be an excellent example for the smart grid becomes a reality. A cluster of interconnected microgrids (Fig.2) gradually replaces the grid.

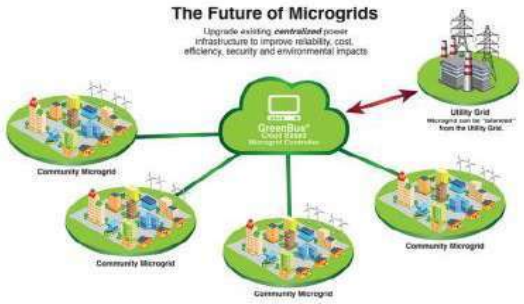

Fig. 2 Future grid architecture [6]

III. Presentation of Microgrid

Microgrids is an important area of study when evaluating smart grid design and deployment, use and integration distributed resources and improved building reliability in the grid.

A. *Definition of Microgrid*

Microgrids are small electrical networks designed to provide reliable electricity supply to a small number of consumers. They aggregate multiple local and diffuse production facilities (micro-turbines, fuel cells, small diesel generators, photovoltaic panels, mini-wind turbines, small hydropower), consumption facilities, storage facilities and monitoring and control tools. demand management. They can be connected directly to a distribution network or operate disconnected from the network (islanding). This concept, likely to concern different scales of the territory (building, district, industrial or artisanal zone, village, etc.) is in the process of being extended to heat and natural gas networks, and can thus be thought of in a multi- fluid.

Fig.3 Microgrid architecture [7]

B. *Benefits of Microgrid*

The benefits of deploying microgrids are numerous: [8-12]

- from a technical point of view: microgrids reflect in particular an optimized management of the production of electricity from renewable sources at the local level. They can provide an auxiliary service to the public distribution network, helping it to keep the voltage stable and "relieving" it when it is cut off from the distribution network.
- from an economic point of view: depending on its size, the microgrid can act as a capacity aggregator. Microgrids also make it possible to defer network investments, the proximity between production and consumption making it possible to optimize the routing of energy. They also make it possible to reduce the volume of technical losses.
- from a societal point of view: a microgrid provides answers to the evolution of the fundamental energy needs of a territory, in particular by guaranteeing a safer and more reliable network in the event of an incident. Because it is a local project, it also facilitates the creation of initiatives and new partnerships between local actors. The development of micro-grids also responds to consumers' appetite for short circuits, especially since the Smart grid functions that can be attached to them considerably reinforce the role of the consumer.
- from an environmental point of view: micro-grids facilitate the integration of energies from renewable sources into the networks, which makes it possible to avoid the installation of thermal power plants in "fragile" areas.

IV. System Modeling Language SysML

SysML (Systems Modeling Language) is a domain-specific modeling language for system engineering. It allows specification, analysis, design, verification and validation many systems. Originally, SysML was developed as part of a specification project open source, and includes an open-source license for its distribution and use.

SysML diagrams can be divided into three types:

- Diagrams that capture system requirements (requirements diagram) and physical constraints (parametric diagram).

ISSN: 1737-9334

- Diagrams that describe the structure of the system (internal block diagram and block definition diagram).
- Diagrams that describe the behavior of the system (use case diagrams, sequence diagram, activity diagram, and state machine diagrams).

V. RESULTATS OF MICROGRID MODELING

The SysML in this article is used to provide a simple objective Powerful description for micro smart grid system modeling. In reality, we present a functional modeling with use case diagram. Next, a complement to functional modeling with requirements diagram. Then, we present a modeling of the behavior with sequence diagram and structural modeling with BDD and IBD.

First, we will present our energy system considered as a microgrid. This system can be connected to the main network or operate in an island mode. The system consists of photovoltaic solar panels (PV) and wind turbine (WT) which are used to produce the local electricity [13],[14]. Moreover, to overcome the intermittency of renewable energy resources and optimize the exploitation of this local production, the use of an electricity storage system is taken into account by means of electric batteries.

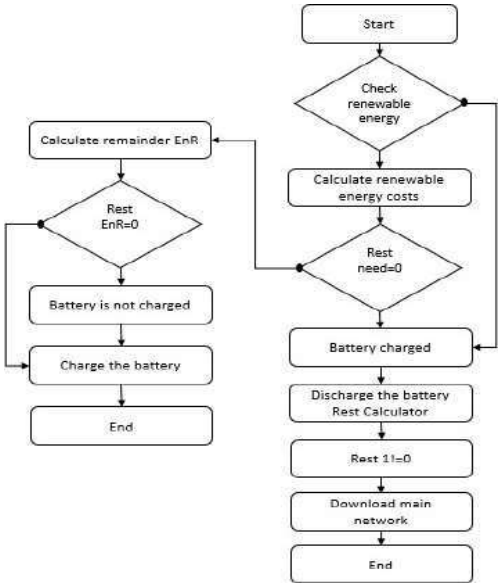

Fig.3 Production algorithm

A. FUNCTIONAL MODELING WITH USE CASE DIAGRAM

use case diagrams model the behavior of a system and help capture system requirements. It's described the general functions and scope of a system. These diagrams also identify the interactions between the system and its actors. Use cases and actors in use case diagrams describe what the system does and how the actors use it, but do not show how the system works internally. In other words, a use case diagrams illustrate and satisfy the context and requirements of an entire system, or essential parts of a system. You can model a complex system with a single use case diagram, or create many uses case diagrams to model system components. You will develop use case diagrams primarily in the early stages of a project and refer to them throughout the development process. In the aim of avoiding too fine decomposition we limit, in the figure below Fig.4, to the essential functions provided by smart micro-grid. it allows consumers to become electricity producers by integrating renewable energies (wind, photovoltaic, etc.), it also gives the possibility of storing energy in batteries. this digital technology allows micro-grid to perform monitoring functions, analysis, control and communication within the supply chain that satisfy the need of its actors to adjust supply to demand and optimize electrical power. All these functions are represented in an ellipse connected to the actor concerned.

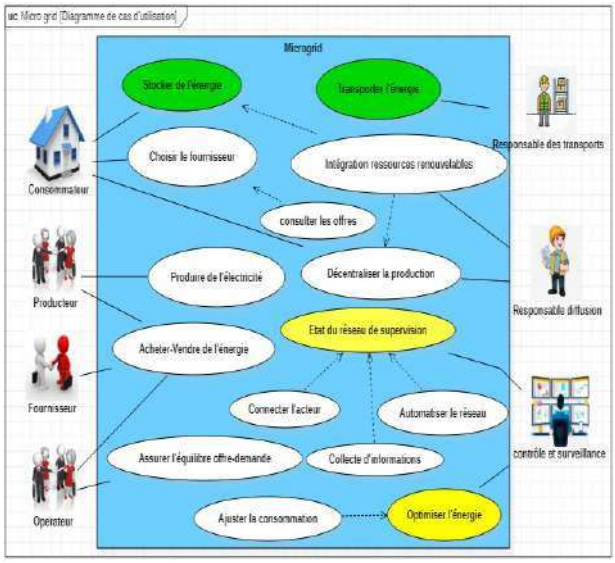

Fig.4 Use case diagram

B. Complements to functional modeling with requirements diagram

This diagram models the requirements to be verified by the system by linking the solutions implemented on the system with the needs defined in the specifications. It translates, through functionalities or constraints (conditions of performance, reliability, security ...), which must be satisfied by the system. The requirements diagram Fig.5. classify multiple requirements of microgrid on physical requirements, functional requirements and performance requirements.

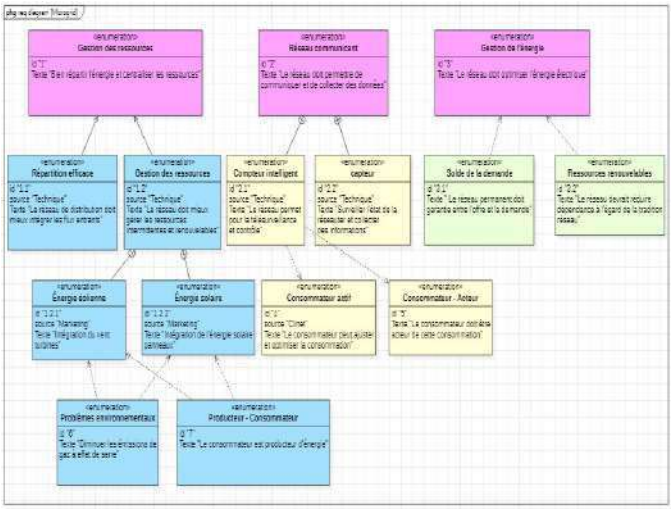

Fig.5 Microgrid requirements diagram

ISSN: 1737-9334

C. Modeling the behavior with sequence diagram

The main operation of the microgrid is based on two modes: connected mode and island mode according to on electricity production: Overproduction, Underproduction and balance. Both generate interactions with the microgrid or within the microgrid itself. Thus, a sequence diagram allows you to map interactions arranged in chronological order among system components or among the actors and the system.

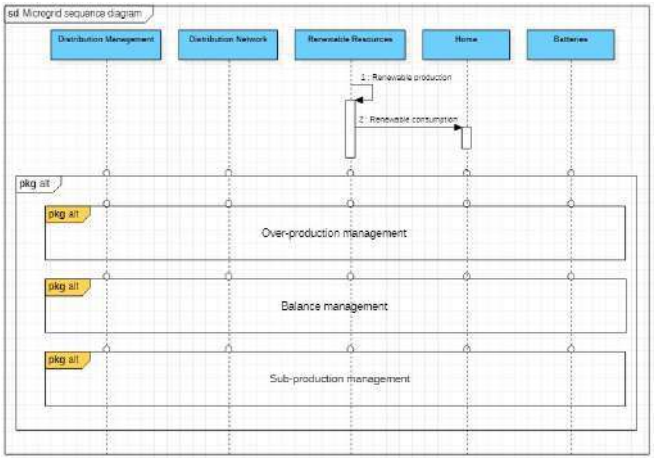

Fig.6 Microgrid sequence diagram

D. Structural modeling with BDD and IBD diagram

SysML Block Definition Diagram (BDD) defines structural elements called blocks, and their composition and classification. Fig.7 shows the different components of microgrid.

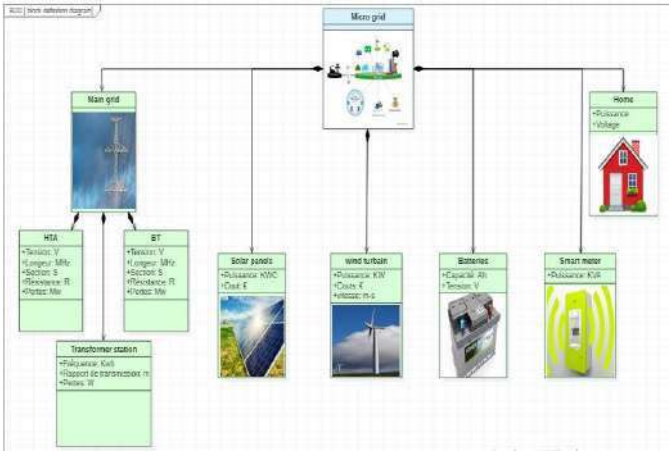

Fig.7 Block definition diagram BDD

A SysML internal block diagram (IBD) describes the internal structure of a block in terms of parts, ports and connectors. The figure below Fig.8 represents the internal block diagram of the microgrid which identifies the flow of data and energy exchanged inside the microgrid.

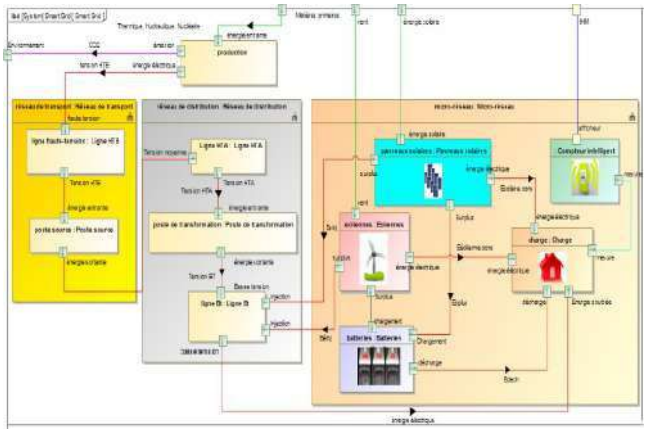

Fig.8 Internal Block diagram

VI. Conclusion

The aim of this paper is to use the SysML modeling language to describe the structure, function and behavior of a microgrid system. These descriptions identify the interactions, data flows, and control between parts of the system that are essential to understanding overall performance and can help in optimizing and designing future power grids, as well as in gaining a better understanding of how the system itself works from the perspective of a multidisciplinary approach.

References

[1] S. M. Metev and V. P. Veiko, *Laser Assisted Microtechnology*, 2nd ed., R. M. Osgood, Jr., Ed. Berlin, Germany: Springer-Verlag, 1998.
[2] J. Breckling, Ed., *The Analysis of Directional Time Series: Applications to Wind Speed and Direction*, ser. Lecture Notes in Statistics. Berlin, Germany: Springer, 1989, vol. 61.
[3] S. Zhang, C. Zhu, J. K. O. Sin, and P. K. T. Mok, "A novel ultrathin elevated channel low-temperature poly-Si TFT," *IEEE Electron Device Lett.*, vol. 20, pp. 569–571, Nov. 1999.
[4] M. Wegmuller, J. P. von der Weid, P. Oberson, and N. Gisin, "High resolution fiber distributed measurements with coherent OFDR," in *Proc. ECOC'00*, 2000, paper 11.3.4, p. 109.
[5] R. E. Sorace, V. S. Reinhardt, and S. A. Vaughn, "High-speed digital-to-RF converter," U.S. Patent 5 668 842, Sept. 16, 1997.
[6] (2002) The IEEE website. [Online]. Available: http://www.ieee.org/
[7] M. Shell. (2002) IEEEtran homepage on CTAN. [Online]. Available: http://www.ctan.org/tex-archive/macros/latex/contrib/supported/IEEEtran/
[8] *FLEXChip Signal Processor (MC68175/D)*, Motorola, 1996.
[9] "PDCA12-70 data sheet," Opto Speed SA, Mezzovico, Switzerland.
[10] A. Karnik, "Performance of TCP congestion control with rate feedback: TCP/ABR and rate adaptive TCP/IP," M. Eng. thesis, Indian Institute of Science, Bangalore, India, Jan. 1999.
[11] J. Padhye, V. Firoiu, and D. Towsley, "A stochastic model of TCP Reno congestion avoidance and control," Univ. of Massachusetts, Amherst, MA, CMPSCI Tech. Rep. 99-02, 1999.
[12] *Wireless LAN Medium Access Control (MAC) and Physical Layer (PHY) Specification*, IEEE Std. 802.11, 1997.
[13] Y. Boukhris, L. Gharbi and N. Ghrab-Morcos., 'Influence of night natural ventilation on Tunisian summer thermal comfort', IREC 2014 - 5th International Renewable Energy Congress, 2014.
[14] A. Chabaud. 'Intelligent microgrid for resource management Energy, January 21, 2016.

ISSN: 1737-9334

Analyzing and optimizing the bi-monthly energy consumption of a Tunisian TCEG (STEG) subscriber

Samir Arfa; Mohsen Ben Ammar; Mohamed Ali Zdiri; Hsan Hadj Abdallah
Control and Energy Management Laboratory, (CEMLab),
University of Sfax, National Engineering School of Sfax
BP 1173, Sfax, 3038, Tunisia
arfa.samir@gmail.com; mohsen.benammar@enis.tn
mohamed-ali.zdiri@enis.tn; hsan.hajabdallah@enis.tn

Abstract

Over the past few decades, we have witnessed a rapid and continuous increase in energy costs worldwide, which has led to economic and ecological problems. To mitigate these consequences, energy conservation has been identified as one of the solutions. It can help control and optimize the methods of using electrical energy. To achieve this goal, we will proceed in several steps. First, we will use an application developed by TCEG (STEG) to estimate the customer's energy consumption and raise awareness about the better use of electrical energy. This will allow us to identify the amount of energy consumed by each electrical load, as well as the daily consumption in winter and summer modes. Next, we will analyze energy consumption and identify the most energy-intensive household appliances to look for ways to conserve energy. Finally, we will demonstrate that we have successfully saved energy by reducing the energy consumption of the lighting load of this subscriber by more than 66.94 % by using energy-efficient lamps. This energy-saving action will help subscribers of the Tunisian TCEG (STEG) to reduce their total energy bill by over 12 %, which is a national and international challenge that affects the economy of both the subscriber and the state.

Keywords

Energy conservation; Household load; Lighting; Energy balance; Bi-monthly bill estimation.

I. INTRODUCTION

The method of using and managing energy is a challenge of great importance for the future [1]. In the face of multiple economic and oil crises, science has focused on energy conservation, which is a strategic sector and holds a privileged place in research and development [2]. Energy conservation can be a crucial axis for energy users, as it can help them better manage their annual budget and increase the value of their assets while ensuring the future of the planet. There are many methods available that can help use energy more efficiently without sacrificing comfort. These easy-to-adopt tips can help reduce our energy bills and are increasingly profitable as energy prices continue to rise [3-4].

Given the rapid and continuous increase in the global cost of energy, the TCEG (STEG) has created an application to estimate the bi-monthly energy consumption of its subscribers, in order to help them optimize their use of electric energy and identify the most energy-intensive household appliances [5]. The application includes an interface that prompts users to provide information about the number of people in their residence, the size of the residence, the number of lamps, refrigerators, televisions, washing machines, ovens, etc. After entering the data, the application estimates the energy consumption during the winter and summer seasons [6-7]. This estimation is based on the historical energy consumption data of TCEG (STEG) subscribers and is prepared by engineers and experts. This method also allows for the estimation of the cost of the bi-monthly electricity and gas bills during the winter and summer seasons, taking into account the park of energy equipment and its mode of use [8].

In this study, we created and analyzed an energy balance for a domestic load of a TCEG (STEG) subscriber. This balance allowed us to determine the daily energy consumption over a period of 24 hours. Next, we attempted to save energy by replacing non-efficient lamps with efficient ones, in order to reduce energy consumption and decrease the cost of the electricity bill. Finally, we explored other targeted energy-saving methods for the same purpose.

This work is divided into four steps. The first part will present the study as a whole. The second part will describe the methodology used to determine the load profile of the household load in question. The third part will present the energy balance of this load, with a detailed analysis of each load in winter and summer modes. The last part will be devoted to the presentation of the results obtained. Finally, a conclusion will conclude this work.

II. DESIGNING A DOMESTIC LOAD PROFILE: A METHODOLOGY

The method used for generating the domestic load profile in this study is illustrated in the following figure [9]:

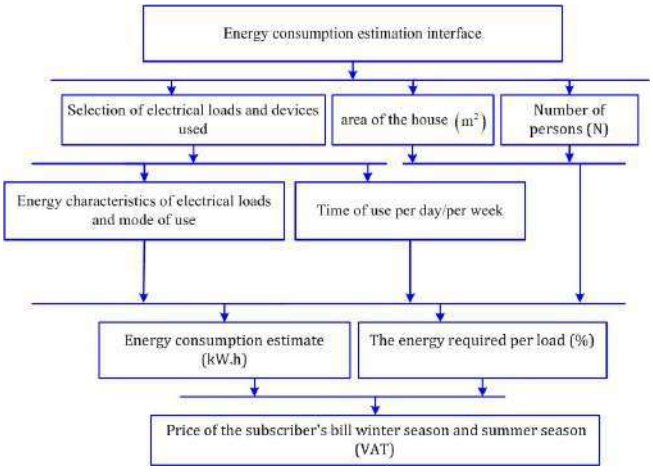

Fig. 1 Diagram of the energy balance sheet creation application interface for TCEG (STEG) subscribers

ISSN: 1737-9334

The load profile of this subscriber is obtained using an interface of an application (shown in the figure above) created by the Tunisian TCEG (STEG). All data about the domestic and electrical loads used (power of each device, number of light points, energy-efficient or non-energy-efficient, type and size, as well as the duration of daily use and the area of the house in m^2) are provided, citing the number of occupants on the site. By filling in this information, the bi-monthly energy balance sheet for this subscriber is obtained, and the daily energy consumption can be determined [10, 12].

The energy and household appliances used by this subscriber are listed in the following table:

TABLE 1. ELECTRIC LOAD USED

Receiver	Nominal electric power (W)	Number of appliances
Lighting lamp	[100-200]	8
Refrigerator	[700-1700]	1
Air conditioner / Heater	[800-1800]	1
TV	[10-450]	1
Washing machine	[50-800]	1
Iron	[70-100]	1
Kitchen (Oven, dishwasher...)	[50-4500]	1
Desktop computer / Multimedia	[5-500]	1
Other equipment*	[50-1000]	1

Other equipment*: portable chargers, Moulinex, internet box, coffee maker, fan, night light, telephone set, printer/scanner, intercom, hair clippers, vacuum cleaners, drill.

III. STUDY AND ANALYSIS OF THE ENERGY BALANCE OF THIS SUBSCRIBER IN WINTER AND SUMMER MODES

Today, the use of new technologies, especially for lighting, such as energy-saving lamps, now allows for the same lighting power to be provided while significantly reducing energy consumption [10-11, 13]. This enables us to achieve energy savings. In this study, we focus solely on energy-saving actions for the lighting load.

III. 1. Estimation of energy consumption during winter and summer seasons (in the case of incandescent lamps)

In this section, we present the bimonthly (two-month) energy balance sheet estimated by TCEG (STEG) in the form of non-modifiable PDF tables that include all the energy data and billing costs for the energy consumption of this subscriber using non-energy efficient incandescent lamps. The results of this balance sheet and the cost of the bill are shown in the following tables:

TABLE 2. ESTIMATION OF ENERGY CONSUMPTION FOR THE WINTER SEASON BY THE SUBSCRIBER USING NON-ENERGY EFFICIENT LAMPS

Electricity use in winter mode	Average usage (kW.h)	%
Lighting	118,096	17,8
Refrigerator	95,4	14,4
TV	41,48	6,2
Washing machine	14,4	2 ,2
Heating	96,075	14,5
Ironing machine	4,8	0,7
Cooking	219,6	33
Micro-computer	47,58	7,2
Other equipments	27,068	4,1
Total	664,499 (kW.h)	
Amount of 1	139,317 (TD)	

TABLE 3. ESTIMATION OF GAS CONSUMPTION FOR THE WINTER SEASON OF THE SUBSCRIBER (USING BOTH ENERGY-EFFICIENT AND NON-ENERGY-EFFICIENT LIGHTING)

Natural gas use	Average usage (m^3)	%
Water heating	15,36	29,6
Cooking	36,6	70,4
Total	51,96 (m^3)	
Amount of 2	12,003 (DT)	

TABLE. 4 ENERGY CONSUMPTION BILL WITH VAT (NON-ECONOMIC LAMPS) FOR THE WINTER SEASON IN TD

Invoice details (TD)	
Total= Amount 1+ Amount 2	151,319
Flat fee	12,8
ERTT	4,258
Taxes	22,392
Total (VAT)	190, 769

TABLE 5 ESTIMATION OF THE ENERGY CONSUMPTION OF THE SUBSCRIBER DURING THE SUMMER SEASON (NON-ENERGY-EFFICIENT LAMPS)

Electricity use in summer mode	Average usage (kW.h)	%
Lighting	118,096	13,9
Refrigerator	148,4	17,4
TV	41,48	4,9
Washing machine	14,4	1 ,7
Air conditioner	227,676	26,7
Ironing machine	4,8	0,6
Cooking	219,6	25,8
Micro-computer	47,58	5,6
Other equipments	29,718	3,5
Total	851,75 (kW.h)	
Amount of 1	204,106 (TD)	

TABLE 6 ESTIMATION OF GAS CONSUMPTION DURING THE SUMMER SEASON FOR THE SUBSCRIBER (ECONOMIC AND NON-ECONOMIC LAMPS

Natural Gas Use	Average usage (m^3)	%
Water heating	7,68	17,3
Cooking	36,6	82,7
Total	44,28 (m^3)	
Amount of 2	10,229 (TD)	

TABLE 7 INVOICE FOR SUMMER ENERGY CONSUMPTION WITH VAT (NO-ENERGY SAVING BULBS) IN TD

Invoice details (TD)	
Total= Amount 1+ Amount 2	214,334
Flat fee	12,8
ERTT	5,007
Taxes	30,356
Total (VAT)	262, 497

ISSN: 1737-9334

III. 2. Estimation of energy consumption for the winter and summer seasons (using energy-efficient lamps)

In this paragraph, we present the second energy balance and the bi-monthly price invoice estimated by STEG for this subscriber, using non-modifiable PDF format tables and economical lamps. The results of this balance are shown in the tables below:

TABLE 8 ESTIMATION OF ENERGY CONSUMPTION FOR THE WINTER SEASON OF THE SUBSCRIBER (USING ENERGY-EFFICIENT LAMPS)

Electricity use in winter mode	**Average usage (kW.h)**	**%**
Lighting	39,04	6,7
Refrigerator	95,4	16,4
TV	41,48	7,1
Washing machine	14,4	2 ,5
Heating	96,075	16,5
Ironing machine	4,8	0,8
Cooking	219,6	37,8
Micro-computer	47,58	8,2
Other equipments	23,115	4
Total		581,49 (kW.h)
Amount of 1		112,872 (TD)

TABLE 9 WINTER ENERGY CONSUMPTION BILL INCLUDING VAT (ENERGY-EFFICIENT LAMPS) IN TD

Invoice details (DT)	
Total = Amount 1+ Amount 2	124,875
Flat fee	12,8
ERTT	3,926
Taxes	19,008
Total (VAT)	160, 609

TABLE 10 ESTIMATION OF SUBSCRIBER'S ENERGY CONSUMPTION DURING THE SUMMER SEASON (WITH ENERGY-EFFICIENT LAMPS)

Electricity use in summer mode	**Average usage (kW.h)**	**%**
Lighting	30,04	5,1
Refrigerator	148,4	19,3
TV	41,48	5,4
Washing machine	14,4	1 ,9
Air conditioner	227,676	29,6
Ironing machine	4,8	0,6
Cooking	219,6	28,6
Micro-computer	47,58	6,2
Other equipments	25,765	3,4
Total		768,741 (kW.h)
Amount of 1		175,385 (TD)

Formulation of the calculation for energy saving on lighting using the following equation:

$$\mathrm{ESL} = \mathrm{ELNEL} - \mathrm{EEEL} \quad (1)$$

- Let $\mathrm{ESL} = 79.056\ \mathrm{kW.h}$

The cost savings rate in summer is obtained using the formula in equation (2):

$$\mathrm{SECR} = \frac{\mathrm{ESL}}{\mathrm{ELNEL}} \quad (2)$$

- Let's assume $\mathrm{SECR} = 66.94\ \%$

TABLE 11 SUMMER SEASON ENERGY CONSUMPTION BILL INCLUDING VAT (ECONOMIC LAMPS) IN TD

Invoice details (TD)	
Total= Amount 1+ Amount 2	185,613
Flat fee	12,8
ERTT	4,675
Taxes	26,676
Total (VAT)	229, 764

All tables from 2 to 11 show the different electrical loads of the household, as well as their values and volume depending on the total load volume for the different seasons and the two economic/non-economic modes. From these tables, one can calculate the average daily consumption for each case.
Indeed, Tables 4, 7, 9, and 11 present the different costs of energy consumption bills with VAT taxes and prices for each case.

Using these tables, we can calculate the average daily consumption value for this subscriber using equation (3):

$$\mathrm{ADC} = \frac{\mathrm{Total}}{60} \quad (3)$$

TABLE 12 BIMONTHLY ENERGY BALANCE

Domestic Load	**Bimonthly energy consumption in kWh**	**Daily average consumption in kWh**
Electric load of the subscriber during the winter season (non-energy-saving lamps)	664.499	11.0749
Electric load of the subscriber during the summer season (non-energy-saving lamps)	851.750	14.1928
Electric load of the subscriber during the winter season (energy-saving lamps)	581.490	9.6915
Electric load of the subscriber during the summer season (energy-saving lamps)	768.741	12.81

TABLE. 13 COST OF THE ENERGY BILL FOR TWO SEASONS

Domestic charge	**Cost of consumption for the bimonthly bill (TD)**
Electric charge for the subscriber during the winter season (non-energy-efficient bulbs)	190.769
Electric charge for the subscriber during the summer season (non-energy-efficient bulbs)	262.497
Electric charge for the subscriber during the winter season (energy-efficient bulbs)	160.609
Electric charge for the subscriber during the summer season (energy-efficient bulbs)	229.764
WSC (TD)	30.16
CSS (TD)	32.733

The equation for calculating the cost saved during winter is determined using the following expression:

$$\mathrm{WSC} = \mathrm{CNEWC} - \mathrm{CEWC} \quad (4)$$

$$\mathrm{WSC} = 30.16\ \mathrm{TD}$$

Likewise, the cost saved during summer is identified by equation 5:

$$\mathrm{CSS} = \mathrm{SNECC} - \mathrm{CNESC} \quad (5)$$

Indeed, the value of the money saved: $\mathrm{CSS} = 32.733\ \mathrm{TD}$

The winter cost savings rate is presented by the following expression:

$$\mathrm{WSCR}(\%) = \frac{\frac{\mathrm{WSC}}{\mathrm{CNEWC}}}{} \quad (6)$$

- $\mathrm{WSCR}(\%) = 15.81\ \%$

In the same way, we can determine the summer cost savings rate just as we did for winter:

$$\mathrm{SECR}(\%) = \frac{\mathrm{CSS}}{\mathrm{SNECC}} \quad (7)$$

- $\mathrm{SECR}(\%) = 12.46\ \%$

ISSN: 1737-9334

IV. RESULTS AND DISCUSSIONS

Figures 2 and 3 display the bimonthly energy balance for a TCEG (STEG) subscriber during the winter and summer seasons, for both non-energy-efficient and energy-efficient lighting modes. These histograms show the amount of energy consumed by each electrical device or appliance based on the total load. Notably, the average daily consumption during summer is higher than during winter.

In detail, Figures 4 and 5 illustrate the energy consumption of lighting loads during the winter season, for both non-energy-efficient and energy-efficient bulbs. Figure 6 presents the cost savings achieved when using energy-efficient lighting.

Analysis of the energy balance of this subscriber reveals that the most energy-intensive electrical loads are the oven, air conditioning/heating, refrigerator, and lighting. The use of energy-efficient bulbs can reduce lighting energy consumption by up to 66.94 %. This reduction in consumption not only helps save energy but also optimizes its use, ultimately allowing the subscriber to reduce their energy bill by 15.81 % during winter and 12.46 % overall. This reduction is a national and international challenge that affects both the subscriber and the state's economy.

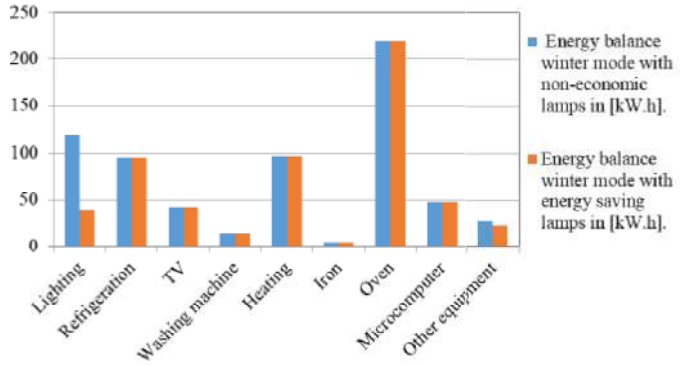

Fig. 2 winter season energy balance

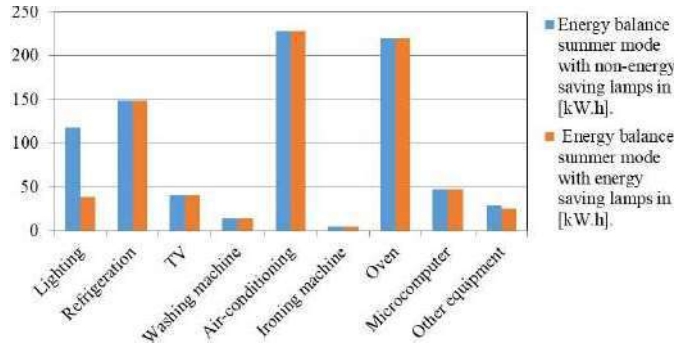

Fig. 3 summer season energy balance

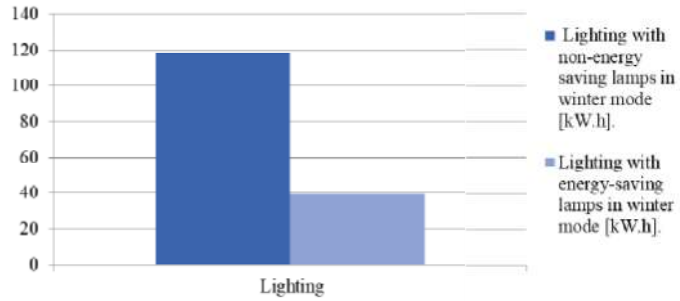

Fig. 4 Winter Season Lighting

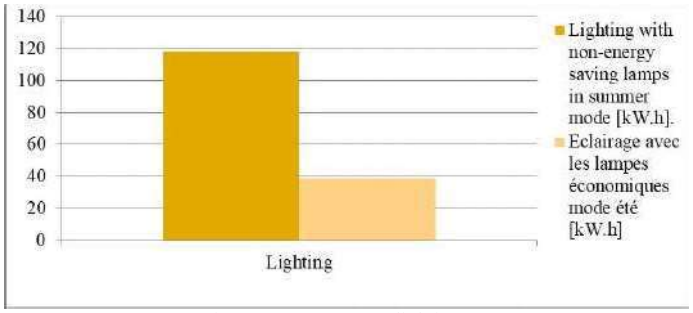

Fig. 5 Summer season lighting

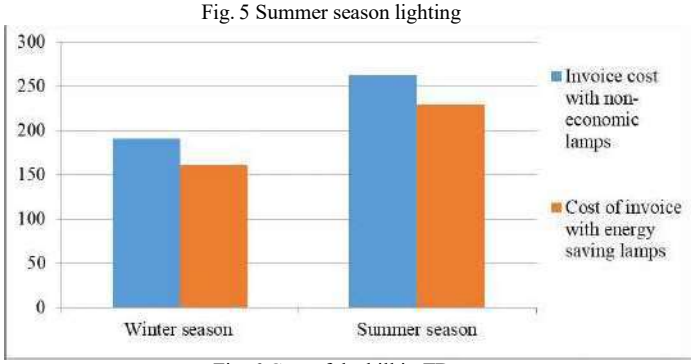

Fig. 6 Cost of the bill in TD

V. CONCLUSION

This work presents several benefits for TCEG (STEG) subscribers by allowing them to better understand their energy consumption for each activity and the amount of energy used in relation to the total domestic load. Additionally, through this study, the client can identify the most energy-consuming charges and save energy by reducing their lighting consumption by up to 66.94 %, which allows them to reduce their energy bill by up to 15.81 %.

Other ways to save energy exist, such as using low-energy-consuming appliances, more energy-efficient technologies, buildings containing insulation and heat exchangers, as well as programmable thermostats and natural lighting.

Electrical appliances used are the most energy-consuming compared to other appliances, consuming more than 80 % of the energy cost. If they are essential, it is important to rationalize their use to save energy.

Finally, to minimize the effects of economic crises caused by uncontrolled growth in oil prices, it is important to control energy use, even when using various natural/renewable energy sources.

APPENDIX

Symbol	Designation	Symbol	Designation
TCEG (STEG)	Tunisian Company of Electricity and Gas	TD	Tunisian Dinar
ATI (TVA)	All Taxes Included	ADC	Average Daily Consumption (kWh)
kW.h	Kilowatt-hour	VATR	Value Added Tax Rate
ELEL	Energy for Lighting with Economical Lamps (kWh)	LSR(%)	Lighting Saved Rate
ATI	All Taxes Included	ESL	Energy Saved for Lighting
ELNEL	Energy for Lighting with No-Economical Lamps (kWh)	WSC	Winter Saved Cost
CNEWC	Cost of No-Economical Winter Consumption	SNECC	Summer No-Economical Consumption Cost
CSS	Cost Saved in Summer	CNESC	Cost of No-Economical Summer Consumption
CEWC	Cost of Economical Winter Consumption	SECR	Summer Economy Cost Rate
WSCR	Winter Savings Cost ate		

ISSN: 1737-9334

REFERENCES

[1] Ç. Ahmet. "Energy consumption and energy saving potential in clothing industry". *Energy*, 159: 74-85 , 2018.

[2] B. Catherine, "Energy consumption and energy saving measures in poultry". *Energy Environ. Eng*, , 5.2: 29-36, 2017

[3] J. Zhu, D. Li,. "Current Situation of Energy Consumption and Energy Saving Analysis of Large Public Building" . *Procedia Engineering*, 121, 1208–1214. (2015)

[4] K. Ghaib, and F.Z. Ben-Fares, "A design methodology of stand-alone photovoltaic power systems for rural electrification", *Energy Conversion and Management*, 148, pp. 1127–1141, 2017.

[5] Tunisian Company of Electricity and Gas (Société Tunisienne de l'Electricité et du Gaz). STEG Tunisie.

[6] A. Soares, A. Gomes, and C. H. Antunes. "Domestic Load Characterization for Demand-Responsive Energy Management Systems". *IEEE International Symposium on Sustainable Systems and Technology (ISSST).* 2012

[7] D. H. Muhsen, H. T.Haider, Y. M. Al Nidawi, & T. Khatib, "Domestic load management based on integration of MODE and AHP-TOPSIS decision making methods". *Sustainable Cities and Society*, 50, 101651, 2019.

[8] C. Bucher, G. Andersson. "Generation of Domestic Load Profiles an Adaptive Top Down Approach". *Proceedings of PMAPS. Istanbul*, Turkey, June 10-14, 2012.

[9] S. Arfa, M. Ben Ammar, M. Al Zidir & Hsan Hadj Abdallah. "Daily energy management system for a house powered by renewable energy"*, Proceedings of Engineering & Technology , 4ème Congrès International sur les Energies Renouvelables et le Développement Durable,* Vol. 69, pp .40-47. 2022.

[10] A. K.. Aliyu, A. Bukar, , L. Ringim, J. G., & A. Musa. "An approach to energy saving and cost of energy reduction using an improved efficient technology". *Open Journal of Energy Efficiency*, 4(04), 61. 2015.

[11] M. W. Akram , M. F. Mohd Zublie, M. Hasanuzzaman, & N. A. Rahim. "Global Prospects, Advance Technologies and Policies of Energy-Saving and Sustainable Building Systems" *A Review. Sustainability, 14*(3), 1316. 2022

[12] M. F. Zublie, M. Hasanuzzaman, & N. A. Rahim. "Feasibility Analysis of Solar Power Generation System for Office Building in Academic Institution". *In IOP Conference Series: Materials Science and Engineering (Vol. 1127, No*. 1, p. 012039). March 2021.

[13] R. Saidur, M. Hasanuzzaman, & N. A. Rahim. Energy use, energy savings and environmental analysis of industrial boilers and compressors*". International Journal of Thermal & Environmental Engineering*, 1(1), 29-36, 2010.

ISSN: 1737-9334

Implementation of the robust MRAC controller based on the Lyapunov's quadratic function:speed control for a DC motor and investigation on adaptivegains

NZANZU Lukogho Luckson
Electrical Engineering Department,LE3PI Laboratory
Polytechnic School of Dakar (ESP)Dakar,Senegal
irnzanzulukogho@gmail.com

GUEYE Samba
Electrical Engineering Department, LE3PI Laboratory
Polytechnic School of Dakar (ESP)
Dakar,Senegal
papesgueye@hotmail.com

NDIAYE Mouhamadou Falilou Electrical Engineering Department, LE3PI Laboratory
Polytechnic School of Dakar (ESP)
Dakar,Senegal
mouhamadouf.ndiaye@ucad.edu.sn

***Abstract*— This paper proposes a robust model reference adaptive controller (MRAC) based on Lyapunov's quadratic function and an investigation on its adaptive gains to control the output speed of dc motor with parameter variations by following a reference model. In this paper, the parameters armature's resistance Ra, armature's inductance La and moment of inertia J of the machine were varied from 10% to 100% of their nominal values. To achieve this, the methodological approach is as follows. The Lyapunov's quadratic functional is chosen. It allows to guarantee the global stability of the system and in which (this function) derives the mechanism of adaptation of the motor parameters. The implemented parameter adjustment mechanism into the Matlab/Simulink environment gives the following results: a settling time of 13.6 milliseconds, a system rise time of 10.25 milliseconds, a final value of 0.165 for a step input. For the reference model this final value is 0.166, hence a tracking error of 0.001004. The overall relative uncertainty of the system is 0.6%; and the measurement uncertainty on the speed at the motor output is 0.000234% by applying a variation of 10% to 100% on its nominal parameters. These simulation results also show and prove the effectiveness of this controller based on the Lyapunov's quadratic function, as it ensures the global stability of the controlled system and a judicious choice of the adaptation gain coefficients of this controller improves the output performances of the controlled system by cancelling the deviation between the two processes, dc motor and reference model, in presence or not of the parametric variations.**

Keywords*— *MRAC controller, Lyapunov's quadratic functional, DC motor, adaptive gains

I. INTRODUCTION

The parametric variations of a real process over the time due to environmental changes and process aging affect the control of the closed loop system with fixed parameter controllers [1], [2]. Under these conditions, it is imperative to find a solution implementing systems capable of adapting to these variations[3], [4]. Gueye et al. show that a dc motor can be considered as a dynamic system whose parameters such as the resistance Ra and inductance La of the armature, and the moment of inertia J of the machine change over time and according to the working environment[5]–[8]. Mouldi also in the positioning study of a dc motor driving the axis of an industrial robot demonstrates the influence of changing friction
Δf as well as inertia Δj of the machine on the response of the system [1]. Another study conducted by Turki in his thesis in 2018 considers an electric motor with a flexible transmission subject to load inertia as a linear time-varying system, LTV [9]. In this situation, the classical approach of control and regulation is limited and inefficient because it cannot meet the precise specifications seen that these classical controllers are fixed parameters [10]–[12]. In [13] the author presents an adaptive gain investigation for a first order system based on the MRAC- MIT rule. His methodology is based on a mathematical background based on the choice of the cost function. The performance improvement is demonstrated on a first-order system under parameter variations [13], [14]. In [15] the author presents a controller based on fuzzy logic to control the speed of a steam turbine in an isolated operating condition, especially in nuclear power plants. In this study he chooses a simple control law and a first order Lyapunov 's algebraic function[15], [16]. This is not in conformity with the theory developed by Landeau in [17] and Nguyen in [18]. It also uses the first order's parameter adjustment mechanism. This is not recommended in [17], [18] because the reference model and the process to be controlled (steam turbine) are modeled by second order transfer functions. This allows us to undertake in this paper researches on a robust MRAC control for a dc motor speed based on the Lyapunov 's quadratic functional and to investigate the adaptation gains to address this problem. The Lyapunov's approach consists in adapting the on-line controllers to the variations of dynamic systems in order to ensure and guarantee a constant quality of performance of the system to be controlled. The Lyapunov's technique is based on the choice of a quadratic functional in which the adjustment mechanism of the dc motor parameters is derived. This

XXX-X-XXXX-XXXX-X/XX/$XX.00 ©20XX IEEE

ISSN: 1737-9334

manuscript is organized as follows; section 2 deals with the modeling of the dc motor and the presentation of the theory based on the Lyapunov's method. Section 3 presents the synthesis of the Lyapunov's MRAC controller. Simulation results and discussion are presented in section 4. The manuscript is closed with a conclusion followed by some research perspectives in section 5.

II. MODELING OF THE DC MOTOR AND PRESENTATION OF THE LYAPUNOV METHOD

A. Modeling of the DC motor

1) Electro kinematic diagram

The modeling of the dc motor is made from the electro kinematic diagram given in figure 1 indicating on the left the electrical part, and mechanical on the right.

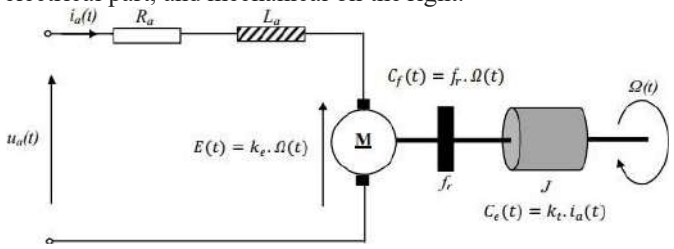

Fig. 1. Schematic and modeling of dc motor

2) DC Motor equations

The model of the studied dc motor is represented by the transfer function (1) [18]–[21].

$$G(s) = \frac{\omega(s)}{V(s)} = \frac{b_0}{s^2 + a_1 * s + a_0} \quad (1)$$

With $b_0 = \frac{K}{J.La}$; $a_1 = \frac{J.Ra+f.La}{J.La}$; and $a_0 = \frac{f.Ra+K^2}{J.La}$ coefficients of the transfer function composed of the electromechanical quantities of the motor. W is the output speed of the motor, V the voltage at the motor terminals, the motor torque constant K, inertia moment of motor J, viscous friction coefficient f, resistance of armature Ra and the inductance of armature winding La. Its equivalent in state space model is given by (2).

$$\begin{cases} \dot{x}_p(t) = A(t) * x_p(t) + B(t) * u(t) \\ y_p(t) = C * x_p(t) \end{cases} \quad (2)$$

Where A, B and C are matrices of appropriate dimensions.

$$A = \begin{bmatrix} 0 & 1 \\ -a_0 & -a_1 \end{bmatrix}; B = \begin{bmatrix} 0 \\ b_0 \end{bmatrix}; \text{and } C = [1 \quad 0]$$

As system state variables, we have x1 the speed and x2 the acceleration of the dc motor. Motor parameters are given in table 1 where Ra is resistance in ohm (Ω), the armature's inductance La is given in henry (H) and J the inertia moment inkilogram meter square ($kg.m^2$).

Table I. PROCESS PARAMETERS SUGJECT TO VARIATIONS

Nominal values	Parameter's variations			
	10 %	30%	50%	100%
Ra=0.59	0.65	0.77	0.89	1.18
La=0.00133	0.00146	0.00173	0.00199	0.00266
J=0.00031	0.00034	0.00040	0.00047	0.00062

B. Presentation of the Lyapunov's method

1) Objective of stability in the Lyapunov sense

Stability means that if a system is in equilibrium, it stays in that state even if time varies. The analysis of Stability in the sense of Lyapunov consists in the study of the trajectories of the system when the initial state is close to an equilibrium state [22]. Based on the properties of the Lyapunov functional of energy type and for a given system, by examining its time derivative along the trajectories of this system; we can predict and have information on the stability of this system around the equilibrium point. If the system reaches the equilibrium point in infinite time, then it is asymptotically stable; if not, the system is stable in finite time. This therefore allows us to say that the objective of the study of stability in the Lyapunov sense is to draw conclusions as to the behavior of systems without explicitly calculating their trajectories [22], [23].

2) Choice of the reference modele

In accordance with the theory developed by Landau in [17] and Nguyen in [18], a reference model of the same order as the plant is chosen. This model is given by (3) and (4) [18]–[21].

$$G_m(s) = \frac{K.\omega_n^2}{s^2 + 2.\xi.\omega_n.s + \omega_n^2} \quad (3)$$

$$\begin{cases} \dot{x}_m(t) = A_m.x_m(t) + B_m.r(t) \\ y_m(t) = C_m.x_m(t) \end{cases} \quad (4)$$

Where K represents the static gain, ξ damping coefficient and ω_n the natural pulsation of the reference modele. A, B and C are matrices with appropriate dimensions.

$$A_m = \begin{bmatrix} 0 & 1 \\ -\omega_n^2 & -2\xi \end{bmatrix}_n; B_m = \begin{bmatrix} 0 \\ K\omega^2 \end{bmatrix}_n; \text{and } C_m = [1 \quad 0]$$

3) Choice of the Lyapunov's quadratic function

This choice is justified in [4], [10], [24]. Although there is no universal formula for constructing a Lyapunov candidate function for a stable system; a good first attempt is to test Lyapunov's quadratic functions for linear or linearizable systems. We choose the function below:

$$\begin{aligned} V(e, K_x, K_r, \Phi(x)) &= e^T(t)P(t)e(t) \\ &+ |b|(K_x(t)\Gamma_x^{-1}K_x^T(t) + \frac{K_r^2(t)}{\gamma_r} \\ &+ \Theta^T\Gamma_\Theta^{-1}\Theta) > 0 \end{aligned} \quad (5)$$

ISSN: 1737-9334

With $\Gamma_x = \Gamma_x^T > 0$ a positive definite matrix of adaptation rate for $K(t)$; and $P = P^T > 0; Q = Q^T > 0 \in \Re^2 \times \Re^2$; matrices which solve the Lyapunov equation:

$$P.A_m + A_m^T.P = -Q \quad (6)$$

Where Q is an identity matrix and P, a symmetric matrix.

III. SYNTHESIS OF THE LYAPUNOV-MRAC

Figure 2 shows the general architecture of a MRAC adaptive control.

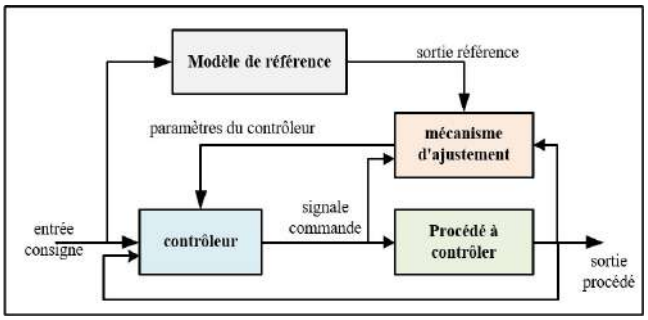

Fig. 2. General architecture of a MRAC adaptive control

The synthesis of the MRAC controller based on the Lyapunov's quadratic function approach is given by the adaptation mechanism as follows:

$$\dot{K}_x^T = \Gamma_x \times x \times e^T \times \bar{P} \times sgn(b) \quad (7)$$

$$\dot{K}_r^T = \gamma_r \times r \times e^T \times \bar{P} \times sgn(b) \quad (8)$$

$$\dot{\Theta} = -\Gamma_\Theta \times \Phi(x) \times e^T \times \bar{P} \times sgn(b) \quad (9)$$

With the nonlinear state feedback control law defined by (10).

$$U_{com} = K_x(t) \times x + K_r(t) \times r - \Theta^T \times \Phi(x) \quad (10)$$

The tracking error between the output of the reference model and that of the dc motor is defined by (11)

$$e(t) = y_m(t) - y_p(t) \quad (11)$$

The symmetric matrix P is determined by solving the Lyapunov algebraic equation (6) by the matlab syntax (12).

$$P = lyap(A_m, Q) \quad (12)$$

The major steps we followed in the methodology to find the stable adaptation laws are:

- Find the structure of the Lyapunov MRAC controller;
- Determine the dynamic tracking error equation;
- Find the candidate quadratic Lypunov's function and finally;
- Implementations in the Matlab / Simulink environment.

The mechanism for adjusting the parameters of the dc motor subject to variations allows the simulation block diagram shown in figure 3 to be constructed.

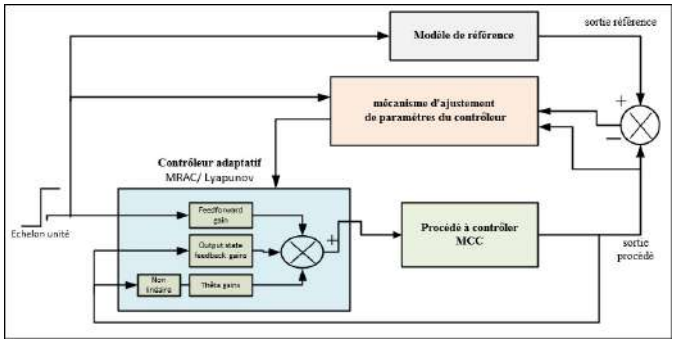

Fig. 3. Simulation block diagram of the Lyapunov-MRAC system

IV. SIMULATION RESULTS AND DISCUSSION

The implementation of the MRAC controller in the Matlab / Simulink environment is done with the following numerical applications. The matrices of scalar adaptation coefficients are $\gamma_{x1} = \gamma_{x2} = \gamma_r = 0.05$ and $\gamma_{\theta 1} = \gamma_{\theta 2} = 20$; with a natural pulsation of the system $\omega_n = 260\ rad * s^{-1}$ and a damping coefficient $\xi = 0.85$.

A. MRAC controller with nominal motor parameters

With nominal motor parameters; we find: The system response is given in figure 4.

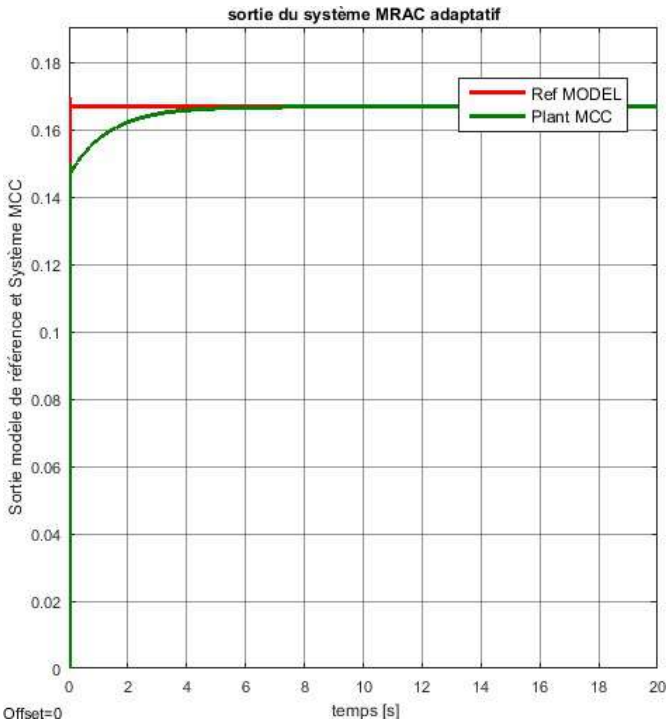

Fig. 4. Sortie du système MRAC-Lyapunov

The figure 5 shows the evolution of adaptive gains taking into account the nonlinearity of the process.

ISSN: 1737-9334

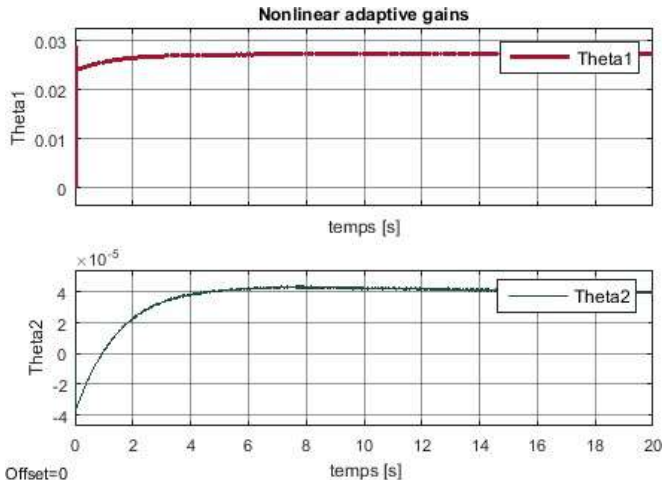

Fig. 5. Adaptive gains with nonlinearity of system

The tracking error output is shown in figure 6.

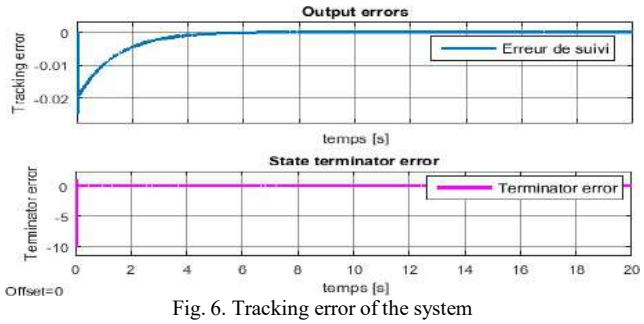

Fig. 6. Tracking error of the system

B. *MRAC controller with parameter variations*

With changes of motor parameters from 10% to100%; we find the following results:

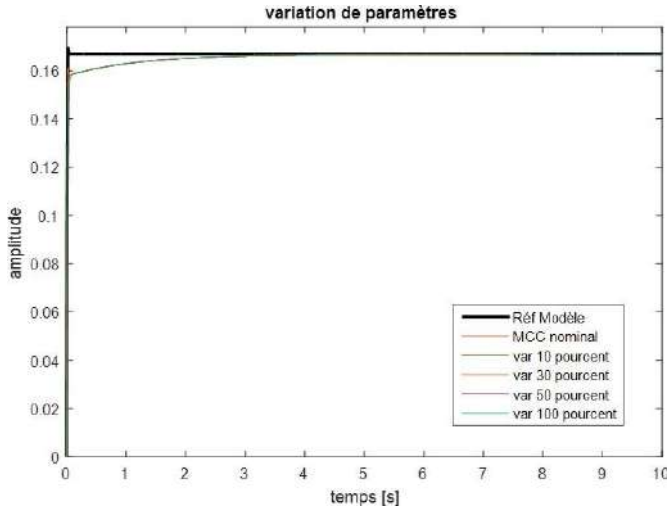

Fig. 7. System output with parametric changes

C. *Investigation on changes in adaptation gains*

For a perfect following of the system, four cases are illustrated in order to decide on the optimal choice of gain coefficients.

- Case 1 : $\gamma_{x1} = \gamma_{x2} = \gamma_r = 0.05$ et $\gamma_{\theta 1} = \gamma_{\theta 2} = 2$;
- Case 2 : $\gamma_{x1} = \gamma_{x2} = \gamma_r = 0.05$ et $\gamma_{\theta 1} = \gamma_{\theta 2} = 20$;
- Case 3 : $\gamma_{x1} = \gamma_{x2} = \gamma_r = 1$ et $\gamma_{\theta 1} = \gamma_{\theta 2} = 2$;
- Case 4 : $\gamma_{x1} = \gamma_{x2} = \gamma_r = 3$ et $\gamma_{\theta 1} = \gamma_{\theta 2} = 2$.

Figure 8 shows that perfect tracking is feasible by choosing the optimal gain coefficients (case 2) such that $\gamma_{x1} = \gamma_{x2} = \gamma_r = 0.05$ for feedback state adaptive gains and $\gamma_{\theta 1} = \gamma_{\theta 2} = 20$ for non-linear adaptive gains.

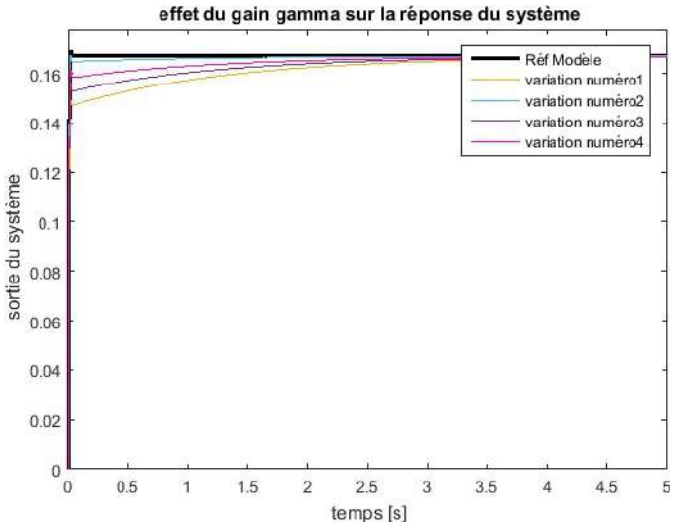

Figure 8 effect of the adaptation gain variation on the system response

D. *Commentary and discussion*

The simulation results show that the implemented MRAC-Lyapunov's controller is robust and guarantees a good tracking of the motor to the reference model with a tracking error of 0.001 and an overall relative uncertainty of the system of 0.6 % for a step input. By applying a variation of 10%; 30%; 50% and 100% on the nominal parameters of the motor; we see that the MRAC-Lyapunov controller always gives desired performance to the motor by faithfully following the reference model. These simulation results also show and prove the effectiveness of this controller . In all cases, it is shown that the output tracking performance depends significantly on the choice of gamma coefficients. The performance is observed for steady state and transient response. The estimated value of adaptation gains in all the cases is giving good transient and steady state performance. The crucial issue of selection of adaptive gains is resolved with complete mathematical analysis and simulation study. By examining the different curves obtained in simulation, we find the optimal range of values for the adaptation gain coefficients. For feedback state adaptive gains,

ISSN: 1737-9334

the optimal performance is obtained for gamma between 0.05 and 3 with zero steady error. And the optimal range for non-linear adaptive gains is between 2 and 20. In this cases study, the best performance is obtained in the senario (case 2) for the feedback state adaptive gains $\gamma_{x1} = \gamma_{x2} = \gamma_r = 0.05$ and for the non-linear adaptive gains $\gamma_{\theta 1} = \gamma_{\theta 2} = 20$. The major advantage of this MRAC controller based on the Lyapunov's quadratic function implemented in this paper is that the system remains stable regardless of the scenario studied. The analysis of different curves in the cases study allows to validate the judicious choice of adaptation gains.

CONCLUSION

This paper proposes a robust model reference adaptive controller (MRAC) based on Lyapunov's quadratic function and an investigation on its adaptive gains to control the output speed of dc motor with parameter variations by following a reference model. The implementation of the parameter adjustment mechanism into the Matlab / Simulink environment gives satisfactory results with a tracking error almost zero for a step input despite the parametric variations of the plant. These results from the analysis of the Lyapunov's quadratic function meet the objectives set because the output of the dc motor faithfully follows that of the reference model. Hence, a perfect tracking and this in critical working conditions due to the change of the environment, temperature increase or aging of the process.

These simulation results also show and prove the efficiency of the implemented MRAC-Lyapunov controller. The major advantage of this controller based on the Lyapunov's quadratic function implemented in this paper is that the system remains stable regardless of the scenario studied. The analysis of different curves in the cases study allows to validate the judicious choice of adaptation gains. In the future, we plan to design an augmented MRAC controller with integral action in order to further improve this implemented model.

REFERENCES

[1] M. M. Ennaceur, « Étude et conception d'un algorithme adaptatif pour la commande de position d'un moteur à courant continu », PhD Thesis, Université du Québec à Trois-Rivières, 1991.

[2] J.-J. E. Slotine et W. Li, *Applied nonlinear control*, vol. 199. Prentice hall Englewood Cliffs, NJ, 1991.

[3] G. Tao, « Multivariable adaptive control: A survey », *Automatica*, vol. 50, nº 11, p. 2737-2764, 2014.

[4] K. J. Åström et B. Wittenmark, *Adaptive control*. Courier Corporation, 2013.

[5] S. Gueye, L. Thiaw, M. F. Ndiaye, I. Ngom, M. Diop, et E. H. M. Ndiaye, « A Sensorless Speed Control of DC Motor Based on an Adaptive Reference Model », in *2021 4th Biennial International Conference on Nascent Technologies in Engineering (ICNTE)*, NaviMumbai, India, janv. 2021, p. 1-5. doi: 10.1109/ICNTE51185.2021.9487787.

[6] Y. Liu, J. Zhao, M. Xia, et H. Luo, « Model reference adaptive control-based speed control of brushless DC motors with low-resolution Hall-effect sensors », *IEEE Trans. Power Electron.*, vol. 29, nº 3, p. 1514-1522, 2013.

[7] S. Mallick et U. Mondal, « Performance Study of different Model Reference Adaptive Control Techniques applied to a DC Motor for Speed Control », in *2019 3rd International Conference on Trends in Electronics and Informatics (ICOEI)*, 2019, p. 770-774.

[8] B. Keziz, S. Ladaci, et A. Djouambi, « Design of a MRAC-Based Fractional order PI λ D μ Regulator for DC Motor Speed Control », in *2018 International Conference on Electrical Sciences and Technologies in Maghreb (CISTEM)*, 2018, p. 1-6.

[9] M. Turki, « Synthèse de contrôleurs prédictifs auto-adaptatifs pour l'optimisation des performances des systèmes », PhD Thesis, Normandie Université, Université de Rouen, 2018.

[10] H. Kaufman, I. Barkana, et K. Sobel, *Direct adaptive control algorithms: theory and applications*. Springer Science & Business Media, 2012.

[11] M. Swathi et P. Ramesh, « Modeling and analysis of model reference adaptive control by using MIT and modified MIT rule for speed control of DC motor », in *2017 IEEE 7th International Advance Computing Conference (IACC)*, 2017, p. 482-486.

[12] P. Swarnkar, S. Jain, et R. K. Nema, « Effect of adaptation gain in model reference adaptive controlled second order system », *Eng. Technol. Appl. Sci. Res.*, vol. 1, nº 3, p. 70-75, 2011.

[13] P. Ramesh, « Investigation on Adaptive Gain in MRAC for First Order Systems », 2016.

[14] P. Ramesh et N. Yadaiah, « MRAC with variable adaptation gain for first order systems », in *TENCON 2017 - 2017 IEEE Region 10 Conference*, nov. 2017, p. 585-590. doi: 10.1109/TENCON.2017.8227930.

[15] A. Feyo, A. Thelkar, C. Bharatiraja, et Y. Adedayo, « Reference design and comparative analysis of model reference adaptive control for steam turbine speed control », *FME Trans.*, vol. 48, nº 2, p. 329-341, 2020, doi: 10.5937/fme2002329F.

[16] A. Hafte, « DESIGN OF LYAPUNOV RULE BASED MODEL REFERENCE ADAPTIVE CONTROL WITH DECOUPLER FOR BOILER-TURBINE-GENERATOR ». January, 2019.

[17] I. D. Landau, « A survey of model reference adaptive techniques—Theory and applications », *Automatica*, vol. 10, nº 4, p. 353-379, 1974.

[18] N. T. Nguyen, « Model-reference adaptive control », in *Model-Reference Adaptive Control*, Springer, 2018, p. 83-123.

[19] G.-Q. Wu, S.-N. Wu, Y.-G. Bai, et L. Liu, « Experimental studies on model reference adaptive control with integral action employing a rotary encoder and tachometer sensors », *Sensors*, vol. 13, nº 4, p. 4742-4759, 2013.

[20] N. M. Raharja, A. Ma'arif, Y. Ramadhan, et P. A. Rosyady, « Pole Placement Based State Feedback for DC Motor Position Control », in *Journal of Physics: Conference Series*, 2021, vol. 1783, nº 1, p. 012057.

[21] J. V. Candy, « Model Reference Adaptive Control (MRAC) for Additive Manufacturing », Lawrence Livermore National Lab.(LLNL), Livermore, CA (United States), 2021.

[22] N. Zoghlami, « Stabilité et stabilisation en temps fini des systemes dynamiques interconnectés et probleme de consensus en temps fini », PhD Thesis, Université d'Évry Val d'Essonne; École nationale d'ingénieurs de Tunis (Tunisie), 2014.

[23] M. Safi, « Stabilité de Lyapunov de systemes couplés impliquant une équation de transport », PhD Thesis, Institut supérieur de l'aéronautique et de l'espace, 2018.

[24] L. Eugene, W. Kevin, et D. Howe, « Robust and adaptive control with aerospace applications », *Engl. Springer-Verl. Lond.*, 2013.

ISSN: 1737-9334

ISSN: 1737-9334